

BRNO UNIVERSITY OF TECHNOLOGY

VYSOKÉ UČENÍ TECHNICKÉ V BRNĚ

FACULTY OF MECHANICAL ENGINEERING

FAKULTA STROJNÍHO INŽENÝRSTVÍ

INSTITUTE OF SOLID MECHANICS, MECHATRONICS AND BIOMECHANICS

ÚSTAV MECHANIKY TĚLES, MECHATRONIKY A BIOMECHANIKY

A SIMULATION OF CLOSED DIE FORGING USING FINITE ELEMENT METHOD

SIMULACE ZÁPUSTKOVÉHO KOVÁNÍ POMOCÍ METODY KONEČNÝCH PRVKŮ

MASTER'S THESIS

DIPLOMOVÁ PRÁCE

AUTHOR

AUTOR PRÁCE

Bc. Michal Nytra

SUPERVISOR

VEDOUCÍ PRÁCE

Ing. Petr Kubík, Ph.D.

BRNO 2019

Master's Thesis Assignment

Institut: Institute of Solid Mechanics, Mechatronics and Biomechanics
Student: **Bc. Michal Nytra**
Degree program: Applied Sciences in Engineering
Branch: Engineering Mechanics and Biomechanics
Supervisor: **Ing. Petr Kubík, Ph.D.**
Academic year: 2018/19

As provided for by the Act No. 111/98 Coll. on higher education institutions and the BUT Study and Examination Regulations, the director of the Institute hereby assigns the following topic of Master's Thesis:

A simulation of closed die forging using finite element method

Brief description:

Create a study from an area of high temperature bulk forming aimed at its simulation. Perform a simulation of a closed die forging process for a chosen mechanical part using the finite element method. Further, perform an analysis of an influence of chosen process parameters (e.g. an initial temperature of an input material, initial dimensions of an input material etc.) on a stress–strain field. This thesis will be solved in cooperation with an industry partner MSV Metal Studénka, a.s.

Master's Thesis goals:

- A study from an area of high temperature bulk forming.
- A simulation of a closed die forging process.
- An analysis of influence of chosen process parameters on a stress–strain field.

Recommended bibliography:

FOREJT M., PÍŠKA M. Teorie obrábění, tváření a nástroje. 1. vyd. Brno: Akademické vydavatelství CERM, s. r. o., 2006. 217 s. ISBN 80-214-2374-9.

NALAWADE R.S., PURANIK A.J., BALACHANDRAN G., MAHADIK K.N., BALASUBRAMANIAN V. Simulation of hot rolling deformation at intermediate passes and its industrial validity. International Journal of Mechanical Sciences, 2013, vol. 77, pp. 8-16.

HAILIN H., SHIQUAN H., YOUPING Y., WANFU G. Simulation and experimental research on isothermal forging with semi-closed die and multi-stage-change speed of large AZ80 magnesium alloy support beam. Journal of Materials Processing Technology, 2017, vol. 246, pp. 198-204.

HARTLEY P., PILLINGER I. Numerical simulation of the forging process. Computer Methods in Applied Mechanics and Engineering, 2006, vol. 195 (48-49), pp. 6676-6690.

Students are required to submit the thesis within the deadlines stated in the schedule of the academic year 2018/19.

In Brno, 24. 10. 2018

L. S.

prof. Ing. Jindřich Petruška, CSc.
Director of the Institute

doc. Ing. Jaroslav Katolický, Ph.D.
FME dean

Summary

This master's thesis is aimed at computational modelling of closed-die forging, which is one of the high temperature bulk forming methods. The objective is to change the ordinary approach of creating of analysis models in specialized programmes based on a finite element method (FEM) and to build-up an analysis model in FEM software Abaqus. A displacement-based variant of FEM and an explicit algorithm are used for the calculations. The solved mechanical part is a spur gear from a car gearbox. A study from an area of bulk forming including specialized programmes for simulation of forming processes is created as a part of this thesis. Next, all constitutive laws for description of an elasto-plastic model of material with ductile damage are mentioned in the thesis. A heat transfer theory follows, there are described all ways how a heat transfer can be realised with their mathematical formulations including methods of solution. A key chapter is that one describing a the process of creating an analysis model in software Abaqus from a geometry creation up to boundary condition. An analysis of results follows and this thesis is ended by the prospect of a possible follow-up on the subject/topic.

Abstrakt

Tato diplomová práce se zabývá výpočtovým modelováním zápusťkového kování, které patří do metod objemového tváření zatepla. Cílem je změnit běžnou praxi tvorby výpočtových modelů ve specializovaných softwarech na bázi metody konečných prvků (MKP) a sestavit výpočtový model v MKP softwaru Abaqus. Pro výpočet jsou zde použity deformační varianta MKP a explicitní algoritmus. Řešenou součástí je ozubené kolo automobilové převodovky. V rámci práce je vytvořena rešerše z oblasti objemového tváření včetně specializovaných programů pro simulace procesů tváření. Dále jsou v práci uvedeny všechny konstitutivní vztahy pro popis elasto-plastického modelu materiálu s tvárným porušením. Následuje teorie přenosu tepla, jsou popsány všechny způsoby jeho realizace s jejich matematickými formulacemi včetně metod řešení. Klíčovou je kapitola popisující postup tvorby výpočtového modelu v softwaru Abaqus od tvorby geometrie až po okrajové podmínky. Následuje analýza dosažených výsledků a práce je zakončena výhledem na možné pokračování v tomto tématu.

Keywords

Closed die forging, bulk forming, finite element method (FEM), explicit algorithm, plasticity, ductile damage, heat transfer

Klíčová slova

Zápustkové kování, objemové tváření, metoda konečných prvků (MKP), explicitní algoritmus, plasticita, tvárné porušování, přenos tepla

Bibliographic Citation

NYTRA, Michal. *A Simulation of Closed Die Forging Using Finite Element Method*. Brno, 2019. 115 p. Master's Thesis. Brno University of Technology, Faculty of Mechanical Engineering. Thesis supervisor Ing. Petr Kubík, Ph.D.

Declaration

I declare that I have written the master's thesis *A Simulation of Closed Die Forging Using Finite Element Method* on my own according to advice of my supervisor Ing. Petr Kubík, Ph.D. and using the sources listed in a bibliography.

In Brno, on
Michal Nytra

Acknowledgement

I would like to say thank you to my supervisor Ing. Petr Kubík, Ph.D. for his valuable advices and remarks during creation of this master's thesis and also for his experience with a FEM software Abaqus.

I would like to say thank you to employees of MSV metal Studénka, a.s. company for consultations to a closed die forging theme, valuable advices and experience during creation of this master's thesis.

I would like to say thank you also to miss Pavlína Zpěváčková and Mr Jan Lukša for language correction of both language versions of this master's thesis.

I would like to say thank you to my family for a support no just during writing this master's thesis, but during the whole university studies.

Contents

1	Introduction	13
1.1	Motivation	13
1.2	Objectives of Thesis	14
2	Problem and Its Analysis	15
2.1	Situation Discussion	15
2.2	Problem formulation and Thesis Goals	15
2.3	Essential Variables System	16
2.4	Solved Mechanical Part	19
2.5	Method Choice	20
3	Forging Technology	27
3.1	Forging Characteristics	27
3.2	Heating of a material	28
3.3	Forging Methods	30
3.4	Forging Process Simulation Possibilities	39
3.5	Mechanical Parts	41
4	Constitutive Laws and Material Characteristics	43
4.1	Elastic Material Behaviour	43
4.2	Plastic Material Behaviour	44
4.3	Ductile Damage	53
4.4	Physical and Thermodynamic properties	58
5	Heat Transfer	59
5.1	Conduction Heat Transfer	59
5.2	Convection Heat Transfer	61
5.3	Radiation Heat Transfer	62
5.4	Initial and Boundary Conditions in Heat Transfer Solution	62
5.5	Heat Transfer Solution	63
6	Build-up of Analysis Model	67
6.1	Units	67
6.2	Dimensions of Input Material	68
		11

6.3	Discretization	70
6.4	Dimensions change due to Thermal Expansion	72
6.5	Model of Material-Steel 12 050	72
6.6	Contacts	74
6.7	Boundary Conditions	77
6.8	Initial Conditions	80
6.9	Series of Operations	81
7	Results	85
7.1	Simulation without Ductile Damage	85
7.2	Simulation with Ductile Damage	99
8	Conclusion	105
8.1	Summarization	105
8.2	Future Works	106
	Bibliography	107
	List of Most Frequent Abbreviations and Symbols	111
A	Tensors for Large Deflections	117
A.1	Strain Tensors	117
A.2	Stress Tensors	121
A.3	Energetically Conjugated Tensors	122
B	Geometry Creation	123
B.1	Mechanical Part	123
B.2	Forging	125
C	Appendix to Results	127
	List of Figures	129
	List of Tables	133

1 Introduction

1.1 Motivation

Manufacturing technologies, where belong also forming technologies, have been connected to the human society for centuries. These methods and its products were used earlier mostly in army industry. After the end of the WW II the situation changed and the main focus was aimed at civil engineering fields (transportation, energetics, mining technology, ...). But the first approaches were very simple, based on an observation, empirical knowledges and experiments and were often uneconomic. An optimization was needed to invent new better approaches. This process has began with a computer technology arrival, because the efficient optimization wouldn't be otherwise possible. Mainly with a finite element method (further only FEM), it was possible to solve bodies with a complicated geometry and non-linear problems (large deformations, non-linear material characteristics, contacts, continuum damage, ...), see Fig. 1.1. Concurrently, the description of possible limit states which should appear during forming (continuum damage initiation, fatigue of tools, ...) had to be improved. For ductile damage analysis, phenomenological models based on a damage cumulation due plastic deformation (see Sec. 4.3) have been built, but its calibration is a tricky and expensive process.

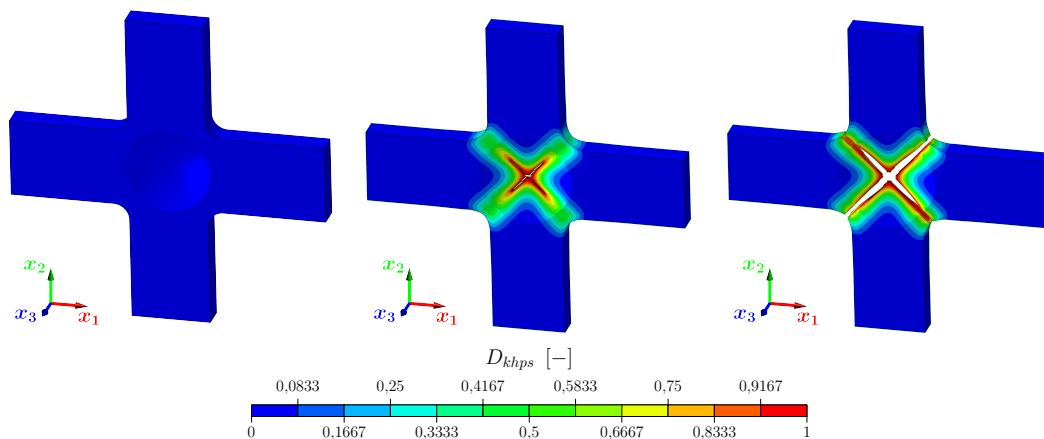


Fig. 1.1: Biaxial tensile specimen¹

¹ D_{khps} is a damage parameter according to KHPS criterion, see Eq. (4.32a) on p. 57.



Fig. 1.2: Central bursting initiation during forward extrusion [1]

e.g. a crack initiation in sheet metal bending, profile rolling, extrusion, forging etc. (see Fig. 1.2). Results of these analysis are used as a background for modifications to reduce risk of defect initiation or for regularization of the process parameters.

Two fields of its usage have been founded. The first one is a simulation of processes, where an initiation of the continuum damage is requested and it serves to observe some process parameters, e.g. shear force value in a bar shear partitioning (see Fig. 1.3) The second one serves to predict defect initiation during manufacturing process,

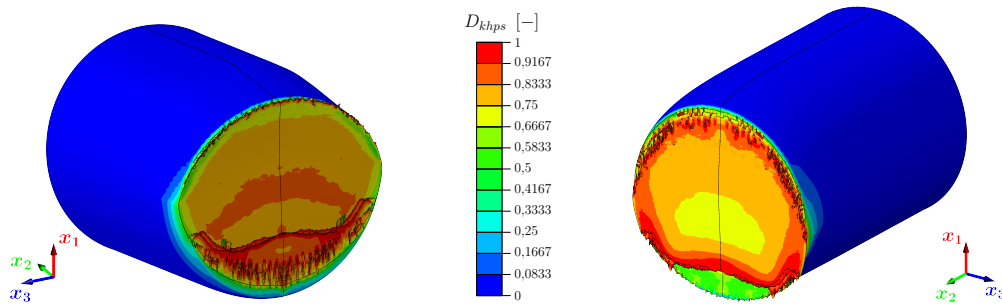


Fig. 1.3: Bar shear partitioning [1]

Very important part is also an analysis verification by experiments, which serve to check if the analysis is correct.² In the case of technologies this process is realized by a production of prototypes which are checked. If their quality is on a requested level, a series production is started. In the opposite case, another modifications are needed

1.2 Objectives of Thesis

For simulations of the forming processes, specialized software containing the mentioned FEM (see Sec. 3.4) were invented. An objective of this thesis is to build a computational model in "universal" commercial FEM software which will be able to describe processes during the hot forming in detail.

²A computational model is only an approximation of a real state, when only some relevant influences on a specific recognition level are considered, other ones are considered as irrelevant.

2 Problem and Its Analysis

2.1 Situation Discussion

Up to now all tasks/problems of a high temperature forming have been solved by specialized programs based on the FEM. There is a will to use existing algorithm in "universal" FEM programs used to solved a wide range of tasks/problems in the solid mechanics and to apply them onto a complex high temperature forming problem containing stress-strain states as well as states connected with a heat transfer

2.2 Problem formulation and Thesis Goals

A problem is to build-up a computational model in a "universal" FEM program to describe a deformation, a stress and a temperature distribution in a mechanical part produced by a closed-die forging method, which belongs into a group of high temperature forming.

It is a *non-linear* problem from an aspect of the solid mechanics because of several reasons:

1. Material non-linearity: during forming plastic deformation occurs that can be in a big range, mainly in case of the volume forming. So the material is not only linear isotropic, but a plasticity model has to be implemented.
2. Geometric non-linearity: during a bulk forming large strain³ occurs, so using of "extended" geometric equation is necessary.⁴ There exist more types of strain tensors, which are mentioned in Chap. A.1.
3. "Mate" non-linearity (contacts): a contact surface is time dependent, so contacts are non-stationary. Contact problems are in an explicit algorithm (see next) solved only with a penalty method based on a change of contact elements normal stiffness according to an actual bodies penetration.⁵

³Large strain is automatically connected with large displacements.

⁴A mate between a field of displacements and a field of strain.

⁵The penetration is an intersecting distance of bodies (non-empty volume intersection). In the reality the bodies are impenetrable.

A solving person is limited in possibilities of experimental verification of results obtained from a FEM solution because of several reasons:

- There isn't a method for measuring deformation (strain) and stress in parts in a plastic state in an enclosed spaced and outside an observer's field of view.⁶
- In the optical way there can be determined a temperature distribution on a body's free surface, not inside it.

Experimentally verifiable quantity is a force required to deform a forging and caused by a forming machine. This force is compared with a machine load capacity to pretend its overloading. Next, it is possible to determine a residual stress in the experimental way, e.g. by a drilling method.

Goals of this thesis are:

- Create a research study in an area of a high temperature forming and possibilities of its solution by a computational modelling.
- Perform a stress-strain analysis of a forging and a temperature distribution in it by a computational modelling.
- Consider an influence of input material parameters (dimensions, temperature) on a deformation and a stress.

2.3 Essential Variables System

This section is based on knowledge from [2].

Surrounding (Environment)

The processes take place in the air atmosphere with temperature T_∞ and no oxidative and corrosive impacts. A heat exchange occurs indeed between surrounding and the formed material defined by a convection coefficient and an emissivity.

⁶A forging is totally enclosed by a die (see further), so there can't be used optical methods for deformation measuring.

Geometry and Topology

An initial geometry of the formed material is a circular cross section rod of a diameter $\varnothing D$ and a length L . The geometry is extended with deformation caused by thermal expansion during heating to a forging temperature. The deformation after previous material parting, mainly in the case of bar shearing, is irrelevant, because it is localized in the shear place and there is no effect on the stress distribution in the rest of the rod.

A geometry of tools is created from surface rigid bodies controlled by reference points. There are used only surfaces that can get in contact with the formed material. All dimensions are considered as deterministic.

Mates with Surrounding

Mates are contacts between the forging and the rigid bodies of the tools defined by a friction coefficient f_f . The next mates are symmetry conditions, if symmetry can be used. Between the forging and the tools occurs also a heat transfer defined by a convection coefficient, sometimes called as a capacitance.

The mates of the rigid bodies are defined in the reference points and in the case of movement are controlled with kinematic conditions.

Activation of The Object

The deformation of the formed material is caused by the contact with tools surfaces, it's a dynamical process. The heat transfer is caused by the contact with the tools surfaces and through outer surfaces into surrounding.

Influencing of The Object

The main influencing variables are tools movement velocity influencing forming velocity, the formed material temperature and a roughness of the dies surfaces depending value of the friction coefficient.

Object's Properties

The formed material is made from a steel 12 050⁷ according to ČSN and its chemical composition is listed in Tab. 2.1. This material is considered as elasto-plastic. Elastic component is linear isotropic defined by Young's modulus E and Poisson's ratio ν . Plastic component is described by Johnson-Cook flow curve which is able to consider a "process rate" and a temperature. A ductile damage is described by Johnson-Cook criterion. All constitutive laws are described in Chap. 4. Furthermore physical and thermodynamic properties as a density ρ_d , a specific heat⁸ c , a thermal conductivity λ_{hc} and a thermal expansion coefficient α_{te} are given. The properties are temperature dependent in a common case.

Tab. 2.1: Steel 12 050 chemical composition [3]

Values in weight %							
C	Mn	Si	Cr	Ni	Cu	P	S
0.42 – 0.5	0.5 – 0.8	0.17–0.37	max 0.25	max 0.3		max 0.04	

Tools are made from tool steel 19 552 according to ČSN. In comparison with a forging's compliance, they are considered as the rigid bodies and the only needed property is the heat capacity⁹ for the heat transfer.

States and Processes

An initial state is the unloaded one with no residual stress. By the forming the deformed state is invoked. After the flash trimming a cooling process is started.

Expressions a consequences

A consequence of a loading of the object is its deformation and stress evocation. Because of forming and a heterogeneous temperature field in the material residual stress remains.

⁷AISI 1045.

⁸Especially constant pressure specific heat.

⁹Specific heat multiplied by a object's mass.

Dynamic Effects Consideration

The problem can not be considered as purely static, because there is an impact between the tool and the forging (see previously). On the other hand there are not evoked any relevant inertia forces, because in a global scale, it is not fast enough. A frequency of the load is also very slow and orderly lower than the first natural frequency of longitudinal waves, so there are no vibrations.

2.4 Solved Mechanical Part

The solved part is displayed in Fig. 2.1. It is an idler spur gear in a reverse transmission of a gearbox F17 used also in vehicles Opel Vectra B (1995–2002) and designed by General Motors (GM).

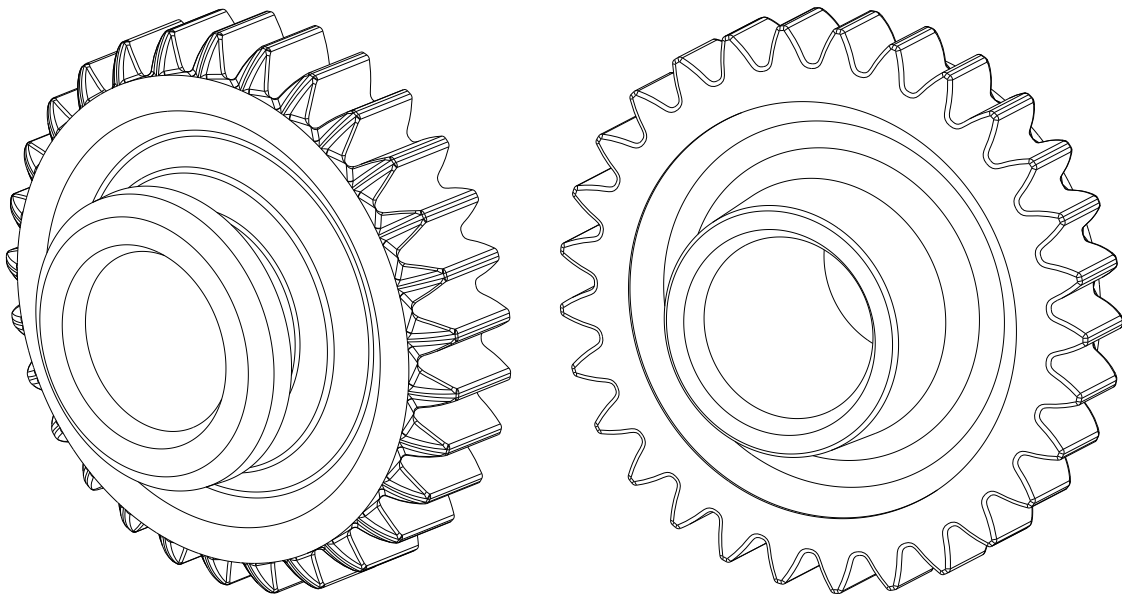


Fig. 2.1: Solved mechanical part

A geometry creation is described in an appendix in Chap. B.

2.5 Method Choice

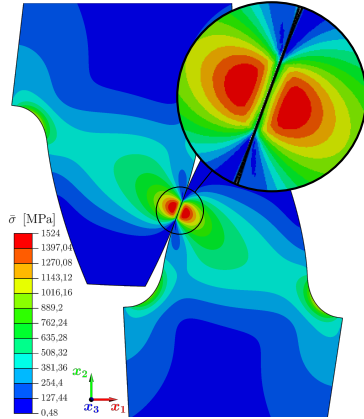


Fig. 2.2: Hertz contact

There can be solved contact stress distribution under the surface of bodies in the contact using this theory, where its geometry can be substituted with an osculating circle. Its basic presumptions are purely the elastic material and the non-frictional contact. However, in the forming an invocation of the plastic strain is required and, what is more, the contacts are non-stationary and frictional.

The only possibility is using the calculus of variations methods, where the FEM also belongs. This method can be used in structural, heat transfer, dynamic analysis etc., where can be situated non-linear problems listed in the introduction of this chapter. Two basic formulations of a FEM displacement-based variant are:

1. Implicit: an unconditionally stable algorithm, suited for solving structural task, slow dynamic processes, heat transfer problems.
2. Explicit: a conditionally stable algorithm, suited for solving very fast processes with big deflections, problems with high amount of contacts, bodies failure.

A description mentioned above, proves that a choice of a solution algorithm strongly depends on a problem/task type: in terms of a process rate, a non-linear behaviour level etc.

¹⁰It is the special case for bi-linear material (linear strain hardening), where a tangential modulus $E_T = 0$ Pa.

¹¹It is used mostly in a contact stress analysis under a gear working profile (see Fig. 2.2, $\bar{\sigma}$ is an von Mises equivalent stress, see Eq. (4.14d) on p. 47) and in a design of a gear transmission against a contact fatigue failure.

We can demonstrate a comparison of an implicit and an explicit algorithm from an aspect of solution time requirements on an analysis of a round bar for an uniaxial tensile test (see Fig. 2.3). Analysis settings is exactly the same for both algorithms from aspects of geometry, material, mesh, boundary conditions etc. Both algorithms are allowed to use an automatic time stepping for a solution. The results are really surprising, because the time requirement of the implicit algorithm 1 min 32 s and of the explicit algorithm 18 h 50 min 15 s for the same task size.¹²

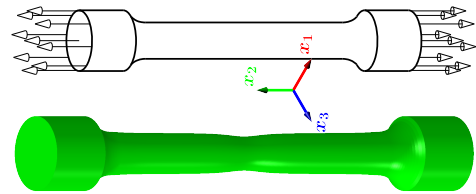


Fig. 2.3: Uniaxial tensile test

Both algorithms are allowed to use an automatic time stepping for a solution. The results are really surprising, because the time requirement of the implicit algorithm 1 min 32 s and of the explicit algorithm 18 h 50 min 15 s for the same task size.¹²

The mentioned time results clearly demonstrate that it is doubtless better to use the implicit algorithm, because the explicit algorithm requires a very small time increment to make it stable (see further). However, there are areas of the solid mechanics, where the implicit algorithm badly converges or even fails, e.g. analysis of thin-wall structures post-critical behaviour (see Fig. 2.4), continuum damage analysis and else.

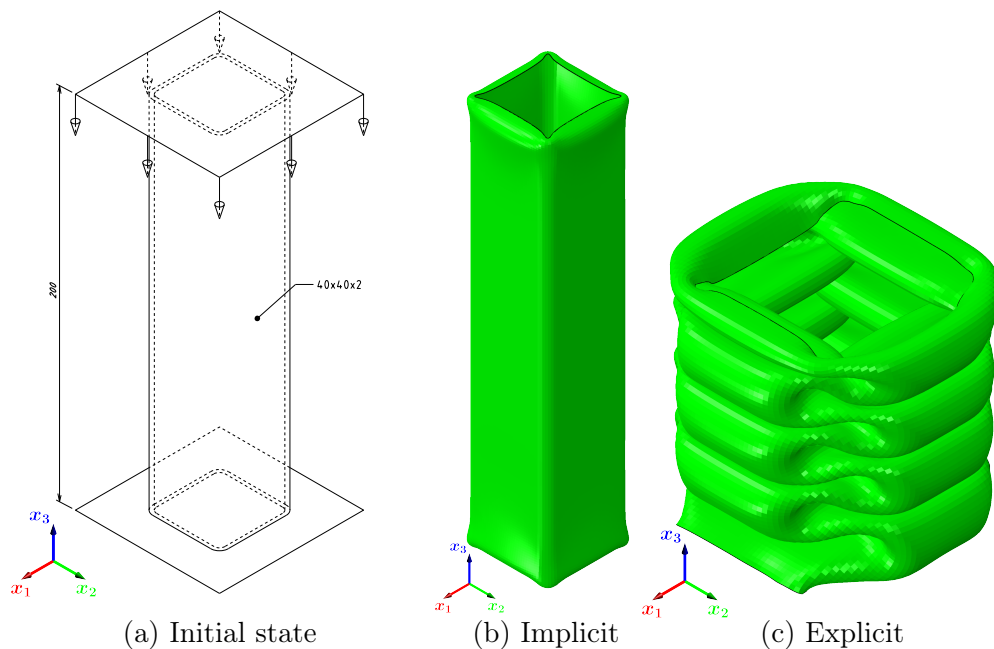


Fig. 2.4: Thin-wall structure post-critical behaviour analysis

¹²A large time increment may cause inaccurate results, so it is appropriate to limit its maximum size.

Because of the big deflections and a requirement of a failure criterion implementation the explicit algorithm will be used. There is a will to solve this specific problem with an "universal" FEM package, because hot forming problems are usually solved by using specially created software (see Sec. 3.4). As a workbench Abaqus CAE, developed by a company Simulia, will be used. It is a part of DAUSSALT SYSTÉMES.

2.5.1 Basic Description of FEM

As was said earlier, the FEM is a numerical method based on a discretization of a solved area to smaller subregions (elements) simpler in a shape having common vertices (nodes), edges and in 3D also surfaces. Nowadays mostly its displacement-based variant, where solved variables are nodal displacements, is used. Displacements are approximated over the element by using basis functions, usually polynomials. There is used the calculus of variations. There are several variational principles, where also belongs a Lagrangian variational principle. It is based on a statement that between all possible displacement functions applying geometric equations and geometric boundary conditions there are realizing functions minimizing of a potential Π

$$\Pi = W_i - W_o = \iiint_{\Omega} \Lambda \, dV - \left(\iiint_{\Omega} \mathbf{U}^T \mathbf{o} \, dV + \iint_{\partial\Omega} \mathbf{U}^T \mathbf{p} \, dS \right), \quad (2.1)$$

where:

- W_i [J] is an internal energy in a body Ω ($\partial\Omega$ is a body's border),
- W_o [J] is an outer forces potential,
- Λ $\left[\frac{\text{J}}{\text{m}^3}\right]$ is an internal energy per a volume unit,
- \mathbf{U} [m] a displacement matrix,
- \mathbf{o} $\left[\frac{\text{N}}{\text{m}^3}\right]$ is a body load matrix and
- \mathbf{p} $\left[\frac{\text{N}}{\text{m}^2}\right]$ is a surface load matrix.

A condition of the functional Π minimal value can be express as

$$\delta\Pi = 0,$$

where δ is a variation operator. A system of equations required for FEM equations built-up:

- Equilibrium equations: equations of a force equilibrium on an internal (Eq. (2.2a), Fig. 2.5a), respectively on a border (Eq. (2.2b), Fig. 2.5b) elementary element.¹³

$$\frac{\partial \sigma_{ji}}{\partial x_j} + o_i = 0 \quad (2.2a)$$

$$\sigma_{ji} \cos \alpha_j = f_{pi} \quad (2.2b)$$

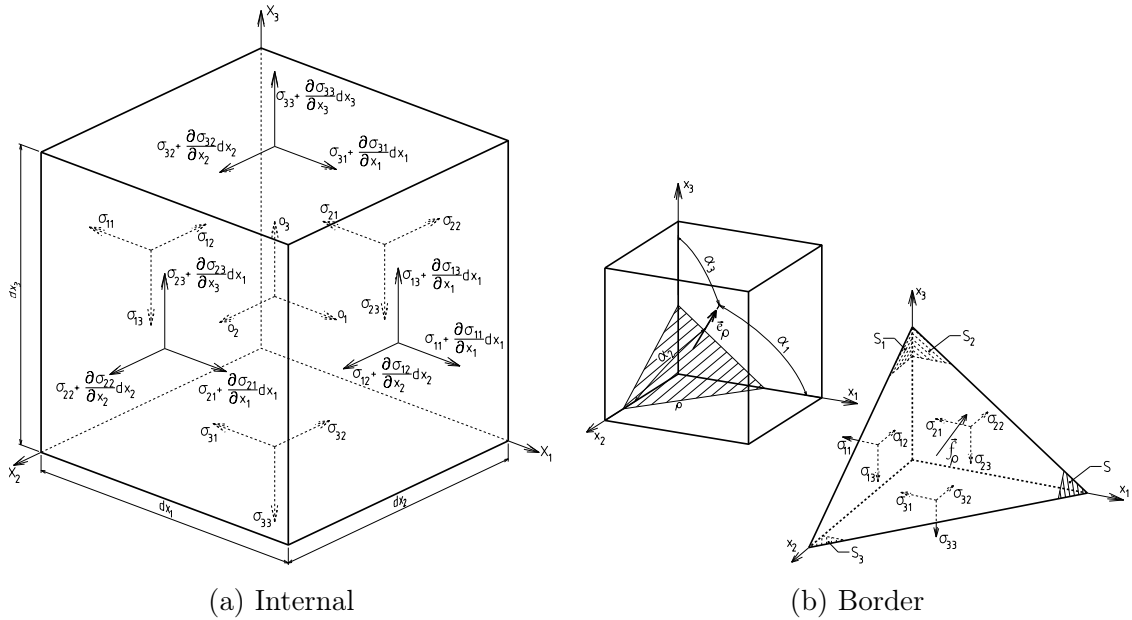


Fig. 2.5: Elementary element [5]

- Geometric equations: relations between a displacement field and a strain field. These relations are described in Chap. A.1, because there are several strain tensors for large deflections.
- Constitutive laws: relations between the strain field and a stress tensor components. These are described in Chap. 4.

¹³Eq. (2.2a) and (2.2b) are vector equations written to its components. There is used the Einstein notation and a summation symbolic.

Explicit Algorithm

As previously said, it is a conditionally stable algorithm. This means the algorithm stability is depends on a solution time increment size, which has to meet a relation

$$\Delta t \leq \Delta t_c,$$

where Δt_c is a critical time increment size given by Eq. (2.3)

$$\Delta t_c = \frac{L_e}{v_w} = \frac{L_e}{\sqrt{\frac{E}{\rho}}} = L_e \sqrt{\frac{\rho}{E}}, \quad (2.3)$$

where:

- L_e [m] is a characteristic dimension of the *smallest* element in a mesh,
- ρ [$\frac{\text{kg}}{\text{m}^3}$] is a material density and
- E [Pa] a Young's modulus [6].¹⁴

The critical time increment value is influenced by the material type, in comparison with the implicit solver, where is its value not dependent on the material type. A typical time increment for the explicit solver is 10^{-6} s and less. To increase a time increment, it is possible to use a mass scaling based on increasing of the density. In the static/quazistatic tasks there is needed to pay attention to keep the systems kinetic energy up to 10% of its internal energy.

A basis of the explicit algorithm is solving a matrix equation

$$\mathbf{M}\ddot{\mathbf{U}} = \mathbf{F}_e - \mathbf{F}_i, \quad (2.4)$$

where:

- \mathbf{M} [kg] is a mass matrix,
- $\ddot{\mathbf{U}}$ [$\frac{\text{m}}{\text{s}^2}$] is an acceleration matrix,
- \mathbf{F}_e [N] is an external load matrix and
- \mathbf{F}_i [N] is an internal force matrix [6].

¹⁴ v_w in the Eq. (2.3) is a wave propagation velocity in the material. An interpretation of the equations is that a stress wave can't get through the mesh's smallest element during one increment.

The internal force matrix depends on a stress state, contact forces and forces caused by a hourglassing (see next). It can be express by relation

$$\mathbf{F}_i = \sum \left(\iiint_{\Omega} \mathbf{B}^T \boldsymbol{\sigma} dV + \mathbf{F}_{\text{hg}} \right) + \mathbf{F}_{\text{cont}}, \quad (2.5)$$

where:

- $\mathbf{B} \left[\frac{1}{\text{m}} \right]$ are strain basis functions¹⁵,
- $\boldsymbol{\sigma}$ [Pa] is a (Cauchy) stress tensor (see Sec. A.2.1),
- \mathbf{F}_{hg} [N] are hourglassing forces and
- \mathbf{F}_{cont} [N] are contact forces [7].

To get velocity and displacement, a central difference method is used in the explicit algorithm

$$\dot{\mathbf{U}}_{i+\frac{1}{2}} = \dot{\mathbf{U}}_{i-\frac{1}{2}} + \frac{\Delta t_{i+1} + \Delta t_i}{2} \ddot{\mathbf{U}}_i, \quad (2.6a)$$

$$\mathbf{U}_{i+1} = \mathbf{U}_i + \Delta t_{i+1} \dot{\mathbf{U}}_{i+\frac{1}{2}}, \quad (2.6b)$$

where:

- $\dot{\mathbf{U}} \left[\frac{\text{m}}{\text{s}} \right]$ is a velocity matrix,
- Δt [s] is the time increment size and
- i [-] is a step time number (integer) [6].

There is only a lumped (diagonal) mass matrix because of its easy inversion. The other advantage is a decomposition to a system of independent equations the solution of which can be easily paralleled into several clusters/threads. The internal forces matrix is composed from every single element and is not necessary to compose a global stiffness matrix and its inversion, this leads to another time save.

A reduced (single-point) integration is often used, where the element has only one Gauss-integration point placed in its center of mass. A time and operational difficulty is decreased for the element matrices composing, on the other hand it can lead to a negative effect known as hourglassing.

¹⁵It is displacement basis functions derivative.

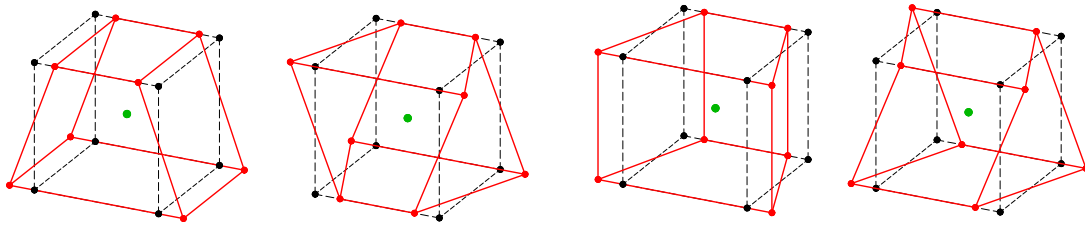


Fig. 2.6: Hourglassing symmetric modes [7]

These are modes of deformation symmetric to the integration point (see Fig. 2.6), but there is a zero deformation energy. To reduce it, it is possible to use:

1. Integration grade increase: the time difficulty to compose the element matrices is increased. What is more, the stiffness of the element/system increases and it can lead to unreal behaviour.
2. Number of elements increase: in one consequence, the size of solved matrices is increased and time required for their solution is increased. The second one is the fact that with increasing number of elements, their size decrease, which leads to the smaller time increment size (see Eq (2.3)).

A tolerated amount of an energy caused by the hourglassing is 5 – 10% of a total internal energy.

According to the fact there is required the small time increment size for the algorithm stability (see Eq. (2.3)), there has to be performed a high amount of time steps¹⁶. Because of the fact that the finite element method is the numerical method, it works just with a finite count of decimal places. That way, using a double precision is recommended. A data type `double` (8 B) has 15 decimal places in comparison with 7 decimal places of the data type `float` (4 B) used for a single precision. In case of using the single precision, an analysis breakdown can appear because of a round error run-out.

¹⁶The number of steps for the explicit algorithm is usually 10^5 and more.

3 Forging Technology

Forging belongs to one of the oldest forming technologies in the world. It originally served mainly for military purpose (army equipment production). In that time it was especially open die forging (see Sec. 3.3.1). There is also used closed die forging (see Sec. 3.3.2), which predominates nowadays.

3.1 Forging Characteristics

It's a method of bulk ("volume") forming¹⁷, which takes place in higher temperature (e.g. for steels 750 °C up to 1300 °C)¹⁸. An upper limit of the forging temperature is often 200 ÷ 300 °C under solidus curve (see Fig. 3.1).

A basis is a transformation of Perlit, respectively of Ferit which is included in Perlit, into Austenit, which has mechanical properties more suitable for forming (natural forming resistance¹⁹ σ_p decrease). On the other hand, there is possibility of a grain grow if the temperature is too high for a long time. As a result, mechanical properties are worsened and this state can be eliminated with an additional heat treatment (normalizing).

The aim is to create stress state in a formed body, which evokes the macroplastic deformation in the whole volume. By increasing of the temperature, substantially bigger plastic deformation before a damage initiation can be obtained than at a room temperature. See Fig. 3.2, where is displayed how big deformation can be made during forging.

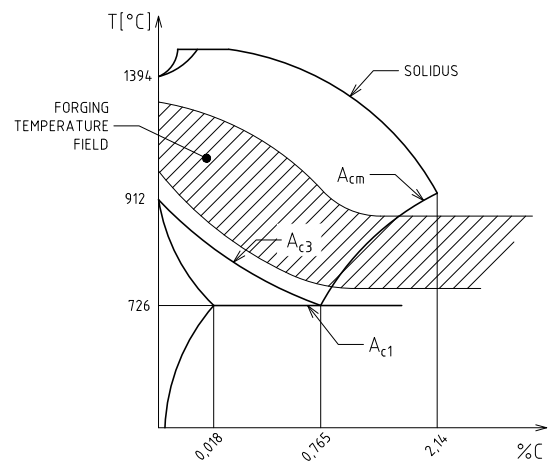
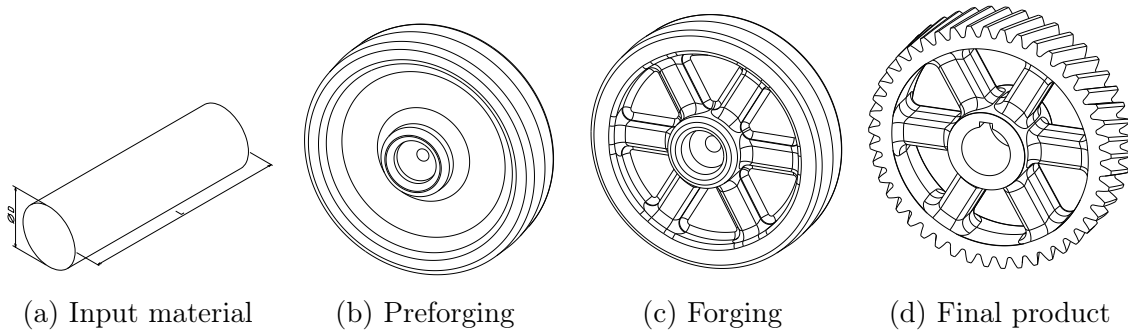


Fig. 3.1: Diagram Fe - Fe₃C [8]

¹⁷It's a way of the forming, when is a shape of a manufactured mechanical part changed in all directions.

¹⁸Forging temperature range is set by chemical composition and is included in material data sheet.

¹⁹Internal material resistance against external forces influence under one-axial stress state conditions when a plastic deformation starts, expressed in Pa. [9]

Fig. 3.2: Gear production process²⁰

With the forming progress, the natural forming resistance of the material increases, so bigger forces are needed for the next deformation. High temperature forming cause that the deformation (strain) hardening particularly disappear in the influence of the temperature. On the other hand, it is needed to consider a thermal expansion of material, which depends on a thermal expansion coefficient and hence to consider this factor in a production process design.

3.2 Heating of a material

A heating way of the input material is crucial for a final surface structure, hardness and quality. During heating can rise these phenomena:

1. Mill scales creation: mill scales are created from iron oxides FeO , Fe_2O_3 and Fe_3O_4 , which are created by a reaction of the iron situated in steel with an oxygen, carbon dioxide and other gases in a furnace atmosphere. Mill scales is necessary to be cleaned up before the forging process starts, because there is a risk of a penetration into the surface of the forging. This makes surface structure worse, but mainly these defects are places, where fatigue cracks may evoke under a cyclic load [8].
2. Decarburization of the surface layer: as well as oxidation takes place in an atmosphere with active gases, but it interferes into a bigger depth. It has an

²⁰The forging is displayed without a flash. The final product is finished with membrane trimming and following machining.

unfavourable influence on the final surface hardness during a heat treatment (e.g. quenching) [8].

3. Steel "burning": it occurs at the temperature close to the melting temperature. The principle is a diffusion of sulfur and phosphorus contained in the steel to the grain border in form of sulphides and phosphides. The consequence is that mechanical properties get worse and there is a higher probability of brittle crack across the grain borders.²¹

3.2.1 Ways of Heating

Induction heating is based on heat generation which cause eddy currents generated in the heated object by a magnetic field of the exciting coil. A high-frequency alternating current (AC) passes through the coil.

Nowadays it is the most frequently used method, because good and economical heating of material is guaranteed. The biggest advantage is suppressing mill scales creation and decarburization of the surface layer to minimum. The other advantage is an easy temperature regulation. On the other hand, it is not suitable for heating of long or shaped profiles, eventually sheet metals or plates.²²

Heating in a furnace is realized through the heat transfer from a surrounding atmosphere created by burning of gaseous or liquid fuels. The material can be exposed directly in flames coming out of the burner, but this cause production of the high amount of mill scales and big decarburization of the surface layer.²³ A better variant is separating heated body from the burners with the impenetrable partition, the influence of the oxidation and decarburization is limited. On the other hand, a heating effectiveness decreases.

Due to the increasing pressure on the emission production and a high frequency current production possibility (using frequency inverter) there is an effort to suppress this way. Heating in a furnace is used mainly in cases when induction heating is not effective, or, in the single-part production.

²¹Known as intercrystalline crack.

²²The coil has to be common in shape and dimensions to the cross section, otherwise losses appear.

²³An addition ca. 3 % to material volume is needed.

3.3 Forging Methods

3.3.1 Open Die Forging

Open die forging belongs to forming methods with one of the biggest work requirements. It is used for a production of the shapes for closed-die forging²⁴ in big series or in small series production of the parts with different sizes.

In open-die forging, basic operations are used, as can be seen in Fig 3.3a up to 3.3d.

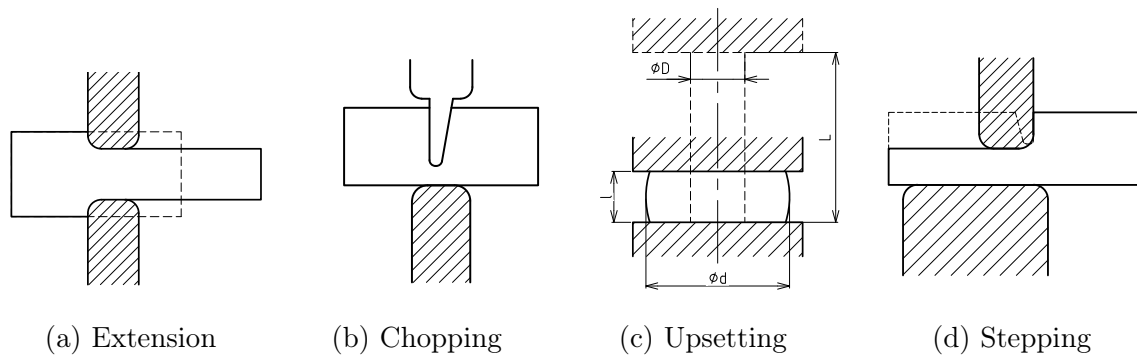


Fig. 3.3: Open-die forging operations examples [8]

Hand-made Forging is rarely used nowadays (mostly for art purposes). In this case hand tools and an anvil are used. However, the principle is the same as in the case when machines are used.

Mechanized Forging is used in a production of parts with mass in units of tonnes.²⁵ For forming there are used drop hammers or hydraulic presses if the bigger forming force is required. As an input material for forging, rolled profiles or ingots are used [8].²⁶ With using special machines it is possible to produce rings with big diameters and thickness which are used as rings for roller bearings.

²⁴A shape for closed-die forging is often called as *preforging* [10, 8].

²⁵Company Vítkovice Heavy Machinery a.s. produce e.g. assembled crankshafts for ship engines.

²⁶A profile after casting.

3.3.2 Closed Die Forging

Closed die forging is a method, where a special tool called die is used to gain a required shape of a forging. It is usually a two-part tool (see Fig. 3.4), where a cavity is created in a shape of the forging.²⁷ The forging is thoughtfully divided by a parting plane, which divides the die into parts to make forging easily releasable after finishing the forming process. In the parting plane there is also situated a flash gutter, where the redundant material flows. This redundant material is called a flash (see Fig. 3.4) and then it's trimmed.

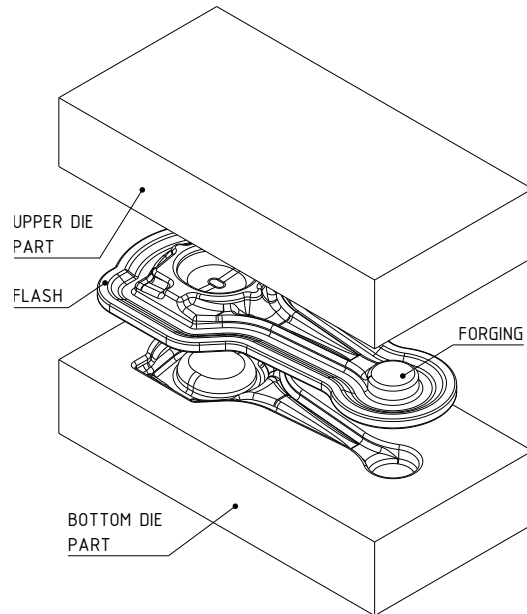


Fig. 3.4: Assembly die-forging

In fact dies are used in big series production, there is needed to put high requirements on mechanical properties. Among the most important ones belong hardness, strength, toughness, fatigue resistance and wear resistance. The dies are loaded with strong impacts during the forging process, this may cause initiation of fatigue cracks from surface defects. That is the reason they are made from tool steel. High hardness (up to 60 HRC and more) is gained by quenching and low temperature tempering. Between the formed material and the die there is a frictional contact, a friction intensity is reduced by a lubricant.²⁸ In the contact, a heat transfer from a forging into the die also takes place.²⁹ Because of a high thermal stress are dies heated at temperature around 250 °C before using.

Only exceptionally it is possible to create the part in one operation, in the most common case, it is before the final shape a "blocking" operation, where a shape similar to the final one is gained. The blocking die cavity has to be designed to fit its output into the finishing cavity with some clearance.

²⁷There is used machining on CNC centres.

²⁸Nowadays it is usually used a mixture of water and carbon in form of a graphite, its concentration is depended by a shape complexity of the produced component.

²⁹2nd law of thermodynamics is valid: "Heat *can't* be transferred by itself from a colder object onto the hotter one."

Forging Design

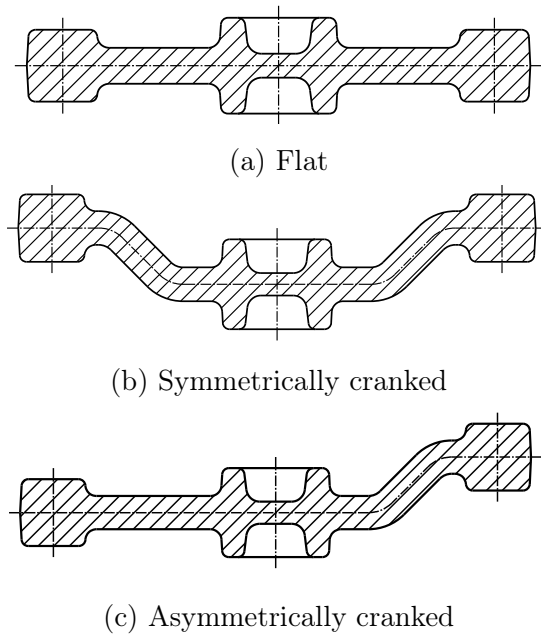


Fig. 3.5: Parting plane shapes [12]

The first step is a choice of the parting plane location, which can be flat or cranked (see Fig. 3.5). The next step is a choice of an addition for machined surfaces. Their size depends on a size of the part and the precision of the forging (see [13]).

All surfaces perpendicular onto the parting plane have to be drafted (outer surfaces usually 3°, inner ones 7°).³⁰ There are tolerated *no* sharp edges, all edges (inner and outer) have to be filleted. A size of the fillet radii depends on a size of characteristic dimensions (see Fig. 3.6) and they are defined according to norms (fraction $\frac{f_i}{h_i}$).

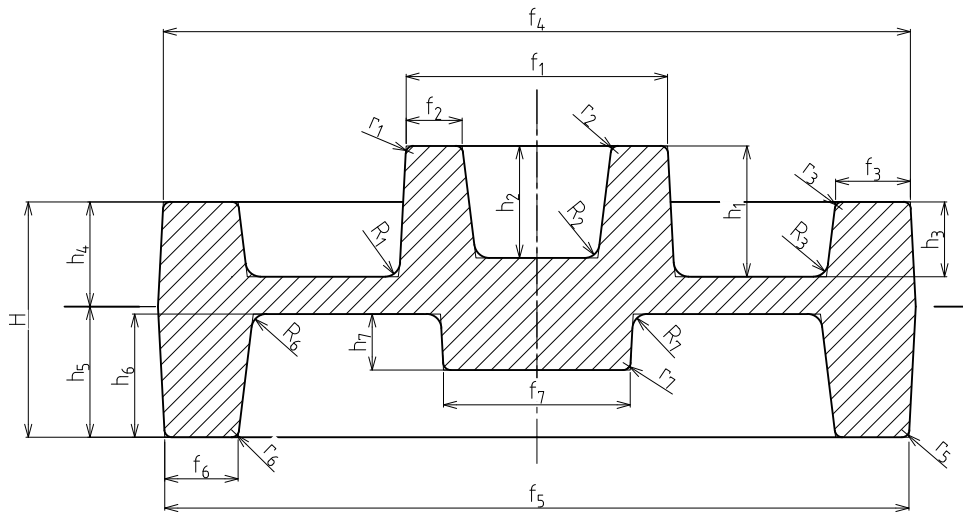


Fig. 3.6: Forging fillet radii [13]

³⁰Size of drafts can be reduced using ejectors (usually in a form of pins) which eject the forging out of a die cavity.

The next speciality of the closed die forging is a fact it is not possible to forge through holes in parts. It is possible only to "preforge" a hole (see Fig. 3.7), this means to create a counterbore with given diameter and depth. In case a membrane³¹ is thin enough, it is possible to trim it through (see further), otherwise it' is removed with machining.

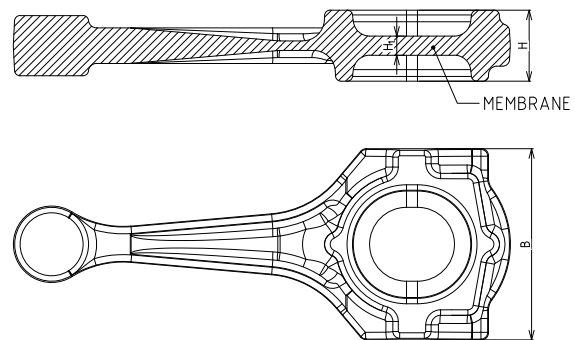


Fig. 3.7: Preforged hole

As previously said, the formed metal shrinks because of cooling. For this reason, the die cavity has to be scaled to gain correct dimensions of the produced part.³²

Input Material for Closed Die Forging

As the input material hot rolled rods³³ are used, mostly with a circular cross section, less then with a square or rectangle one. Profiles are delivered in big lengths, therefore is needed to divide the rod into required lengths.³⁴ This can be done using several methods:

1. Band saw cutting: dividing of the big cross section profiles, a principle is a linear displacement of a band with teeth.
2. Bar shear: waste-less rod dividing, based on damage due to shear between a punch and a fixed blade. This method is limited by a load capacity of a machine to be able to create stress state leading to the bar partitioning. In case of bigger cross sections, it is useful to shear at a higher temperature (up to 500 °C) for decreasing required shear forces .
3. Oxygen cutting, plasma cutting, waterjet etc.

³¹A remaining layer of metal under preforged hole

³²For carbon steels is stated a scale ratio 1.015 – 1.03.

³³Eventually cold drawn rods.

³⁴The usual rod length is {3;6} m.

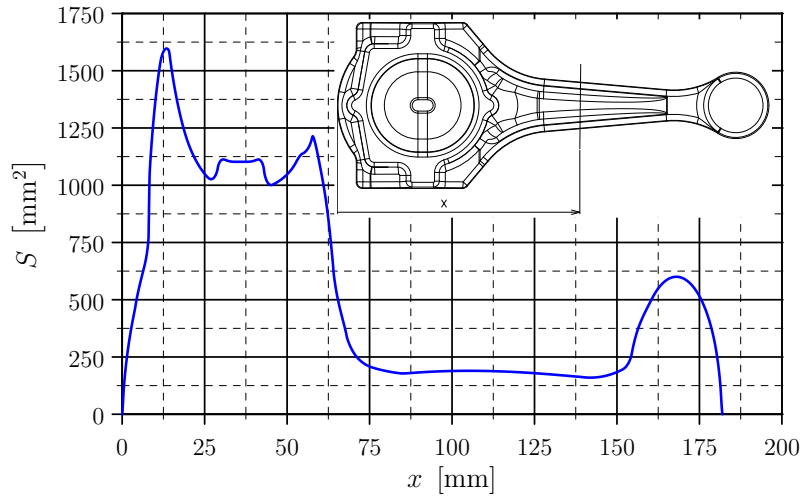


Fig. 3.8: Cross section diagram

After getting a piece of rod its extension and the cross section reduction may be needed. Cross section can be very variable (see Fig. 3.8). There exist several methods how to extend the rods.

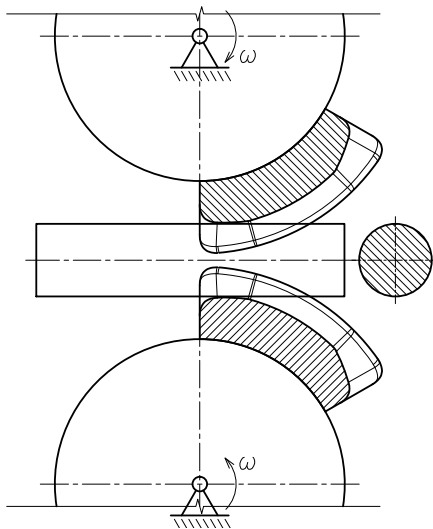


Fig. 3.9: Roll-forging scheme

Open die forging is the least productive and has high work requirements. It is used rarely. It works at a principle of repeated hits by flat or shaped dies perpendicularly to a rod axis (see Fig. 3.3a).

Roll forging works at a principle of two parallel cylinders rotating an angular velocity ω in the opposite direction, where a rod axis does not intersect any cylinder axis (see Fig. 3.9). Into cylinders cavities the rolled piece shape is onto a circle "winded". In most cases it is not possible to create the rolled part at once and that is the reason to partition rolling into several operations,

mostly 3 – 6. The cavity shape is usually oval or quadrilateral, the maximum reduction occurs in a case the shapes are swapped periodically.

Cross wedge rolling as the roll forging works at the principle of two parallel cylinders, but rotating in the same direction in this case. A rolled part is inserted between cylinders, where its axis is parallel with theirs and rotates in the opposite direction than cylinders (see Fig. 3.10). A tool's working part has a shape of a cutting edge winded up to the cylinder in a helix. From the mentioned descriptions it is visible it is possible to create only rotary shapes. Moreover, the whole shape has to be finished during *one* revolve and the rolled part should leave a working space itself. The parts rolled by this method may be used also as final products for machining, e.g. pins, shafts etc. (see Fig. 3.16d).

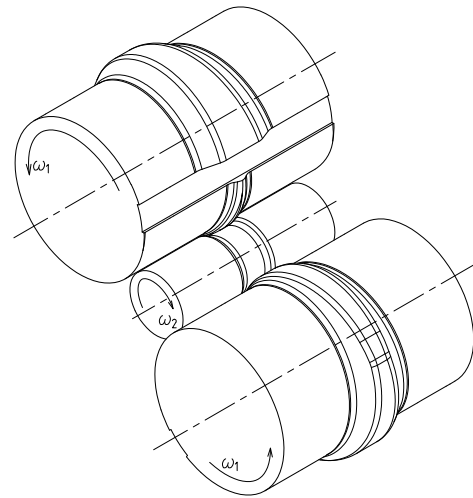


Fig. 3.10: Cross wedge rolling scheme

Drop Hammer Forging

Drop hammers are machines, where a kinetic energy of a ram in a form of an impact is used. An amount of the energy is a machine's parameter. There exist more kinds of hammers:

1. Single acting: there is used only the ram's own weight, where the die's upper part is situated. The bottom part is situated in an anvil.
2. Double-acting: the principle is similar to the single acting drop hammer, moreover, the ram is accelerated by a pneumatic system.
3. "Counter-running": the both parts of the die are moving, these are suitable for larger forgings, where the higher energy is required.

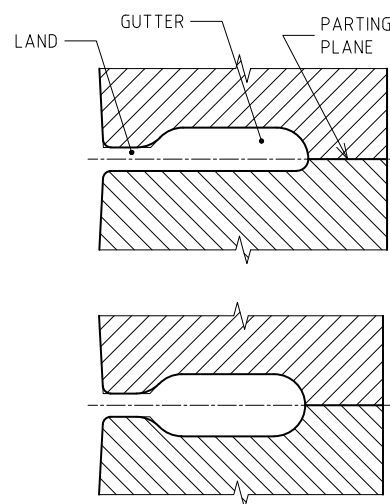


Fig. 3.11: Flash gutters for drop hammers [8, 15]

The forging is shaped in several strokes, where the required energy for next forming is increased with each stroke. This is the reason, why there has to be calculated the energy required for the *last* stroke to choose a drop hammer. There are empirically derived relations for its estimation (e.g. (3.1) and (3.2a) according to ČSN 22 8308), but these are only an approximation, so there is needed to have some backup. On the other hand there is not recommended to use the drop hammer with an unnecessarily high amount of energy to reduce wear on the dies. A surplus energy is absorbed by surfaces in the parting plane. The flash gutter in completely closed (see Fig. 3.11). For the axisymmetric forging, the relation for the estimation of energy required for the last stroke applies

$$W = 18 \left(1 - 0.005 D_f \right) \left(1.1 + \frac{2}{D_f} \right)^2 \left(0.75 + 0.001 D_f^2 \right) D_f \sigma_s, \quad (3.1)$$

where:

- D_f [cm] is the biggest diameter of the forging and
- σ_s [MPa] is a natural forming resistance at the finishing temperature [14, 9].³⁵

For a non-circular forging, a similar expression applies

$$W_n = W \left(1 + 0.1 \frac{L_D}{B_m} \right), \quad (3.2a)$$

$$D_{eq} = 1.13 \sqrt{F_D}, \quad (3.2b)$$

$$B_m = \frac{F_D}{L_D}, \quad (3.2c)$$

where:

- W [J] is a work evaluated according to Eq. (3.1) with $D_f = D_{eq}$ from Eq. (3.2b) (equivalent diameter),
- L_D [cm] is a forging's maximum length,
- F_D [cm²] is a forging's area projected into the direction of the stroke,
- B_m [cm] is a mean forging's height according to Eq. (3.2c) [14, 9].

³⁵The variables are necessarily to be put in stated units, there is not possible to use basic SI units. Work W is in J.

Vertical Crank Press Forging

In comparison to the drop hammers, a main parameter of a crank press is a forming force. There is used kinematics of a crank mechanism (see Fig. 3.12), which has a given trajectory by its components. In consequence of this property it is possible to perform *just one* operation per one working stroke. The next difference from the drop hammer is the shape of the flash gutter. In comparison to the drop hammers, the upper and bottom parts of the die are not in a contact and there is always preserved some clearance, which is given by a land height. Some shapes of the flash gutter are displayed in Fig. 3.13.

Similarly to the drop hammer, where the maximal energy has to be determined, for the crank press the maximal force has to be specified. There were developed some approaches for its calculation, one of them is normalised and described in the norm ČSN 22 8306 for the axisymmetric and non-circular forgings. The crank presses of this type are produced in a force capacity from units up to tens of MN.

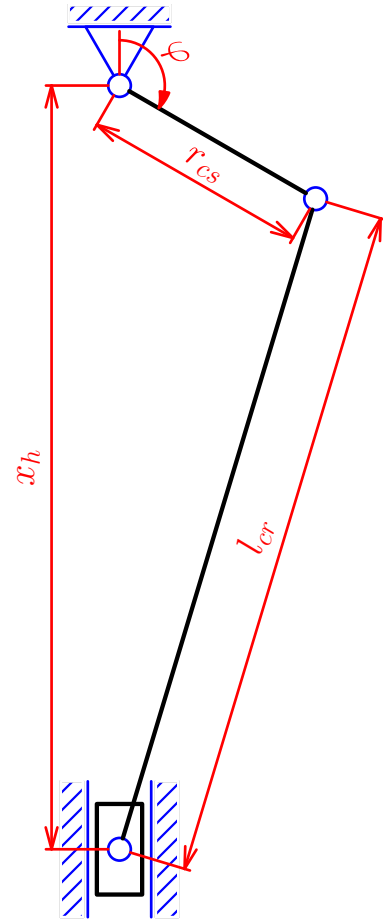


Fig. 3.12: Crank mechanism scheme

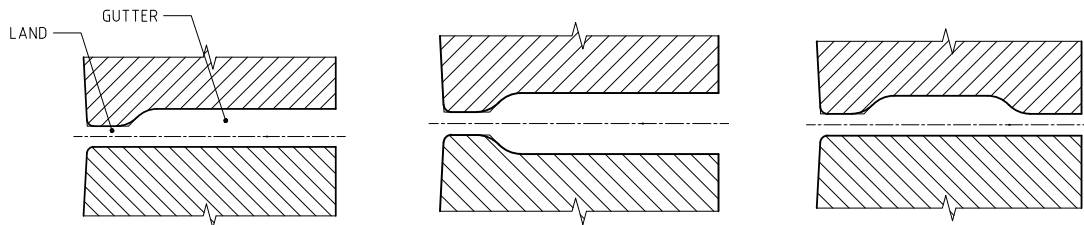


Fig. 3.13: Flash gutters for vertical crank presses [8, 16]

As it was said, a crank mechanism has a given kinematics according to its components. Kinematic quantities of a piston are given by formulas

$$x_h(\varphi) = -r_{cs} \cos \varphi + \sqrt{l_{cr}^2 - r_{cs}^2 \sin^2 \varphi}, \quad (3.3a)$$

$$\dot{x}_h(\varphi) = \frac{dx_h}{dt} = r_{cs} \dot{\varphi} \sin \varphi - \frac{r_{cs}^2 \dot{\varphi} \sin(2\varphi)}{2\sqrt{l_{cr}^2 - r_{cs}^2 \sin^2 \varphi}}, \quad (3.3b)$$

$$\ddot{x}_h(\varphi) = \frac{d^2x_h}{dt^2} = r_{cs} (\dot{\varphi}^2 \cos \varphi + \ddot{\varphi} \sin \varphi) - \frac{r_{cs}^2}{4\sqrt{l_{cr}^2 - r_{cs}^2 \sin^2 \varphi}} \left(4\dot{\varphi}^2 \cos(2\varphi) + \sin(2\varphi) \left[2\ddot{\varphi} + \frac{r_{cs}^2 \dot{\varphi}^2 \sin(2\varphi)}{l_{cr}^2 - r_{cs}^2 \sin^2 \varphi} \right] \right), \quad (3.3c)$$

where:

- r_{cs} [m] is a crank radius,
- l_{cr} [m] is a length of a connecting rod and
- φ [rad] is a crankshaft angle of rotation and
- t [s] is a time.

The crankshaft of the press revolves with a constant angular velocity ω [rad \perp s], so the angle of rotation is a linear function of the time $\varphi(t) = \omega t$. The kinematic quantities can be transformed to an expression

$$x_h(t) = -r_{cs} \cos(\omega t) + \sqrt{l_{cr}^2 - r_{cs}^2 \sin^2(\omega t)}, \quad (3.4a)$$

$$\dot{x}_h(t) = r_{cs} \omega \sin(\omega t) - \frac{r_{cs}^2 \omega \sin(2\omega t)}{2\sqrt{l_{cr}^2 - r_{cs}^2 \sin^2(\omega t)}}, \quad (3.4b)$$

$$\ddot{x}_h(t) = r_{cs} \omega^2 \cos(\omega t) - \frac{r_{cs}^2 \omega^2}{4\sqrt{l_{cr}^2 - r_{cs}^2 \sin^2(\omega t)}} \left(4 \cos(2\omega t) + \frac{r_{cs}^2 \sin^2(2\omega t)}{l_{cr}^2 - r_{cs}^2 \sin^2(\omega t)} \right). \quad (3.4c)$$

A mentioned model does not consider any eccentricity.³⁶

³⁶The piston's axis can be shifted out of a centre of mass perpendicularly to a movement direction or the crankshaft and the piston can be shifted from each other in the way the axes of the crankshaft, the piston and the movement direction are not in the same plane.

Trimming in The Forging Technology

As previously said, in the closed die forging the flash created from the redundant material flowing out of the die cavity is formed and is needed to be removed after finishing. This is carried out by using a special trimming tool that is copying an outer contour of the forging. The forging is laid on the trimming tool³⁷ and struck by using a punch. The trimmed forging fall through and the flash stays laying on the trimming tool (see Fig. 3.14).

There can be trimmed also the membrane of the pre-forged hole, if it is possible according to its thickness. In that case trimming is often partitioned into several operations, because the forgings are often complex in the shape.

The trimming is most often performed immediately after the forging finishing, because there are needed much less shear forces.

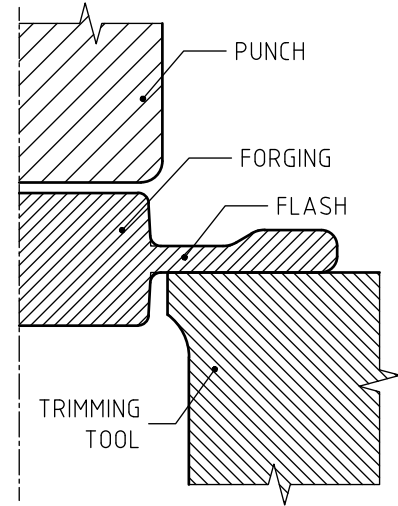


Fig. 3.14: Flash trimming

3.4 Forging Process Simulation Possibilities

Forge[®] NxT is a software developed by a French company TRANSVALOR. It enables to simulate processes of a hot and a cold forming, heat treatment processes etc. through the FEM. It involves a package of prepared libraries for load settings (drop hammer/press), contacts (friction coefficients) and mechanical properties of specific materials (mostly steels). There is used Hansel-Spittel flow curve to describe a strain hardening, expressed by the equation for a yield stress σ_y

$$\sigma_y = A_h T^{m_9} \exp \left(m_1 T + \frac{m_4}{\bar{\epsilon}_p} + m_7 \bar{\epsilon}_p \right) \bar{\epsilon}_p^{m_2} (1 + \bar{\epsilon}_p)^{m_5 T} \bar{\epsilon}_p^{m_3 + m_8 T}, \quad (3.5)$$

where:

- A_h [MPa] is a material constant,
- $m_i, i = \{1, \dots, 9\}$ [-] are material constants,

³⁷Tool storage surface has to be adapted according to the flash shape.

- T [°C] is a actual temperature of the material and
- $\bar{\varepsilon}_p$ [–] is an equivalent plastic strain (see furtherer).

There is omitted an elastic strain component.³⁸ For 3D analysis a tetrahedral mesh is only used and there can be used adaptive meshing during the simulation. For more information see a website <http://www.transvalor.com/en/cmspages/forge-nxt.32.html>.

QForm 3D was created by QuantorForm Ltd. company from the Russian Federation. It enables to solve same types of task as the program Forge described above. For more information see a website <http://www.qform3d.com/>.

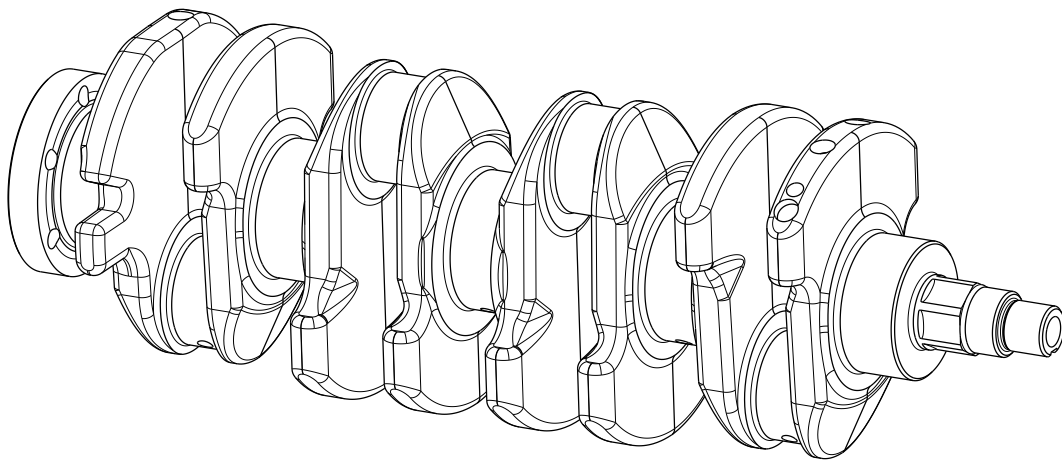
FormFEM is a software developed by ITA s.r.o. company from Ostrava in the Czech Republic. It enables to solve forming task through the finite element method. In comparison with programs above there is possible to solve only axisymmetric and plane strain tasks, so its using is strongly limited, because the forgings have usually the complex shape. For more information see a website <http://www.ita-tech.cz/cs/produkty-a-sluzby/pocitacove-simulace-mkp/objemove-tvareni>.

Simufact Forming is a software developed by an American company MSC Software Corp., which has developed a very successful program MSC Nastran for solving problems through the finite element method. It enables to solve various forming operations (rolling, forging, bending etc.), the heat treatment processes and more. It includes an implicit and explicit solver type. For more information see a website <https://www.simufact.com/simufactforming-forming-simulation.html>.

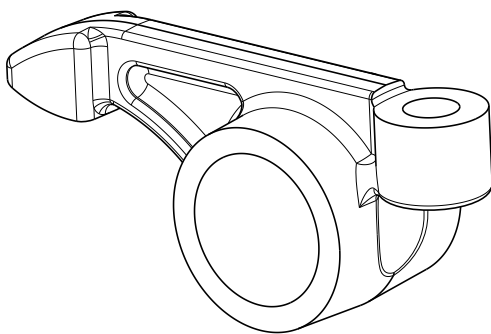
³⁸The elastic strain component is in the order of up to 10^{-2} , but the plastic strain is often in the order of 10^{-1} up to 10^0 .

3.5 Mechanical Parts

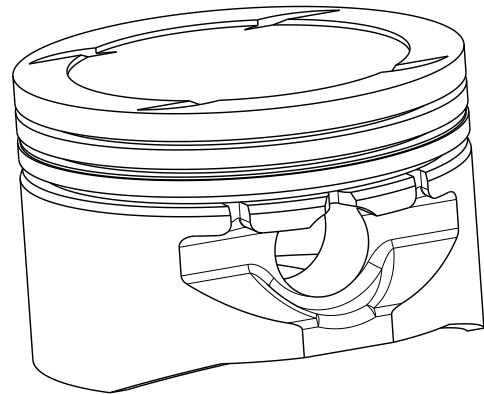
Forged mechanical parts have, in comparison with the machined ones, better mechanical properties, mainly in a strength aspect. This is a reason for using them in areas where high bearing capacity is needed (e.g. hooks for train assemblies, roller bearings rings) or where the part is under a dynamic load and resistance against fatigue damage is needed (crankshafts³⁹, gears⁴⁰). Forged mechanical parts examples are shown in Fig. 3.15a up to 3.16d (all parts are displayed after machining).



(a) Combustion engine crankshaft



(b) Combustion engine rocker

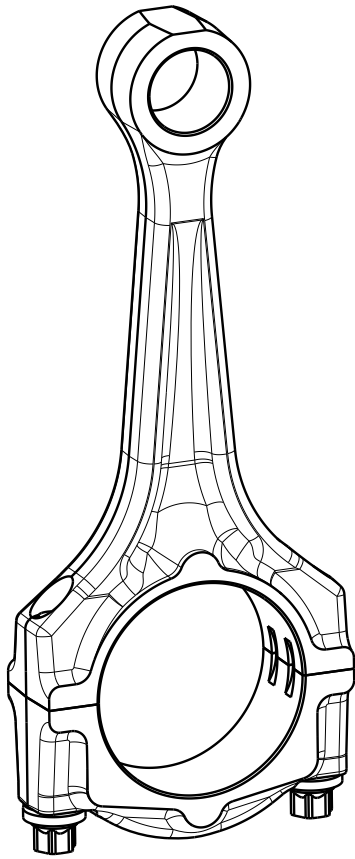


(c) Combustion engine piston

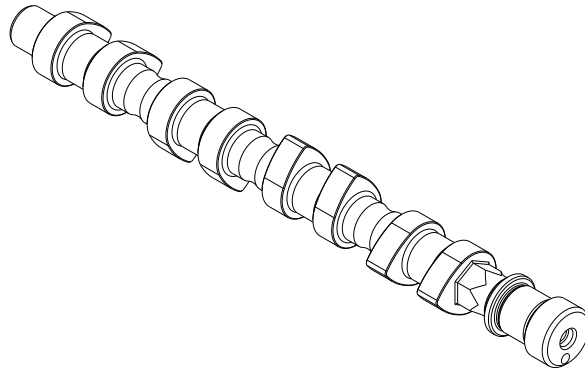
Fig. 3.15: Forged parts examples 1

³⁹A crankshaft is stressed with rotating bending and with often variable torque shear.

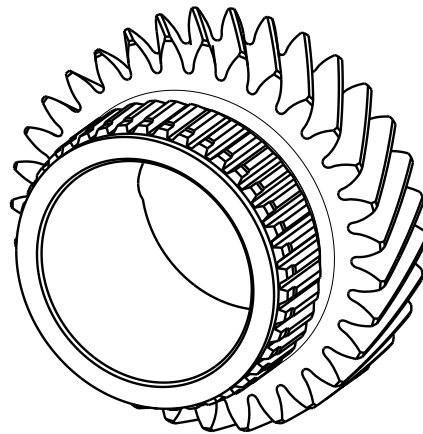
⁴⁰A gear tooth is stressed with alternating bending in tooth's root and with contact stress in tooth's side curve.



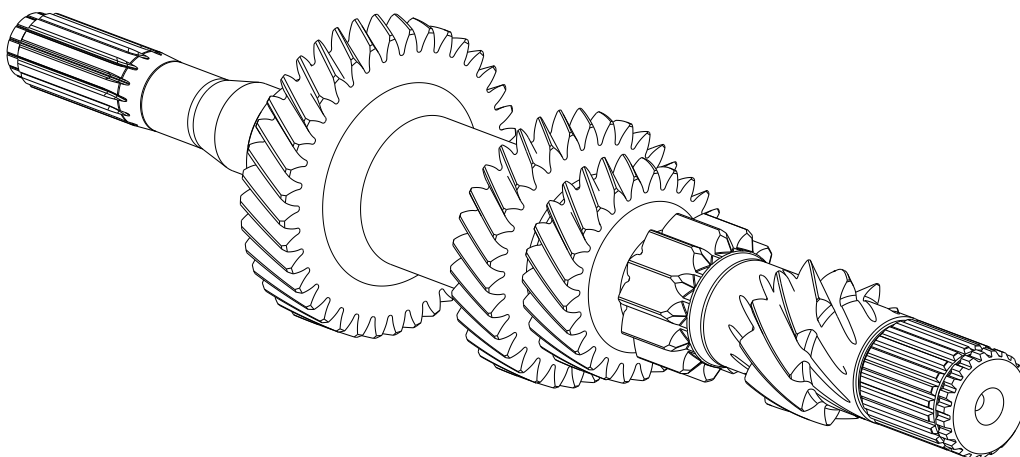
(a) Combustion engine connecting rod



(b) Combustion engine camshaft



(c) Gear



(d) Gearbox maindrive shaft

Fig. 3.16: Forged parts examples 2

4 Constitutive Laws and Material Characteristics

4.1 Elastic Material Behaviour

As previously said, a material's elastic model is linear isotropic defined with a Young's modulus E and a Poisson's ratio ν , where both depend on the temperature (see Fig. 4.1). A relation between stress components and deformation (strain) components is defined by a generalised Hooke's law (here for the isotropic material), which can be expressed in a Voight's notation as

$$\sigma_{ij} = \lambda_l \delta_{ij} \varepsilon_{kk_e} + 2G \varepsilon_{ij_e}, \quad (4.1)$$

where:

- λ_l [Pa] is a Lamé's constant,
- $\delta_{ij} = \begin{cases} 1 & \text{pro } i = j \\ 0 & \text{pro } i \neq j \end{cases}$ [-] is a Kronecker delta,
- ε_{kk_e} [-] is a *elastic* strain tensor ε_e first invariant⁴¹,
- G [Pa] is a shear modulus,
- ε_{ij_e} [-] are *elastic* strain tensor components [17].

The parameters in the relation (4.1) can be expressed for the isotropic material by Eq. (4.2a) and (4.2b) [17].

$$\lambda_l = \frac{E\nu}{(1-2\nu)(1+\nu)} \quad (4.2a)$$

$$G = \frac{E}{2(1+\nu)} \quad (4.2b)$$

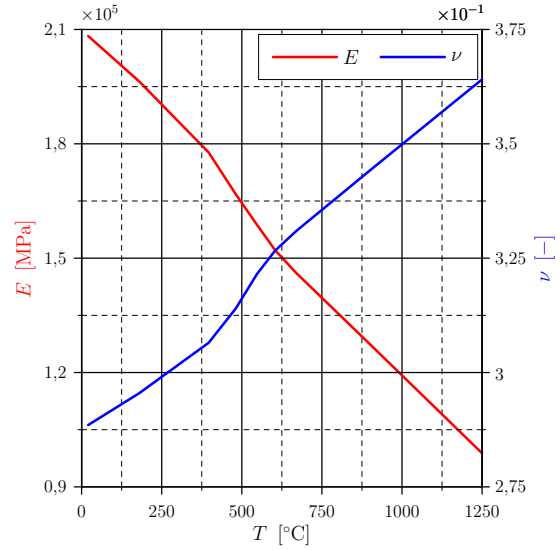


Fig. 4.1: Elastic parameters of the linear isotropic material

⁴¹It expresses a volume change during the deformation.

4.2 Plastic Material Behaviour

4.2.1 Yield Conditions, Operations with Tensors

There has to be determined a criterion, which is used to decide, if the plastic strain increases or not. This criterion is called a yield *condition*, which can be expressed mathematically as

$$\Phi(\sigma_{eq}, \sigma_y(\bar{\varepsilon}_p, T, \dot{\bar{\varepsilon}}_p, \dots)) = 0, \quad (4.3)$$

where:

- Φ is a yield *function*,
- σ_{eq} [Pa] is an equivalent stress and
- σ_y [Pa] is an *actual* yield stress, described by a flow curve (see Sec. 4.2.3), and it can depend on several parameters, e.g. an equivalent plastic strain $\bar{\varepsilon}_p$, an equivalent plastic strain rate $\dot{\bar{\varepsilon}}_p$, a temperature T etc. [18].

There is very often used von Mises (HMH⁴²) yield condition expressed as

$$\Phi = \sigma_{eq} - \sigma_y = 0, \quad (4.4)$$

and can be displayed in Haigh-Westergaard space as a cylindrical surface according to Fig. 4.2. This yield condition belongs to a group of isotropic yield conditions. The yield surface can be described by using 3 stress invariants p , q , r (see further) [6]. All formulas for the equivalent stress and the equivalent plastic strain apply to von Mises yield condition. The equivalent stress is further denoted as $\bar{\sigma}$.

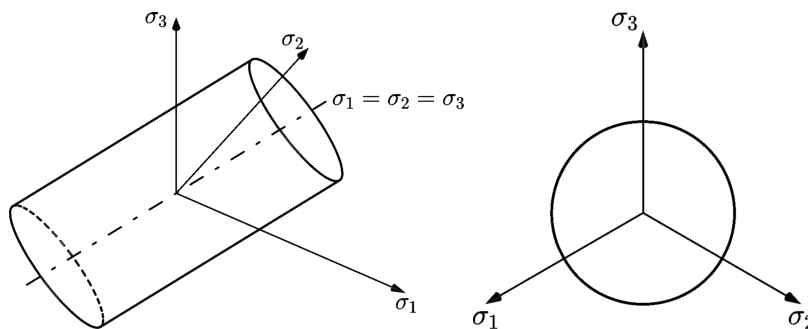


Fig. 4.2: von Mises yield surface [18]

⁴²Huber-Mises-Hencky.

But there has to be distinguished an *actual* equivalent plastic strain calculated from an actual plastic strain tensor $\boldsymbol{\varepsilon}_p$ (see Eq. (4.5)) and a *cumulative* equivalent plastic strain calculated according to Eq. (4.11), which still increases its value during load.

$$\boldsymbol{\varepsilon}_p = \begin{bmatrix} \varepsilon_{11p} & \varepsilon_{12p} & \varepsilon_{13p} \\ \varepsilon_{21p} & \varepsilon_{22p} & \varepsilon_{23p} \\ \varepsilon_{31p} & \varepsilon_{32p} & \varepsilon_{33p} \end{bmatrix} \quad (4.5)$$

The *actual* equivalent plastic strain is given by Eq. (4.6)

$$\bar{\varepsilon}_{p_a} = \sqrt{\frac{2}{3} (\mathcal{D}\boldsymbol{\varepsilon}_p : \mathcal{D}\boldsymbol{\varepsilon}_p)}, \quad (4.6)$$

where $\mathcal{D}\boldsymbol{\varepsilon}_p$ is a deviatoric component of a plastic strain tensor described by the formula

$$\mathcal{D}\boldsymbol{\varepsilon}_p = \boldsymbol{\varepsilon}_p - \frac{\boldsymbol{\varepsilon}_p : \mathbf{I}}{3} \mathbf{I}, \quad (4.7)$$

where \mathbf{I} is a second order identity tensor [1]. Because there is no volume change caused by the plastic strain, $\boldsymbol{\varepsilon}_p : \mathbf{I} = 0$ applies and the deviatoric component of the plastic strain tensor is the tensor itself. For the case of the plastic strain, there are not distinguished the tensor and its deviatoric component in this thesis anymore.

For an explanation it is necessary to describe the meaning of an operator ":" in Eq. (4.6). This operator is called "Double Dot Product" and it represents an operation expressed by Eq. (4.8) between 2 matrices of the same dimensions, its result is a scalar

$$a = \mathbf{A} : \mathbf{B} = \sum_{i=1}^m \sum_{j=1}^n A_{ij} B_{ij}, \quad (4.8)$$

where \mathbf{A} a \mathbf{B} are matrices with a size $m \times n$. Eq. (4.6) can be modified for plastic strain tensor components (see Eq. (4.5)) as

$$\bar{\varepsilon}_{p_a} = \frac{\sqrt{2}}{3} \sqrt{\frac{(\varepsilon_{ii_p} - \varepsilon_{jj_p})^2 + 6\varepsilon_{ij_p}^2(1 - \delta_{ij})}{2}}. \quad (4.9)$$

Eq. (4.9) can be expressed for principal plastic strain applying to a relation $\varepsilon_{1p} \geq \varepsilon_{2p} \geq \varepsilon_{3p}$ [-] as

$$\bar{\varepsilon}_{p_a} = \frac{\sqrt{2}}{3} \sqrt{\frac{(\varepsilon_{ip} - \varepsilon_{jp})^2}{2}} [1]. \quad (4.10)$$

The *cumulative* equivalent plastic strain is evaluated according to Eq. (4.11)

$$\bar{\varepsilon}_{pc} = \int_0^{t_a} \sqrt{\frac{2}{3} (\dot{\varepsilon}_p : \dot{\varepsilon}_p)} dt, \quad (4.11)$$

where:

- $\dot{\varepsilon}_p$ [s⁻¹] is a plastic strain *rate* tensor and
- t_a [s] is an analysis duration [1, 6].

According to Abaqus manual there is used *cumulative* equivalent plastic strain in models of plasticity [6] and this equivalent plastic strain is further denoted as $\bar{\varepsilon}_p$.

4.2.2 Implementation of Plasticity to FEM

With a plastic straining an energy dissipation is connected. This means the system is not conservative.⁴³ The main attribute of the conservative systems is the fact, line integrals are path independent and they depend only on an initial and a final position.

This doesn't apply to elasto-plastic task, where the final state depends on all previous ones, this means on the whole straining history.⁴⁴ That is why the plasticity in FEM is implemented in its incremental (integral) form, where a new stress state is determined as

$$\boldsymbol{\sigma}^{t+\Delta t} = \boldsymbol{\sigma}^t + \Delta\boldsymbol{\sigma}(\Delta\varepsilon_e), \quad (4.12)$$

where:

- $\boldsymbol{\sigma}^t$ [Pa] is a previous stress state and
- $\Delta\boldsymbol{\sigma}$ [Pa] is a stress increment which depends on an elastic strain increment $\Delta\varepsilon_e$ [6].⁴⁵

⁴³A conservative system a type of system where an inserted energy/work into a system is totally given back.

⁴⁴A straining path is in general a curve in the Haigh-Westergaard principal stress coordinate system.

⁴⁵There exists also a deformation plasticity theory which enables to formulate finite relations between a stress tensor and a strain tensor with a presumption that a straining path in the Haigh-Westergaard principal stress coordinate system is a straight line (proportional straining), so quantities characterizing stress state do not change (a stress triaxiality and a Lode angle, see Sec. 4.3).

This approach is based on a predictor-corrector principle. A prediction is based on a presumption the strain increment $\boldsymbol{\varepsilon}$ gained from displacements is pure elastic and, based on this hypothesis, a trial stress tensor according to the Hooke's law (see Eq. (4.1) on p. 43) is evaluated. The equivalent stress is calculated from the trial stress (see further). If the yield condition is fulfilled (see Eq. (4.2) on p. 44), the strain increment includes a plastic component. Except the yield condition there has to be also stated a flow rule bounding the plastic strain increment and the stress increment

$$\Delta\varepsilon_{ijp} = \Delta\lambda_p \frac{\partial Q_p}{\partial \sigma_{ij}}, \quad (4.13)$$

where:

- $\Delta\lambda_p$ [-] is a plastic multiplier and
- Q_p [$\frac{\text{J}}{\text{m}^3}$] is a yield functional, usually identified with the yield function Φ [18, 6].⁴⁶

In case of an associated flow rule, a derivative of the yield functional is a von Mises yield surface normal \mathbf{n}

$$\mathbf{n} = \frac{3}{2} \frac{\mathcal{D}\boldsymbol{\sigma}}{q}, \quad (4.14a)$$

$$\mathcal{D}\boldsymbol{\sigma} = \boldsymbol{\sigma} + p\mathbf{I}, \quad (4.14b)$$

$$p = -\frac{1}{3} \underbrace{(\boldsymbol{\sigma} : \mathbf{I})}_{=I_1} = -\frac{\sigma_{kk}}{3}, \quad (4.14c)$$

$$q = \bar{\sigma} = \underbrace{\sqrt{\frac{3}{2} (\mathcal{D}\boldsymbol{\sigma} : \mathcal{D}\boldsymbol{\sigma})}}_{=\sqrt{3}J_2} = \frac{\sqrt{2}}{2} \sqrt{\frac{(\sigma_{ii} - \sigma_{jj})^2 + 6\sigma_{ij}^2(1 - \delta_{ij})}{2}}, \quad (4.14d)$$

where:

- p [Pa] is a hydrostatic pressure and
- $\mathcal{D}\boldsymbol{\sigma}$ [Pa] is a deviatoric component of the Cauchy stress tensor [1, 6].⁴⁷

⁴⁶Then is the flow rule called as associative.

⁴⁷A member $p\mathbf{I}$ in Eq. (4.14b) is volumetric (hydrostatic) component of the stress tensor and it is related to a material's volume change. The deviatoric component is related to a shape change. In the Abaqus manual [6], the deviatoric stress tensor component is denoted as \mathbf{S} .

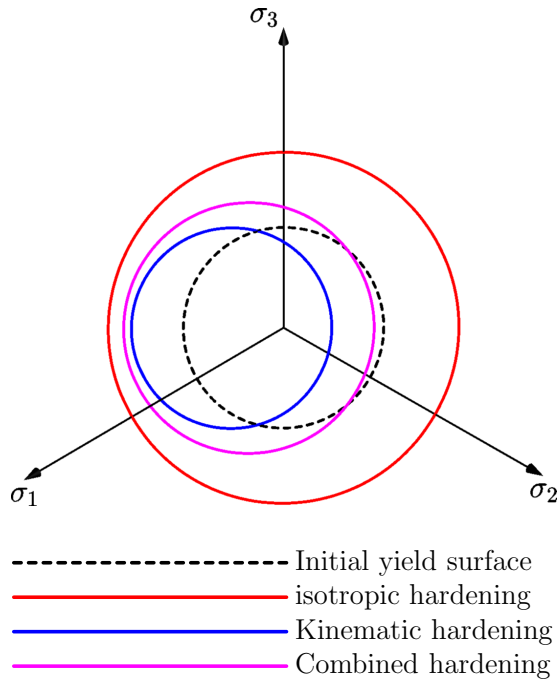


Fig. 4.3: Hardening types [18]

The plastic multiplier is identified with the equivalent plastic strain increment $\bar{\varepsilon}_p$ in the case of the von Mises yield condition and is evaluated as

$$\Delta \bar{\varepsilon}_p = \frac{\bar{\sigma}^* - \sigma_y^t}{3G + H}, \quad (4.15a)$$

$$H = \frac{\partial \bar{\sigma}}{\partial \bar{\varepsilon}_p}, \quad (4.15b)$$

where:

- $\bar{\sigma}^*$ [Pa] is the equivalent stress from the trial stress,
- σ_y^t [Pa] is the yield stress according to the actual equivalent plastic strain and
- H [Pa] is a flow curve slope (see further) [6].

The final step is to correct the stress increment according to

$$\Delta \boldsymbol{\sigma} = \lambda_l \left[\underbrace{(\Delta \boldsymbol{\varepsilon} - \Delta \boldsymbol{\varepsilon}_p)}_{=\Delta \boldsymbol{\varepsilon}_e} : \mathbf{I} \right] \mathbf{I} + 2G(\Delta \boldsymbol{\varepsilon} - \Delta \boldsymbol{\varepsilon}_p). \quad (4.16)$$

4.2.3 Flow curve (stress–strain curve)

In FEM programs, the stress–strain curve for the plastic material is assigned as a dependency of the *equivalent* stress $\bar{\sigma}$ on the *equivalent* plastic strain $\bar{\varepsilon}_p$. Material data are gained from a mechanical test, most often from a uni-axial tensile test. there is necessary to consider the output of the uni-axial tensile test is an engineering tensile diagram⁴⁸ (see Fig. 4.4). So it is necessary to perform a transformation to *true*⁴⁹ diagram by using formulas

$$e^{\text{true}} = \log(1 + e^{\text{eng}}), \quad s^{\text{true}} = s^{\text{eng}}(1 + e^{\text{eng}}) \text{ for } s \leq \sigma_u,$$

$$e^{\text{true}} = \log \frac{S_0}{S}, \quad s^{\text{true}} = s^{\text{eng}} \frac{S_0}{S} \text{ for } s > \sigma_u.$$

For the second case, it is necessary to perform a correction because of a triaxial stress state and a stress concentration at the neck. S [m²] is an *actual* bar cross section, S_0 [m²] is an initial cross section and σ_u [Pa] is ultimate strength stress.⁵⁰

The material's plastic behaviour can be also influenced by other factors as a temperature, a strain rate, a stress state etc. There exist a lot of flow curve models, which are able to consider different influences on the plastic behaviour. On the other hand, a calibration of these models can be a bit tricky because of high costs or it is not possible to perform experiments to gain relevant data.

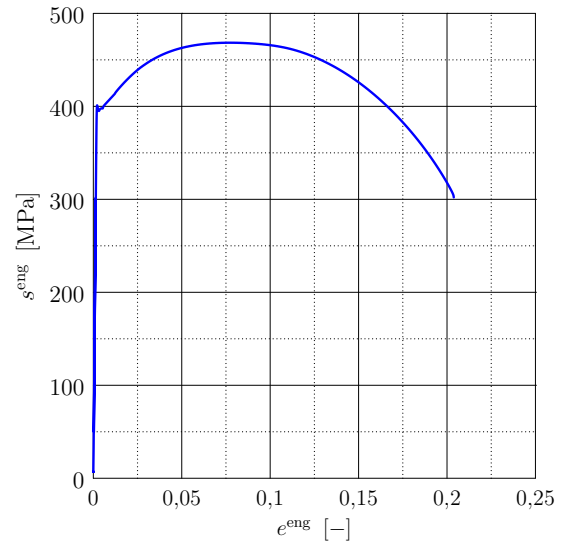


Fig. 4.4: Engineering tensile diagram

Because the closed-die forging is the focus of this thesis and it is also the high temperature bulk forming method, there has to be used a model of material, which is able to take into account the influence of the temperature. The non-negligible influence can also have a strain rate, because forging processes are usually fast.⁵¹

⁴⁸Stress is related to a *initial* cross section.

⁴⁹Stress related to a *actual* cross section

⁵⁰log is a natural logarithm (e base).

⁵¹A total shape change can be performed in the time of about 10^{-1} s.

One of the basic model able to take into account these effects is the Johnson-Cook flow curve with the isotropic hardening described by Eq. (4.17a), (4.17b) and (4.17c)

$$\bar{\sigma}(\bar{\varepsilon}_p, \dot{\varepsilon}_p^*, T^*) = (A_{jc} + B_{jc} \bar{\varepsilon}_p^{n_{jc}}) (1 + c_{jc} \log \dot{\varepsilon}_p^*) (1 - T^{*m_{jc}}), \quad (4.17a)$$

$$\dot{\varepsilon}_p^* = \frac{\dot{\varepsilon}_p}{\dot{\varepsilon}_{0p}}, \quad (4.17b)$$

$$T^* = \begin{cases} 0 & \text{for } T < T_r, \\ \frac{T-T_r}{T_m-T_r} & \text{for } T \in \langle T_r; T_m \rangle, \\ 1 & \text{for } T > T_m, \end{cases} \quad (4.17c)$$

where:

- A_{jc} ⁵², B_{jc} [Pa] are material constants,
- n_{jc} [–] is a strain hardening exponent,
- $\dot{\varepsilon}_p^*$ [–] is a dimensionless plastic strain rate (see Eq. (4.17b)),
- $\dot{\varepsilon}_p$ [s⁻¹] is a equivalent plastic strain rate,
- $\dot{\varepsilon}_{0p}$ [s⁻¹] is a reference equivalent plastic strain rate,
- c_{jc} [–] is a strain rate hardening exponent (coefficient),
- T^* [–] is a homological temperature (see Eq. (4.17c)),
- T [K] is an actual material's temperature,
- T_m [K] is a material's melting temperature,
- T_r [K] is a room temperature and
- m_{jc} [–] is a temperature softening exponent [6].

It is a function of three independent variables. Because there is not the projection $f : \mathbb{R}^3 \rightarrow \mathbb{R}$, it is possible to display the equivalent stress dependency only

⁵²It can be found out, that A_{jc} in Eq. (4.17a) is a yield strength of the material at the room temperature.

in two variables and one selected parameter. The consequence is, that it is a set of surfaces in the 3-D space (see Fig. 4.5).

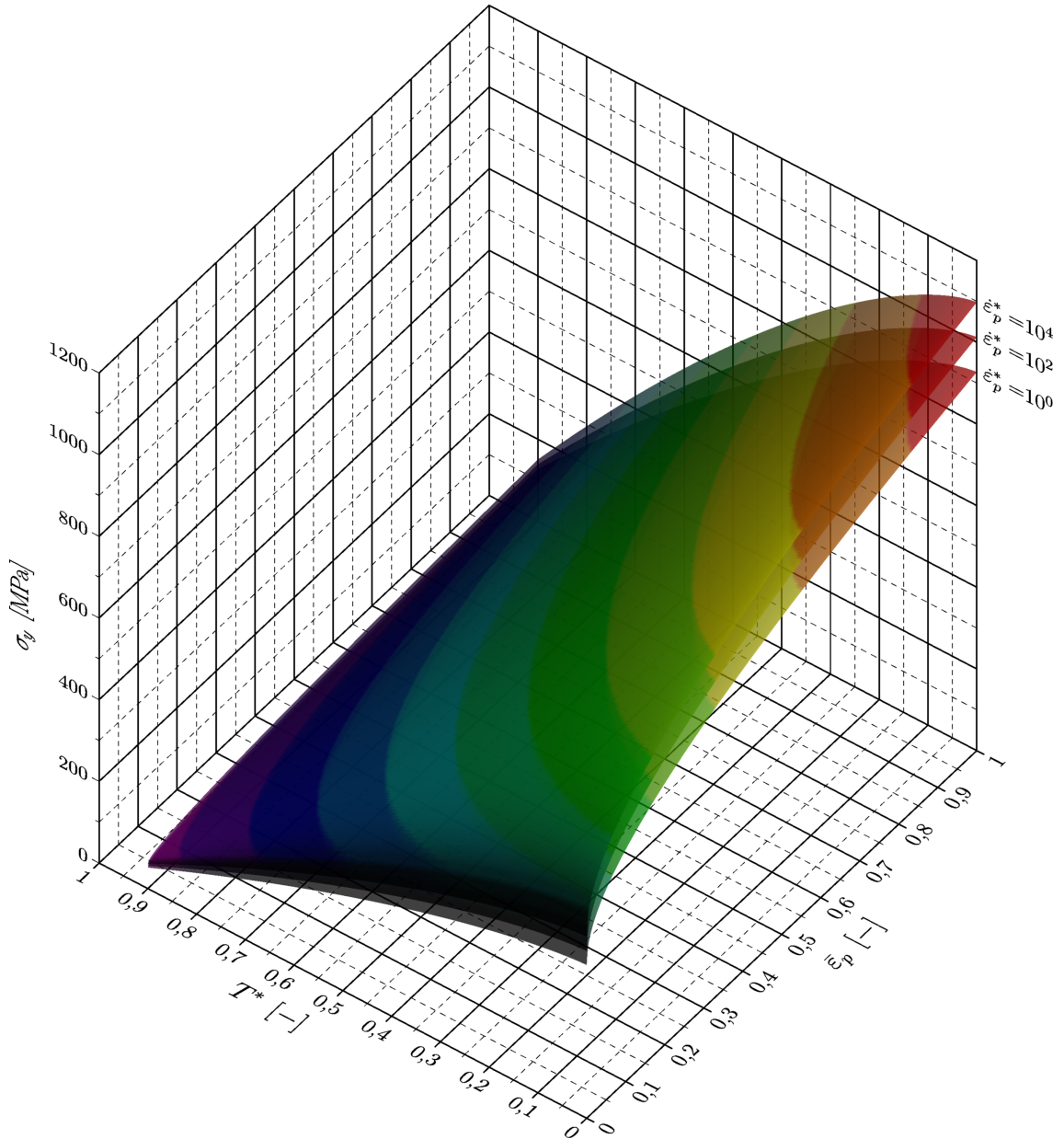


Fig. 4.5: Johnson-Cook yield stress surfaces

The temperature dependency is displayed in Fig. 4.6a and strain rate dependency in Fig. 4.6b. From the graphs it can be stated that the influence of the

temperature on material's properties is far much bigger than the influence of the strain rate.

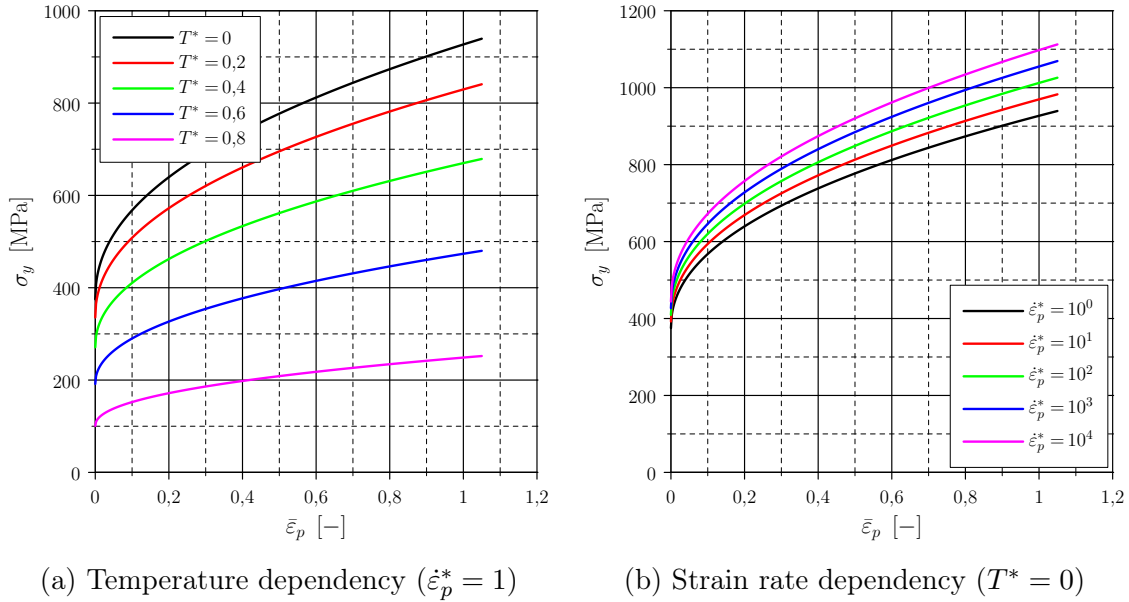


Fig. 4.6: Johnson-Cook flow curves

4.2.4 Plastic Strain Work to Heat Transformation

On the basis of experiments, it was found out that a part (fraction) of the plastic (inelastic) deformation energy is changed into heat. As shown earlier, the temperature increase leads to a change of material properties, which can have undesirable consequences. A heat generation due to a plastic deformation can be taken into account in a fully-coupled analysis⁵³, where the changed heat is estimated as the inelastic deformation energy multiplied with a multiplier called as inelastic heat fraction, usually in a form of a unit volume heat power [4]. The unit volume heat power can be estimated as

$$r_p = \eta_{ihf} (\boldsymbol{\sigma} : \dot{\boldsymbol{\varepsilon}}_p), \quad (4.18)$$

where η_{ihf} [-] is the inelastic heat fraction [6].⁵⁴ The unit volume heat power enters into a heat balance (see p. 59, 60).

⁵³The analysis, where a temperature field influences the deformation and conversely. The opposite is a partly-coupled analysis, where the deformation is influenced by the temperature field, not conversely.

⁵⁴The most used value is 0.9.

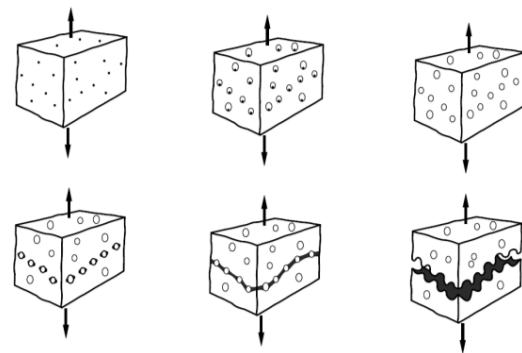
4.3 Ductile Damage

As previously said, the explicit FEM allows to provide a continuum damage analysis, crack initiation, its propagation etc. One of the most important variables influencing a ductile damage mechanisms is a stress triaxiality factor η defined by a relation

$$\eta = -\frac{p}{q}. \quad (4.19)$$

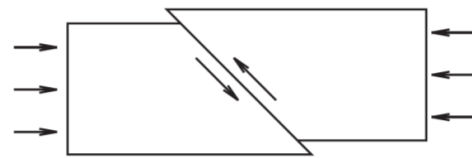
4.3.1 Ductile Damage Mechanisms

A **cavity mechanism** is based on an initiation of voids on an interface of the basic material and foreign phase particles which grow up during a load incrementation, they connect to each other (coalescence) and the consequence is a crack of a part (see Fig. 4.7a). It is typical for higher stress triaxiality values. A crack surface is rough with visible holes [1].



(a) Cavity

A **shear mechanism** is typical of low stress triaxiality regions. A crack initiation and its propagation performs in a maximal shear stress plane (see Fig. 4.7b). In comparison with the cavity mechanism the crack surface is smooth [1].



(b) Shear

Fig. 4.7: Ductile damage mechanisms [7, 1, 19]

4.3.2 Ductile Damage Criteria

The first criteria describing the ductile damage had only one variable and it was a stress triaxiality η . In last years it was found out that with using of experiment it is not possible to describe all stress states only with the stress triaxiality. That is why parameters like a Lode angle θ and derived variables, a Lode parameter μ and a normalized third invariant of the deviatoric stress tensor ξ have been defined

$$\theta = -\frac{1}{3} \arcsin \xi, \quad (4.20a)$$

$$\xi = \left(\frac{r}{q}\right)^3, \quad (4.20b)$$

$$r = \sqrt[3]{\frac{9}{2} [(\mathcal{D}\sigma \cdot \mathcal{D}\sigma) : \mathcal{D}\sigma]} = \underbrace{\sqrt[3]{\frac{27}{2} \det(\mathcal{D}\sigma)}}_{= \sqrt[3]{\frac{27}{2} J_3}}, \quad (4.20c)$$

$$\mu = \frac{2\sigma_2 - \sigma_1 - \sigma_3}{\sigma_1 - \sigma_3} = \sqrt{3} \tan\left(-\frac{1}{3} \arcsin \xi\right), \quad (4.20d)$$

where $\sigma_1 \geq \sigma_2 \geq \sigma_3$ [Pa] are principal stresses [1].⁵⁵ The Lode angle is often normalized to make its range exactly the same as for the Lode parameter μ or the normalized third invariant of the deviatoric stress tensor ξ according to the relation

$$\bar{\theta} = -\frac{6\theta}{\pi} = \frac{2}{\pi} \arcsin \xi \quad [1]. \quad (4.21)$$

The variables describe above are listed in Tab. 4.1 with its values ranges included.

Tab. 4.1: Variables ranges for ductile damage description

Variable	Sign	Range
Stress triaxiality	η	\mathbb{R}
Lode angle	θ	$\langle -\frac{\pi}{6}; \frac{\pi}{6} \rangle$
Normalized third invariant of the deviatoric stress tensor	ξ	$\langle -1; 1 \rangle$
Lode parameter	μ	
Normalized Lode angle	$\bar{\theta}$	

A fracture plastic strain criterion is the simplest criterion for the implementation, but its usage is strongly limited. Critical fracture strain $\bar{\varepsilon}_f$ is particularly smooth surface in a coordinate system $\eta - \bar{\varepsilon}_p$ set by discrete points. The element is deleted⁵⁶ when

⁵⁵ r [Pa] in Eq. (4.20c) is a third invariant of the deviatoric stress tensor, according to Abaqus.

⁵⁶The element deletion is a very widespread method for the crack initiation and propagation. The element's stiffness and the stress value is zero after deletion.

$$D_d = \int \frac{d\bar{\epsilon}_p}{\bar{\epsilon}_f(\eta, \dot{\epsilon}_p, T)} = 1 \quad [1, 6]. \quad (4.22)$$

A Johnson-Cook (J-C) criterion is a criterion, where the fracture strain $\bar{\epsilon}_f$ is expressed by the equation

$$\bar{\epsilon}_f(\eta, \dot{\epsilon}_p^*, T^*) = (D_1 + D_2 e^{-D_3 \eta}) (1 + D_4 \log \dot{\epsilon}_p^*) (1 + D_5 T^*), \quad (4.23)$$

where $D_{1, \dots, 5}$ are material constants. The element deletion is performed when

$$D_{jc} = \int \frac{d\bar{\epsilon}_p}{\bar{\epsilon}_f(\eta, \dot{\epsilon}_p^*, T^*)} = 1 \quad [1, 6]. \quad (4.24)$$

In comparison with the previous criterion, there is nothing new, but the fracture strain $\bar{\epsilon}_f$ is given by an equation, so there is some time saving.

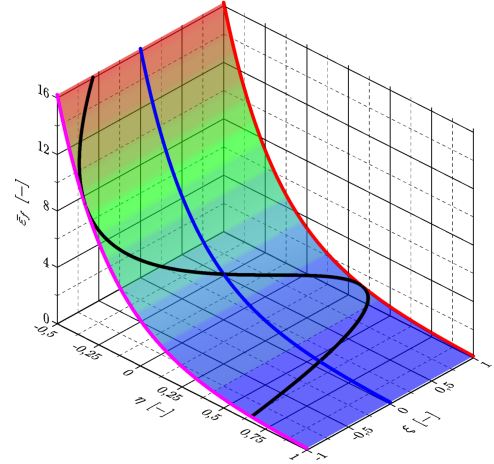


Fig. 4.8: Johnson-Cook criterion

A shear criterion is determined for cases the dominant stress character is the shear one. It is based on damage accumulation expressed by the equation

$$D_s = \int \frac{d\bar{\epsilon}_p}{\bar{\epsilon}_f(\theta_s, \dot{\epsilon}_p)}, \quad (4.25)$$

where θ_s [-] is a shear stress fraction given by the equation

$$\theta_s = \frac{q + k_s p}{\tau_{\max}}, \quad (4.26)$$

where:

- k_s [-] is a material parameter and
- τ_{\max} [Pa] is the maximal shear stress [6].

The element elimination is performed when

$$D_s = 1 \quad [6].$$

The criteria described above are available in user interface Abaqus CAE. In case of needs an implementation of a different criterion, a user has to create his own procedure (FORTRAN subroutine VUMAT⁵⁷) for the solution.⁵⁸ The other existing criteria are described now.

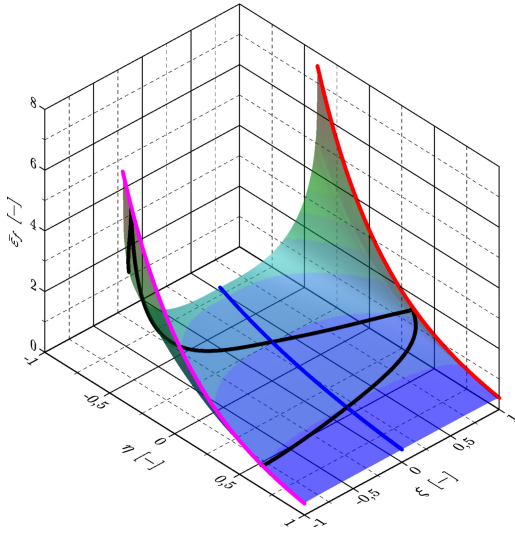


Fig. 4.9: Xue-Wierzbicki criterion

A Xue-Wierzbicki (X-W) criterion is one of the criteria, where the fracture strain is not only a function of the stress triaxiality η , but also of the normalized third invariant of the deviatoric stress tensor ξ . The fracture strain is given by the equation

$$\bar{\varepsilon}_f(\eta, \xi) = C_1 e^{-C_2 \eta} - (C_1 e^{-C_2 \eta} - C_3 e^{-C_4 \eta}) \left(1 - |\xi|^{\frac{1}{n_{sh}}}\right)^{n_{sh}}, \quad (4.27)$$

where:

- $C_{1,\dots,4}$ [-] are material constants and
- n_{sh} [-] is a strain hardening exponent [7].

The element deletion is performed when

$$D_{xw} = \int \frac{d\bar{\varepsilon}_p}{\bar{\varepsilon}_f(\eta, \xi)} = 1 \quad [7, 1]. \quad (4.28)$$

A Bai-Wierzbicki (B-W) criterion has, in comparison with X-W criterion, the normalized Lode angle $\bar{\theta}$ as the second variable. The fracture strain function is

$$\bar{\varepsilon}_f(\eta, \bar{\theta}) = \left(\frac{1}{2}N_1 e^{-N_2 \eta} + N_5 e^{-N_6 \eta} - N_3 e^{-N_4 \eta}\right) \bar{\theta}^2 + \frac{1}{2} (N_1 e^{-N_2 \eta} - N_5 e^{-N_6 \eta}) \bar{\theta} + N_3 e^{-N_4 \eta}, \quad (4.29)$$

⁵⁷Vectorised User MATerial

⁵⁸For the fracture plastic strain criterion (see previous page), it is possible to change the strain rate $\dot{\varepsilon}_p$ dependency to the normalised third invariant of the deviatoric stress tensor ξ by change in a *.inp file, this approach is not available in Abaqus CAE.

where $N_{1,\dots,6}$ are material constants [1]. The element deletion is performed when

$$D_{bw} = \int \frac{d\bar{\varepsilon}_p}{\bar{\varepsilon}_f(\eta, \theta)} = 1 \quad [1]. \quad (4.30)$$

KHPS⁵⁹ Criterion was designed by Ing. Petr Kubík, Ph.D. from the Institute of Solid Mechanics, Mechatronics and Biomechanics. This criterion involves also a cut-off region (region *without* damage cumulation) and its border is defined by a second order polynomial of ξ . The fracture strain is then given by formulas

$$\bar{\varepsilon}_f(\eta, \xi) = \frac{P_5}{\eta + h(\xi)} + \frac{P_4 - P_5}{\eta + h(\xi)} \frac{\xi + 1}{2}, \quad (4.31a)$$

$$h(\xi) = \left(P_3 + \frac{P_1 - P_3}{2} - P_2 \right) \xi^2 + \frac{P_1 - P_3}{2} \xi + P_2 \quad (4.31b)$$

where $P_{1,\dots,5}$ [-] are material constants. The element deletion is performed when

$$D_{khps} = \int dD_{khps} = 1, \quad (4.32a)$$

$$dD_{khps} = \begin{cases} \frac{d\bar{\varepsilon}_p}{\bar{\varepsilon}_f(\eta, \xi)} & \text{if } \eta + h(\xi) > 0, \\ 0 & \text{if } \eta + h(\xi) \leq 0 \quad [1, 20]. \end{cases} \quad (4.32b)$$

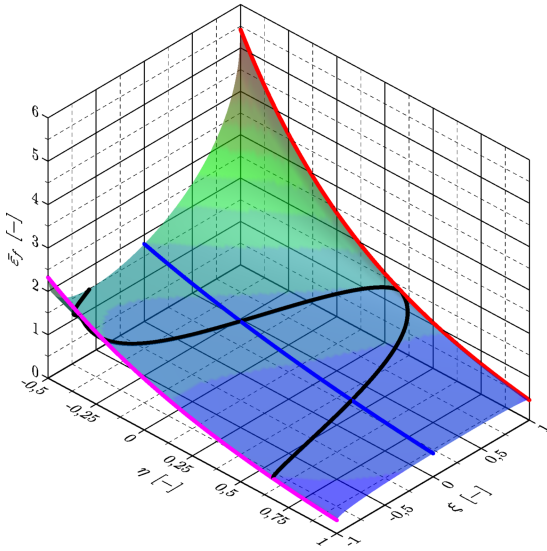


Fig. 4.10: Bai-Wierzbicki criterion

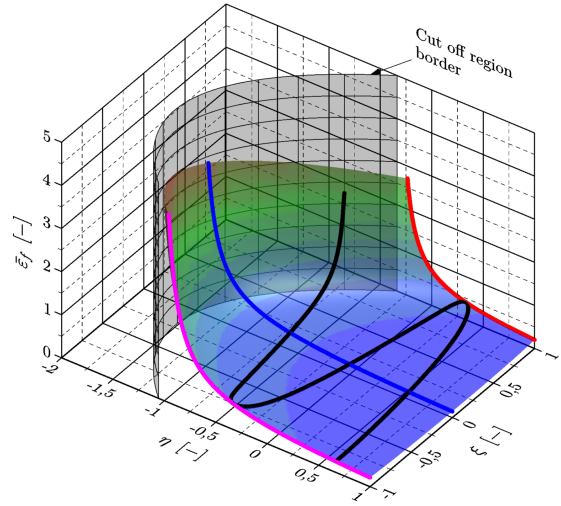


Fig. 4.11: KHPS criterion

⁵⁹Kubík, Hůlka, Petruška, Šebek

4.4 Physical and Thermodynamic properties

Except the mechanical properties the density ρ_d ⁶⁰ is also required as well as thermodynamic properties for a heat transfer analysis: a thermal conductivity λ_{hc} , a specific heat c and a thermal expansion coefficient α_{te} .

Data were provided by Professor Stětina from the Energy Institute at FME BUT through a program IDS (InterDendritic Solidification), where mean values of the chemical contribution from Tab. 2.1 were used. From the program, the *instant* values of the thermal expansion⁶¹ as well as values of the density, the specific heat and the thermal conductivity were determined. Abaqus requires an integral form of the thermal expansion coefficient according to the equation

$$\alpha_{tei} = \frac{1}{T_i - T_{ref}} \int_{T_0}^{T_i} \alpha_{te}^* dT, \quad (4.33)$$

where:

- α_{te}^* [K⁻¹] are *instant* values of the thermal expansion coefficient and
- T_{ref} [K] is a reference temperature [6].

Temperature dependencies of the required properties are shown in Fig. 4.12

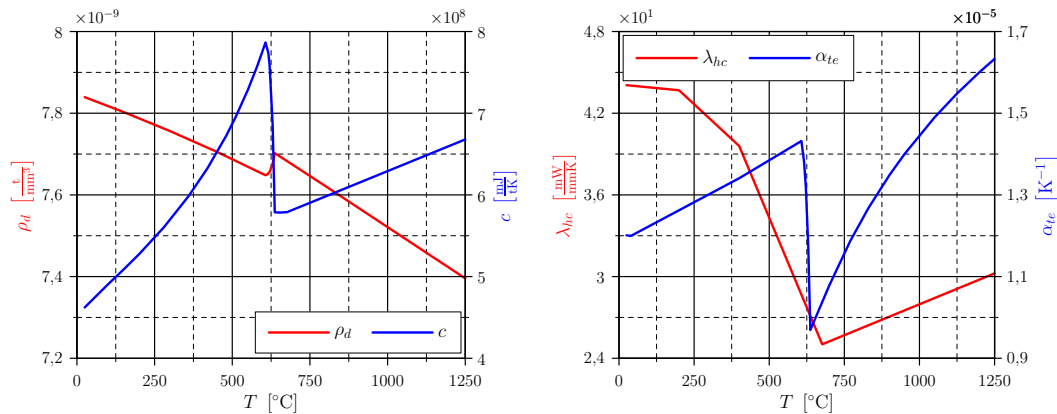


Fig. 4.12: Physical and thermodynamic characteristics of the steel 12 050

⁶⁰Density is required for the time increment estimation for the explicit algorithm and for a transient thermal analysis.

⁶¹A central difference method was used to determine these from the density.

5 Heat Transfer

In this part of the thesis there are the basics heat transfer principles in thermodynamics described and used further in the simulation of the closed die forging process. Among heat transfer ways belongs:

1. a conduction,
2. a convection and
3. a radiation.

Each of the above listed ways will be described in detail.

5.1 Conduction Heat Transfer

This is a heat transfer inside material that can be described using equations

$$\frac{\partial}{\partial x_1} \left(\lambda_{hc} \frac{\partial T}{\partial x_1} \right) + \frac{\partial}{\partial x_2} \left(\lambda_{hc} \frac{\partial T}{\partial x_2} \right) + \frac{\partial}{\partial x_3} \left(\lambda_{hc} \frac{\partial T}{\partial x_3} \right) + \dot{Q}^* = \rho_d c \frac{\partial T}{\partial t}, \quad (5.1a)$$

$$\frac{1}{\rho} \frac{\partial}{\partial \rho} \left(\lambda_{hc} \rho \frac{\partial T}{\partial \rho} \right) + \frac{1}{\rho^2} \frac{\partial}{\partial \phi} \left(\lambda_{hc} \frac{\partial T}{\partial \phi} \right) + \frac{\partial}{\partial x_3} \left(\lambda_{hc} \frac{\partial T}{\partial x_3} \right) + \dot{Q}^* = \rho_d c \frac{\partial T}{\partial t}, \quad (5.1b)$$

$$\begin{aligned} & \frac{1}{\rho^2} \frac{\partial}{\partial \rho} \left(\lambda_{hc} \rho^2 \frac{\partial T}{\partial \rho} \right) + \frac{1}{\rho^2 \sin^2 \psi} \frac{\partial}{\partial \phi} \left(\lambda_{hc} \frac{\partial T}{\partial \phi} \right) + \\ & + \frac{1}{\rho^2 \sin \psi} \frac{\partial}{\partial \psi} \left(\lambda_{hc} \sin \psi \frac{\partial T}{\partial \psi} \right) + \dot{Q}^* = \rho_d c \frac{\partial T}{\partial t}, \end{aligned} \quad (5.1c)$$

where:

- $\frac{\partial T}{\partial t} \left[\frac{K}{s} \right]$ is a temperature time variation and
- $\dot{Q}^* \left[\frac{W}{m^3} \right]$ are internal thermal resources [21].⁶²

It is the 2nd order partial differential equation. Eq. (5.1a) is valid for the Cartesian coordinate system, Eq. (5.1b) for the cylindrical coordinate system and Eq. (5.1c) for the spherical coordinate system. According to the right side value there are distinguished two analysis types:

⁶²The internal thermal resource can be e.g. plastic deformation work, it's conversion has been described in Sec. 4.2.4 and can be quantified using Eq. (4.18) on p. 52.

1. Steady-state: it serves for temperature distribution analysis in the moment of the steady state ($\frac{\partial T}{\partial t} = 0$).
2. Transient: it serves for temperature distribution analysis and its time variation ($\frac{\partial T}{\partial t} \neq 0$).

In case the thermal conductivity is independent on the coordinates, it is possible to simplify e.g. Eq. (5.1a) into

$$\lambda_{hc}\Delta T + Q^* = \rho_d c \frac{\partial T}{\partial t}, \quad (5.2)$$

where Δ is a Laplace operator.

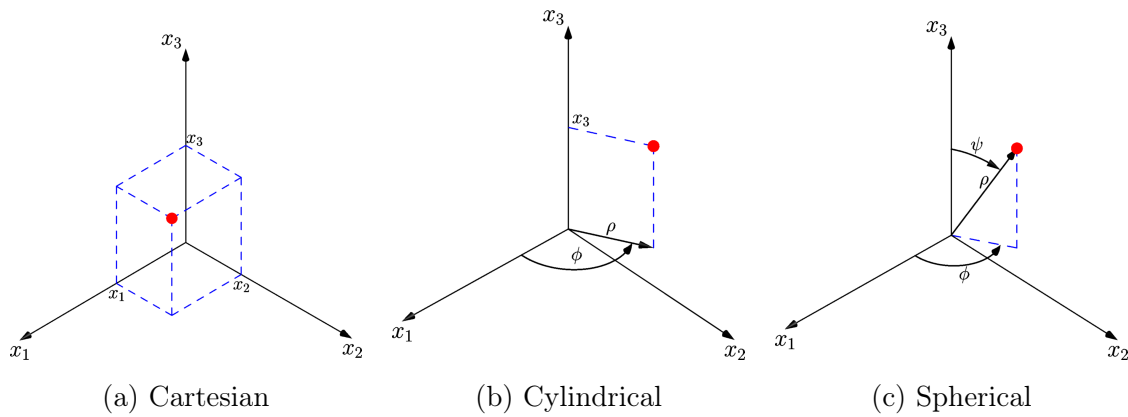


Fig. 5.1: Coordinate systems

The coordinate transformations for the cylindrical system are given by Eq. (5.3a) upto (5.3b), for the spherical system

$$x_1 = \rho \cos \phi \quad (5.3a) \quad x_1 = \rho \cos \phi \sin \psi \quad (5.4a)$$

$$x_2 = \rho \sin \phi \quad (5.3b) \quad x_2 = \rho \sin \phi \sin \psi \quad (5.4b)$$

$$x_3 = \rho \cos \psi \quad (5.4c)$$

A specific heat flux⁶³ caused by the conduction can be written as

$$\dot{q}_k = -\lambda_{hck} \frac{\partial T}{\partial x_k}, \quad (5.5)$$

where $\frac{\partial T}{\partial x_k} \left[\frac{K}{m} \right]$ expresses a change of T in x_k direction. In general it is a three-dimensional vector. Eq. (5.5) is also called Fourier's heat transfer law [21].

⁶³A heat flux through the unit surface, the unit is $\frac{W}{m^2}$.

5.2 Convection Heat Transfer

The heat transfer from a surface takes place in interaction with a fluid (steady/flowing) or in the interaction between bodies. In both mentioned cases the specific heat flux is expressed using Newton's cooling law

$$\dot{q} = \alpha (T_A - T_B), \quad (5.6)$$

where:

- $\alpha \left[\frac{\text{W}}{\text{m}^2 \text{K}} \right]$ is the heat transfer coefficient and
- T_A , respectively T_B [K] is the surface temperature [21].

The most important thing is the determination of the heat transfer coefficient and it is carried out on the basis of the experiments. There are several factors that influence the heat transfer coefficient [22]. In reality there can be distinguished:

1. Natural convection: it is the natural process that isn't influenced by any outer factors, e.g. cooling in stationary air.
2. Forced convection: the process is controlled purposefully, it can be speeded up (compressors, ventilators) or slowed down (annealing furnaces), e.g. for gaining the required material heat treatment.

5.2.1 Interaction of a Body with Fluid

If the heat transfer takes place between a body and fluid, so the temperature T_B in Eq. (5.6) is replaced by temperature T_∞ which is the fluid temperature in a sufficient distance from the body, where is not the fluid influenced by the body presence. The magnitude of the heat transfer coefficient is influenced the body surface structure, the fluid velocity, its density, viscosity, temperature, a type of flow (laminar/turbulent) etc. For heat transfer coefficient determining, experimental measurements and the theory of the dimensionless similarity numbers are used.

5.2.2 Bodies Interaction

A contact pressure is generated in a bodies contact, a friction takes place and leads to the heat generation. The contact pressure p_c is an important quantity

that has an influence on the heat transfer coefficient (conductance). Among the other important factors belong the surface structure and the temperature.⁶⁴ The managed quantities influence was experimentally researched in [22, 23].

5.3 Radiation Heat Transfer

The heat transfer due to a radiation does not need any material environment in comparison with conduction or convection. It works also in the vacuum. But it appears significantly at higher temperature differences between the surface and the surrounding. The specific heat flux due to radiation from the surface with the temperature T can be expressed as

$$\dot{q} = \sigma_{sb} \varepsilon_{rd} (T^4 - T_{\infty}^4), \quad (5.7)$$

where:

- $\sigma_{sb} = 5.67 \times 10^{-8} \frac{\text{W}}{\text{m}^2 \text{K}^4}$ is Stefan-Boltzmann constant,
- ε_{rd} [-] is a surface emissivity⁶⁵ and
- T_{∞} [K] is an environment temperature [21].⁶⁶

Eq. (5.7) is called Stefan-Boltzmann law. For an ideal black body applies $\varepsilon_{rd} = 1$ (an ideal emitter).

The fact that every body with a temperature $T \neq 0$ K emits some radiation spectrum (infra-red) is used to measure with a thermovision device, which can determine a surface temperature based on a emitted infra-red radiation density and a surface emissivity.

5.4 Initial and Boundary Conditions in Heat Transfer Solution

A initial condition is a temperature field distribution inside the region at the start of a process, so $T_0 = f(x, y, z, t = 0)$ [21].

⁶⁴In case of Abaqus it is average surfaces temperature $\bar{T} = \frac{T_A + T_B}{2}$ [6].

⁶⁵It depends on the surface, colour, structure etc.

⁶⁶In solving problems with radiation it *is needed* to set temperature in units of K.

There are several types of boundary conditions, which can be set to the region's border. Some of them are mentioned and described.

Dirichlet boundary condition specifies the temperature distribution on the border in time, so $T = f(x, y, z, t)$ [21]

Neumann boundary condition specifies the specific heat flux distribution on the border in time, so $\dot{q} = f(x, y, z, t)$ [21].

Newton boundary condition specifies the heat transfer coefficient distribution on the border in time, so $\alpha = f(x, y, z, t)$ [21].

If there is no boundary condition prescribed on the border, the homogeneous Neumann boundary condition is explicitly fulfilled, so the specific heat flux in a surface's normal direction has zero value.

5.5 Heat Transfer Solution

The temperature distribution in the closed form is possible to find only for simple domain shapes (a flat plate, a cylindrical/spherical solid body), simple material models (homogeneous, isotropic, temperature independent) and simple boundary conditions. But materials can be a bit more complicated (inhomogeneous, anisotropic-e.g. composites), what is more, properties can be temperature dependent. In these cases and in cases when boundary conditions and solved region shape are complicated, it is necessary to use numerical methods to solve differential equations. In the closed form, it is tricky to solve transient problems.

One of the possibilities is the FEM based on the calculus of variations, where it is possible to solve large and complicated tasks (contact of bodies, different material types, complicated regions, transient/steady states). What is more, it is possible to solve particularly and fully coupled problems (see earlier). A illustrative example

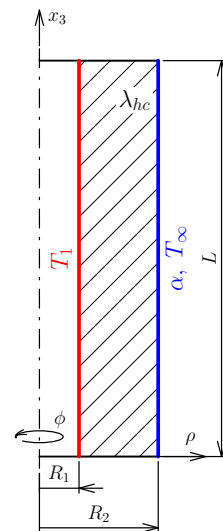


Fig. 5.2: Illustrative example

follows, where a solution performed by the differential calculus and the calculus of variations are compared.

It is a tube according to Fig. 5.2, where the temperature on a inner wall and the heat transfer coefficient value on a outer wall are known. The heat conductivity is constant. A steady state is considered.

$$\begin{aligned} R_1 &= 10 \text{ mm} & R_2 &= 30 \text{ mm} & L_1 &= 50 \text{ mm} \\ \lambda_{hc} &= 50 \frac{\text{W}}{\text{m K}} & \alpha &= 2 \times 10^3 \frac{\text{W}}{\text{m}^2 \text{K}} & T_1 &= 300 \text{ }^\circ\text{C} & T_\infty &= 20 \text{ }^\circ\text{C} \end{aligned}$$

For solution is used Eq. (5.1b), whereas $\dot{Q}^* = 0$ a $\frac{\partial T}{\partial t} = 0$. The task is axisymmetric, so $\frac{\partial T}{\partial \phi} = 0$. There is no heat transfer in the axial direction, so $\frac{\partial T}{\partial x_3} = 0$. Because of the constant heat conductivity there has to be solve an equation

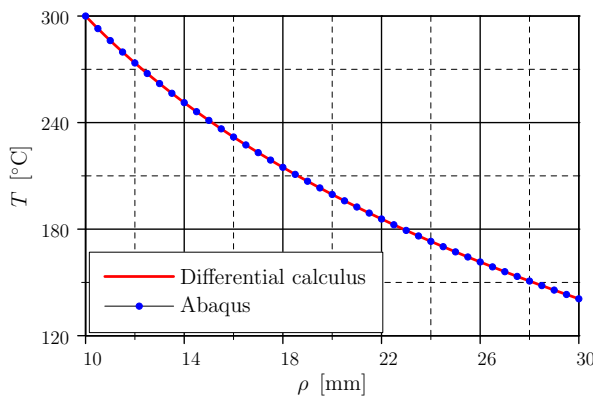


Fig. 5.3: Illustrative example-results

$$\frac{d^2 T}{d\rho^2} + \frac{1}{\rho} \frac{dT}{d\rho} = 0, \quad (5.8)$$

what is an 2nd order ordinary homogeneous differential equation with inconstant coefficients. There is performed a substitute $w = \log \rho$ to gain solution

$$T(\rho) = a_0 + a_1 \log \rho, \quad (5.9)$$

where a_0 a a_1 are constants of integration determined from boundary conditions. The boundary conditions are

$$\begin{aligned} T(\rho = R_1) &= T_1, \\ \dot{q}(\rho = R_2) &= -\lambda_{hc} \left. \frac{dT}{d\rho} \right|_{\rho=R_2} = \alpha(T(\rho = R_2) - T_\infty). \end{aligned}$$

By setting the boundary conditions a solution is obtained in a shape

$$T(\rho) = T_1 + \frac{T_1 - T_\infty}{\log \frac{R_1}{R_2} - \frac{\lambda_{hc}}{R_2 \alpha}} \log \frac{\rho}{R_1}. \quad (5.10)$$

For the FEM solution Abaqus workbench and its solver Abaqus Standard are used. The task is solved as planar axisymmetric, as a geometry serves a rectangle

with dimensions according to Fig. 5.2. A mesh is created by 2nd order quadrilaterals with a size $L_e = 0.25$ mm. The material is homogeneous isotropic with the heat conductivity λ_{hc} . On the edge with a coordinate $x_1 = R_1$ there is specified "Temperature" boundary condition type with a value T_1 . On the edge with a coordinate $x_1 = R_2$ there is specified "Surface Film Condition" boundary condition in the „Interaction“ section. The analysis is "Steady State". Results gained from the both methods are displayed in Fig. 5.3. There can be stated there is a negligible difference between the methods.

6 Build-up of Analysis Model

6.1 Units

An important step is a choice of a unit system because of its compatibility. Abaqus as well as Ansys APDL has dimensionless number input and output. The most often used unit systems are mentioned in Tab. 6.1.

Tab. 6.1: Compatible unit systems

Quantity	Symbol	kg, m, s	t, mm, s
Mass	m	kg	t
Length	l	m	mm
Time	t	s	
Density	ρ	$\frac{\text{kg}}{\text{m}^3}$	$\frac{\text{t}}{\text{mm}^3}$
Force	F	N	
Stress, pressure	σ, p	Pa	MPa
Energy, work, heat	E_{en}, W, Q	J	mJ
Temperature	T	K	
Specific heat	c	$\frac{\text{J}}{\text{kg K}}$	$\frac{\text{mJ}}{\text{t K}}$
Heat conductivity	λ	$\frac{\text{W}}{\text{m K}}$	$\frac{\text{mW}}{\text{mm K}}$
Heat transfer coefficient	α	$\frac{\text{W}}{\text{m}^2 \text{K}}$	$\frac{\text{mW}}{\text{mm}^2 \text{K}}$
Thermal expansion coefficient	α_{te}	K^{-1}	
$1 \frac{\text{kg}}{\text{m}^3} = 1 \times 10^{-12} \frac{\text{t}}{\text{mm}^3}, 1 \frac{\text{J}}{\text{kg K}} = 1 \times 10^6 \frac{\text{mJ}}{\text{t K}}, 1 \frac{\text{W}}{\text{m}^2 \text{K}} = 1 \frac{\text{mW}}{\text{mm}^2 \text{K}}, 1 \frac{\text{W}}{\text{m}^2 \text{K}} = 1 \times 10^{-3} \frac{\text{mW}}{\text{mm}^2 \text{K}}$			

In this thesis unit system t, mm, s is used because of easier check of results.⁶⁷ What is more, °C can be used as a temperature unit if the absolute zero temperature is modified.⁶⁸

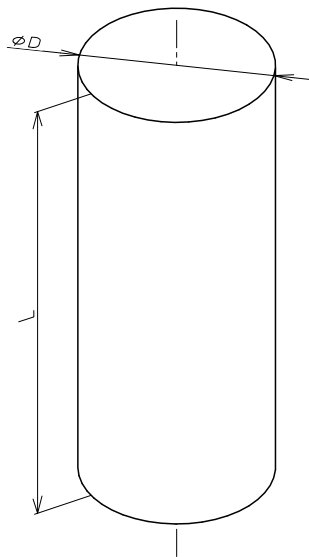
⁶⁷A base unit of the length for mechanical engineers is mm. Strength properties are usually given in MPa.

⁶⁸The absolute zero temperature is 0 K, a transformation between unit is $T_K = T_C + 273.15$.

6.2 Dimensions of Input Material

The first step is to determine dimensions of a input material, which is a circular rod. It is based on a volume of the finished forging V_f , which can be determined by boolean operations with primitives for simple shapes. An easier approach is to use a created CAD model of the forging, its geometric properties (volume, surface, centre of mass) are evaluated with an numerical integration. The volume is necessary to be extended with a volume for the flash, a mill scales addition etc.. This can be performed the extend volume is a multiple of the initial one

$$V_f^* = V_f(1 + \delta_f),$$



where δ_f is chosen in units of %.⁶⁹ The rod has to be design to avoid buckling, this can be expressed in conservative was as a maximal ratio of a rod's length and a rod's diameter

$$\lambda_u = \frac{L}{D} \leq 2.5. \quad (6.1)$$

By expressing of the rod's length L and by putting into a formula for a cylinder's volume $V = \frac{\pi D^2 L}{4}$ the rod's diameter is gained

$$d_r = \sqrt[3]{\frac{4V_f^*}{\pi \lambda_u}}. \quad (6.2)$$

Rods are supplied only in a specific diameter series. Hot rolled circular rods are used most frequently, their dimensions with tolerances are specified e.g. in norm EN 10060. As the rod's diameter D the closest bigger one than the diameter calculated according to Eq. (6.2) is chosen. The rod's length is determined from the cylinder's volume

$$L = \frac{4V_f^*}{\pi D^2}$$

and rounded with 1 decimal precision.

⁶⁹It is necessary to pay attention to the fact that the elastic strain causes the volume change. This change is tricky to estimate because the deformation process is very difficult and a stress distribution is inhomogeneous, so it may be necessary to increase the material's volume.

The whole approach described above was programmed into a GUI application (see Fig. 6.2), created in a programming language Pascal and IDE Delphi.

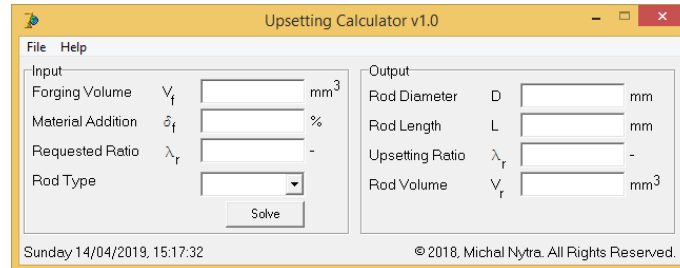


Fig. 6.2: Application GUI

Dimensions of the finished forging are prescribed in a drawing `vykres_vykovku.pdf` created from a CATIA CAD model. In CATIA a measuring tool was used and the forging's volume is $V_f = 79\,292.2 \text{ mm}^3$. The addition for a flash $\delta_f = 0.03$ and the maximal length ratio $\lambda_u = 2.5$ were chosen. An calculation's output is listed below.

====UPSETTING ANALYSIS REPORT====

Sunday 5/12/2019, 4:38:36 PM

-----INPUT PARAMETERS-----

Forging Volume: 79292.2 [mm³]

Material Addition: 3 [%]

Requested Length Ratio: 2.5 [-]

Rod Type: EN 10060

-----ROD PARAMETERS-----

Rod Diameter: 35 [mm]

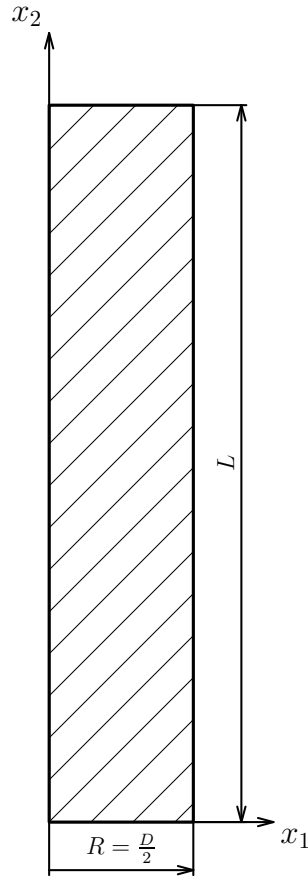
Rod Length: 84.9 [mm]

Length Ratio: 2.425 [-]

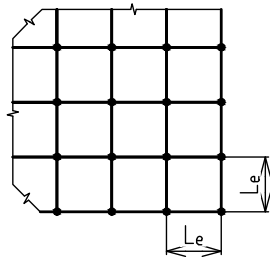
Status: OK

Based on the simulations, it was found out the rod's volume was not big enough because of the volume change caused by elastic strain and its length was extend up to $L = 89.5 \text{ mm}$.

6.3 Discretization



(a) Geometry



(b) Mesh

Fig. 6.3: Rod

Due to the geometric shape, ties and load, the task is solved as planar axisymmetric. This option makes solution easier for an adaptive remeshing during straining (see further) and a computational difficulty is decreased significantly

6.3.1 Rod

Geometry of the rod is a rectangle with dimensions $R = 18 \text{ mm}$ and $L = 89.5 \text{ mm}$ in the plane x_1x_2 first quadrant, where the x_2 axis is an axis of rotation (see Fig. 6.3a). The dimensions are extended by thermal expansion

Mesh of the rod is composed of CAX4RT elements having a quadrilateral shape, a linear basis function and reduced integration for axisymmetric analysis. Each node has three degree of freedom (displacement in a direction x_1 , x_2 and a temperature). Due to very simple geometry, the mesh is very regular (see Fig. 6.3b). The element size is $L_e = 0.06 \text{ mm}$.

Because the forming processes are connected with large deflections and changes of the shape, there occurs a distortion of the elements leading to inaccurate results (mainly in areas with large curvature changes) or a premature termination of the analysis. Because of this fact, it is necessary to change the mesh adaptively, this is ensured by ALE⁷⁰ algorithm. A disadvantage is the elements/nodes contained in a remeshing area have to create one domain in a processor (it has to be included in one physical core). The ALE algorithm is used for the whole domain, so the analysis has to be performed with one processor's core leading to not negligible slowdown.⁷¹

⁷⁰Arbitrary Lagrangian-Euler

⁷¹Here is the advantage of the planar discretization reducing a computational time.

6.3.2 Tools

Geometry of each tool is formed by a curve (see Fig. 6.4a) imported from CATIA and considered as rigid⁷² Geometry of a finishing tool is extended by 1.5% because the material shrinks during cooling. The rigid body is controlled by a reference point where the boundary conditions are prescribed.

Mesh of the tools is composed from RAX2 linear rigid line elements (see Fig. 6.4b). Each node has two degrees of freedom (displacement in a direction x_1 and x_2).⁷³ The element size is $L_e = 0.3$ mm.

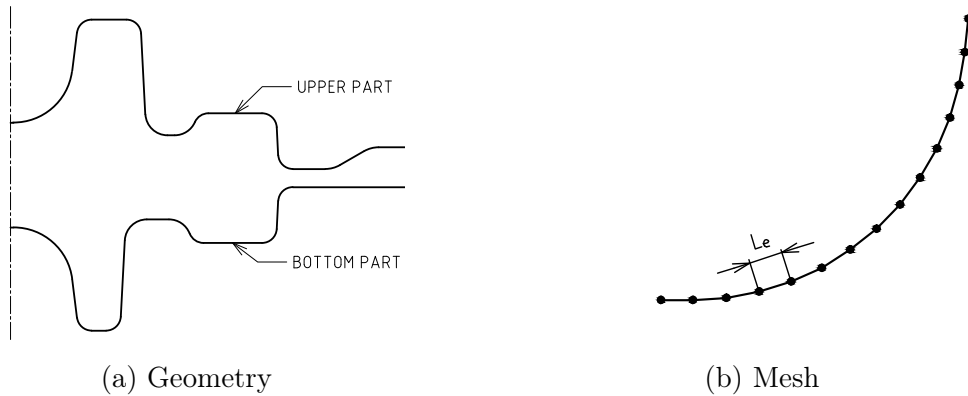


Fig. 6.4: Tool

Into the reference point of each tool, a heat capacity (Part \rightarrow Engineering Features \rightarrow Inertias \rightarrow Heat capacitance) corresponding to a product of tool's mass and the specific heat for the specific temperature is prescribed. Each tool is considered with mass 50 kg. Temperature dependency of the steel 19 552 specific heat is displayed in Fig. 6.5.

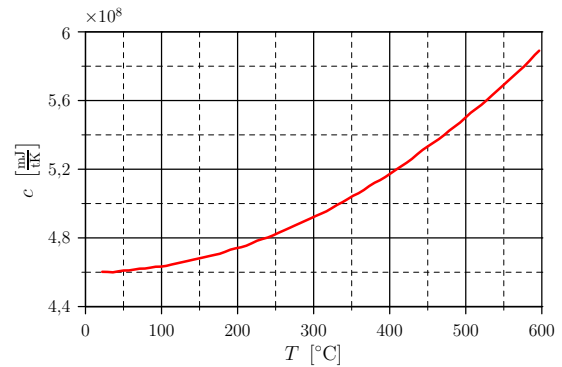


Fig. 6.5: Specific heat-steel 19 552 [25]

⁷²Discrete Rigid.

⁷³A reference node also includes a rotation around an axis x_3 .

6.4 Dimensions change due to Thermal Expansion

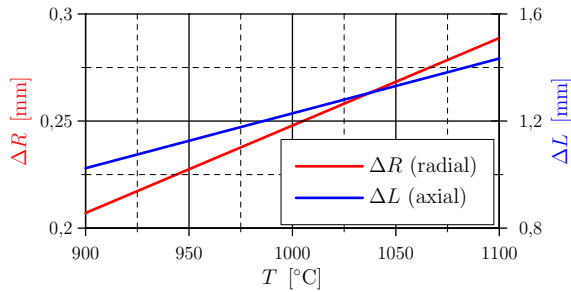


Fig. 6.6: Rod's dimensions change

By using of FEM analysis a dependency between a forging temperature and a rod's dimensions change in each direction during a heat-up from a room temperature was stated. The solution was implemented by using an implicit fully-coupled thermal analysis. The dependency for the rod with dimensions described in Sec. 6.3 is shown in Fig. 6.6.

6.5 Model of Material-Steel 12 050

As mentioned earlier in Chap. 2 and 4, it is necessary to define a series of mechanical, physical and thermomechanical properties. Their list including path in Abaqus CAE and their settings is described below. It is also necessary to mention a couple of points about using the model of plasticity.

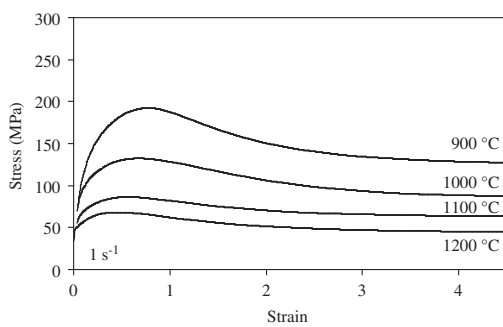


Fig. 6.7: Flow curve for high temperature [26]

Based on experiments it was proved that steels (mainly low alloy ones) in higher temperatures harden from the beginning, but after reaching a specific level of strain they soften slightly because there occurs self-propelled recrystallization due to the high temperature. Unfortunately, Abaqus does not include solvers able to compile decreasing flow curve, conversely it has to be non-decreasing⁷⁴ ones. As well

as for the ductile damage, there has to be created VUMAT subroutine to implement decreasing flow curve.⁷⁵ That is why there is used the Johnson-Cook plasticity,

⁷⁴This means increasing or constant.

⁷⁵The softening is performed on a basis of damage parameter cumulation according to some criterion (see earlier). There is still a *non-decreasing* flow curve as an input. Through this approach, a bonded model of plasticity and ductile damage is created.

which is available in Abaqus CAE workbench.

Jan Bořkovec calibrated the flow curve for steel 12 050 in his thesis. However, there were not performed high temperature experiments to calibrate the temperature softening exponent in Eq. (4.17a) and its value was only assumed (see p. 31 in [7]). Constants of the calibrated curve are in Tab. 6.2.

Tab. 6.2: Johnson-Cook flow curve parameters for steel 12 050 [7]

A_{jc} [MPa]	B_{jc} [MPa]	n_{jc} [-]	c_{jc} [-]	$\dot{\epsilon}_{p0}$ [s ⁻¹]	m_{jc} [-]	T_m [°C]	T_r [°C]
375	552	0.457	0.02	0.1	1.4	1520	24

However, this calibrated material is stiffer in comparison with the values of stress resistances mentioned in Tab. 5 on p. 10 in [16]. That is why it was necessary to modify the value of the constant m_{jc} for a bigger softening up to value $m_{jc} = 0.4$.

Johnson-Cook ductile damage criterion is used, it's material constants are mentioned in Tab. 6.3.

Tab. 6.3: Johnson-Cook ductile damage parameters for steel 12 050 [1, 27]

D_1 [-]	D_2 [-]	D_3 [-]	D_4 [-]	D_5 [-]
0	1.9583	1.3824	0	0.58

- Density: General → Mass Density: temperature dependent,
- Elasticity: Mechanical → Elasticity → Elastic: isotropic, temperature dependent,
- Plasticity: Mechanical → Plasticity → Plastic: Johnson-Cook,
- Ductile damage: Mechanical → Damage for ductile metals → Johnson-Cook damage,
- Thermal expansion: Mechanical → Expansion: isotropic, temperature dependent,
- Heat conductivity: Thermal → Conductivity: isotropic, temperature dependent,
- Inelastic heat fraction: Thermal → Inelastic heat fraction: 0.9,

- Specific heat: Thermal \rightarrow Specific heat: constant pressure, temperature dependent.

The values of the above mentioned quantities (expect Johnson-Cook plasticity and ductile damage) are for steel 12 050 listed in *.txt files on an attached CD. Their graphical interpretation is in Fig. 4.1 and 4.12.

6.6 Contacts

6.6.1 Interaction forging-tool

Contacts are defined in a module "Interactions" in Abaqus, where the user chooses a pair of surfaces, which could possibly get into interaction, and assigns properties to the contact pair defined in a module "Interaction Properties". An advantage is, if more contact pairs have the same properties, it is not necessary to fill them for each one as in the case of Ansys. The contacts for the axisymmetric discretization and the explicit algorithm are defined through "Surface-to-surface contact (Explicit)".

There is used Coulomb's law of friction, where a frictional force \vec{F}_T depends on a normal force \vec{F}_N according to the formula

$$|d\vec{F}_T| = f_f |d\vec{F}_N| \quad (6.3)$$

where f_f [–] is a friction coefficient and a direction of the frictional force is counter-wise to the movement direction. There is not distinguished a static/kinetic friction coefficient for simplification and it is set as a constant value. As has been mentioned in Chap. 2, the only available algorithm for the contact solution is the penalty method. Other methods, e.g. Lagrange multiplier method, are available only for the implicit FEM algorithms.

Contact properties between a tool and a forging:

- Normal direction: Mechanical \rightarrow Normal Behaviour \rightarrow Pressure-Overclosure: "Hard" Contact, Constraint enforcement methods: Default, Allow separation after contact: Yes.
- Tangential direction: Mechanical \rightarrow Tangential Behaviour \rightarrow Friction formulation: Static-Kinetic Exponential Decay, Coefficients.

- Heat transfer: Thermal \rightarrow Thermal Conductance: Tabular, use pressure-dependency data, temperature dependent.

Value of the frictional coefficient is chosen $f_f = 0.4$ according to [16].

Based on experiments in Heat Transfer and Fluid Flow Laboratory, a multi-parameter linear regression function describing dependency of the film coefficient between bodies on a temperature T , a contact pressure p_c and as well as an arithmetic average profile roughness R_a

$$\alpha_c(T, p_c, R_a) = 9.25644T + 168.11p_c + 346,166R_a + 0.121614p_cT - 10.4959p_cR_a - 0.61TR_a - 0.00947Tp_cR_a, \quad (6.4)$$

where $T \in \langle 300; 900 \rangle$ °C, $p_c \in \langle 25; 100 \rangle$ MPa and $R_a \in \langle 0.8; 7.2 \rangle$ μm was calibrated [22].

A contact pressure range is strongly limited, so in case of a higher value of the contact pressure, the values of the film coefficient are extrapolated according to the same formula. The exactly same approach is applied for the temperature. Its implementation is based on creating a text file⁷⁶ loaded into a table in Abaqus.⁷⁷ The arithmetic average profile roughness is chosen $R_a = 6.3 \mu\text{m}$.

6.6.2 Interaction forging-surrounding

Through outer surfaces of a forging, a heat transfer into surrounding through the convection and the radiation takes place. Theirs mathematical description was explained in Chap. 5. An implementation in Abaqus is following:

- Convection: Interactions \rightarrow Surface film condition \rightarrow Film coefficient, Sink temperature,
- Radiation: Interactions \rightarrow Surface radiation \rightarrow Emissivity, Ambient temperature.

The surface film coefficient is set to $\alpha = 20 \frac{\text{W}}{\text{m}^2\text{K}}$ and the surface emissivity to $\varepsilon_{rd} = 0.88$. The surroundings temperature for the both ways is $T_\infty = 24$ °C.

⁷⁶E.g. in MATLAB software.

⁷⁷Dataset has to be ordered the way to make the last independent variable ascending.

For the heat transfer through the radiation, it is necessary to define the Stefan-Boltzmann constant and in case a temperature unit is °C, it is necessary to change an absolute zero temperature. This is performed in a model's settings through the menu: Model → Edit Attributes → Physical Constants → Absolute zero temperature, Stefan-Boltzmann constant.

Interactions with tools (see before) are defined on all outer domain's surfaces except the axis of rotation. With available algorithms, it is impossible to detect which part of the contact pair is already in the interaction. Through this surface part, the convection and the radiation to the surroundings do not take place. Heat fluxes caused by them are orderly lesser than heat fluxes between a forging and a tool, so for simplification, the convection and the radiation take place during the whole analysis.

6.7 Boundary Conditions

There are used only *displacement-based (kinematic)* boundary conditions.

Tab. 6.4: Used machines parameters

Parameter	Symbol	Machine	
		LMZ 2500 ⁷⁸	LDO 315A ⁷⁹
Stroke	z^{80} [mm]	320	200
Connecting rod length	l_{cr} [mm]	1070	885
Revolve rate	n [min ⁻¹]	70	44

Moving tools perform only a necessary part of their trajectory to decrease a time of calculation. Let us consider the Δh distance between an initial and a final position, where a ram's deflection is maximal. Based on parameters mentioned in Tab. 6.4 there can be determined a time required to overcome the distance Δh by using Cosine formula

$$l_{cr}^2 = x_h^2 + r_{cs}^2 + 2r_{cs}x_h \cos(\omega t) \quad (6.5)$$

according to Fig. 3.12 on p. 37 and with this there can be stated an initial time t_i and a final time t_f

$$t_i = \frac{1}{\omega} \arccos\left(\frac{l_{cr}^2 - (l_{cr} + r_{cs} - \Delta h)^2 - r_{cs}^2}{2r_{cs}(l_{cr} + r_{cs} - \Delta h)}\right), \quad (6.6a)$$

$$t_f = \frac{T_\omega}{2} = \frac{2\pi}{2\omega} = \frac{30}{n}, \quad (6.6b)$$

where T_ω [s] is a period. A graphical interpretation of above mentioned knowledges is in Fig. 6.8.

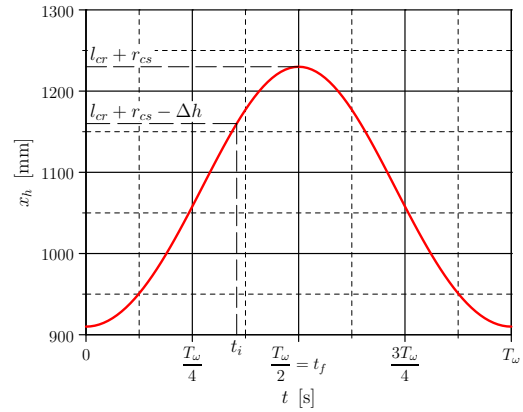


Fig. 6.8: Position of ram in time

⁷⁸ $z = 2r_{cs}$.

⁷⁹Vertical forging crankpress.

⁸⁰Trimming press.

A time range $\langle t_i; t_f \rangle$ defines a time between zero load up to its maximal value. It is necessary to add some time for a smooth unload and release an elastic strain energy. Due to the shape complexity, the forces in boundaries are assured to be zero after ending a step. It is sufficient if the force at the end of the step is orderly lower than the maximal force. There appears a negative effect during a reverse movement of the tool. Contact surfaces are not separated properly (see Fig. C.1 on p. 127). The problem could not be eliminated by change of contact settings.

In case it is necessary to set a boundary condition (force-based or displacement-based) as time dependent, an amplitude in Abaqus has to be used serving as a multiplier of a set boundary condition value according to

$$val(t[i]) = val_{in} \cdot amp(t[i]).$$

There are 2 options for time variable setting for the amplitude in Abaqus. **STEP TIME** is a default option and time values in the amplitude are related to a time measured through a step, which has zero value at the beginning of each step. In comparison, **TOTAL TIME** measures the time from an analysis beginning and has a cumulative character regardless to a number of steps [6]. In this thesis, the default settings **STEP TIME** is used, but it is necessary to norm time values to zero, this means

$$t[i] = t[i] - t[0] \text{ for } \forall i = 0, 1, \dots$$

The easiest way to set the amplitude is through tabular discrete values in the time with a linear interpolation, this creates a multi-linear curve.⁸¹

Now it is necessary to choose a controlling kinematic quantity. Their time running through one period is plotted in Fig. 6.9a.⁸²

⁸¹Other possibilities to set the amplitude are available on <http://130.149.89.49:2080/v6.11/books/usb/default.htm?startat=pt07ch32s01aus110.html#usb-prc-pamplitude> in [6].

⁸²Formulas are taken from Chap. 3.3.2, Eq. 3.4a up to 3.4c on p. 38.

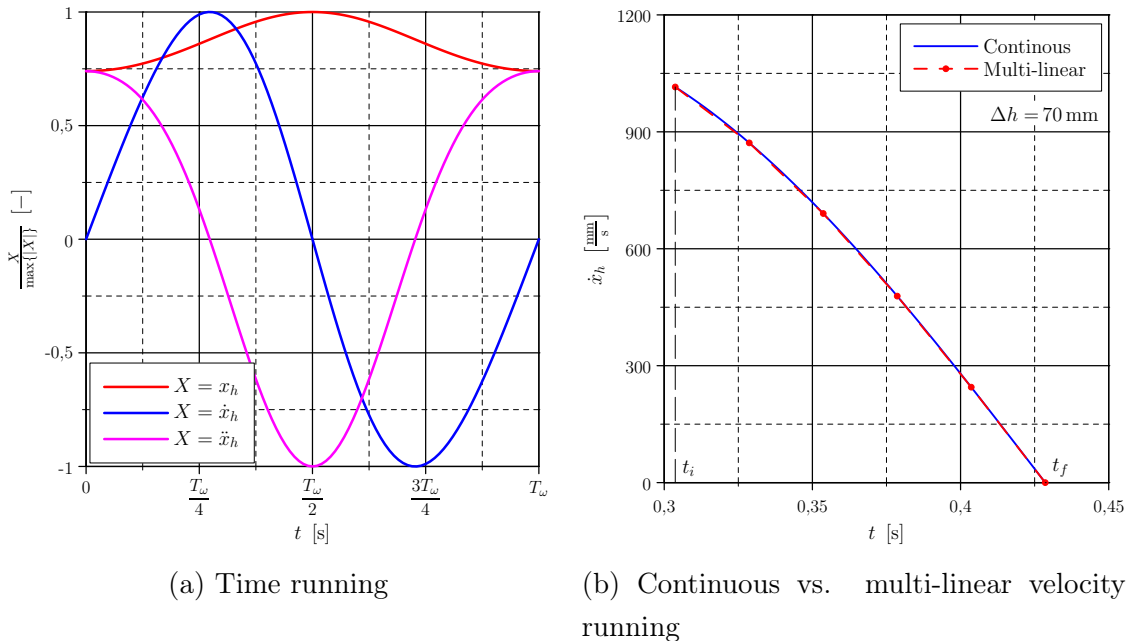


Fig. 6.9: Kinematic quantities

Displacement is not really inappropriate. Its running has a large curvature close to a dead position, so there are required a lot of points for a good approximation. The main disadvantage are its derivatives (piecewise constant of the first derivative and Dirac's pulses for the second one), this can lead to numerical instability.

Velocity is the most appropriate one. Its running around the dead position is very close to the linear one, so the approximation is precise with a low number of points (see Fig. 6.9b). There applies a homogeneous initial condition for the displacement ($x_0 = 0$). The discontinuity appears only in the first derivative in tabular points.

Acceleration is the most appropriate in terms of connection, because of the fact that the second derivative of the displacement is continuous. As well as for the displacement, it is necessary to use more points for the sufficient approximation. What is more, there does not apply homogeneous initial conditions for the velocity ($\dot{x}_0 \neq 0$), so an implementation is a bit tricky.

An amplitude creation for an Abaqus input is again programmed in a form of the GUI application in Pascal and IDE Delphi (see Fig. 6.10). Its output is `txt`

files containing 2 columns and a number of rows corresponding to a number of the division.

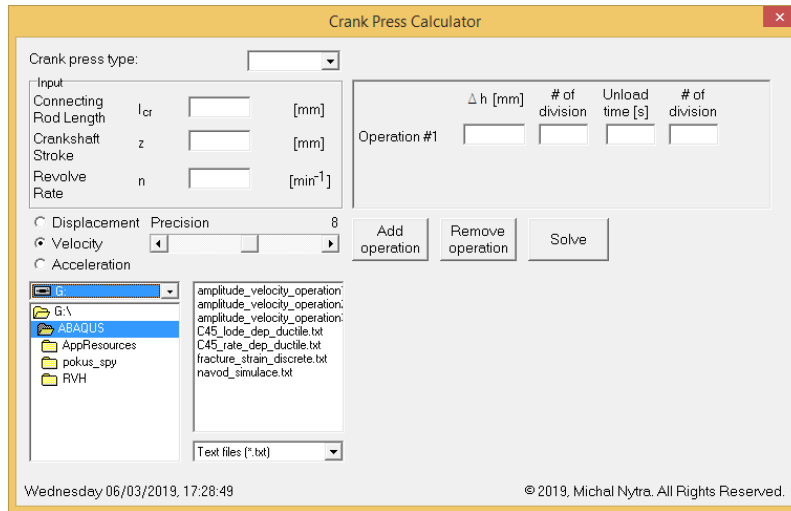


Fig. 6.10: Crank press amplitude GUI application

There is used the axisymmetric discretization, so it is not necessary to prescribe any additional boundary conditions for the rod's domain, because a $u_1(x_1 = 0) = 0$ condition is fulfilled automatically and the rest of conditions is contacts with the tools. However, in some cases some nodes on the axis of rotation changed their radial coordinate, because of very large deflections and the hourglassing. Because of this fact, the condition $u_1(x_1 = 0) = 0$ was prescribed and this negative issue was suppressed.⁸³ Boundary conditions allow tools to move only in a rod axial direction.

6.8 Initial Conditions

Initial conditions are related only to a temperature and they are defined in Pre-defined Fields → Other → Temperature. There is considered a homogeneous temperature distribution in a rod. Temperature is also defined for each tool, where the initial condition is prescribed into a reference point. An initial temperature for a rod is $T = 1000\text{ }^\circ\text{C}$, for upsetting and trimming tools $T = 20\text{ }^\circ\text{C}$ and for other tools $T = 250\text{ }^\circ\text{C}$.

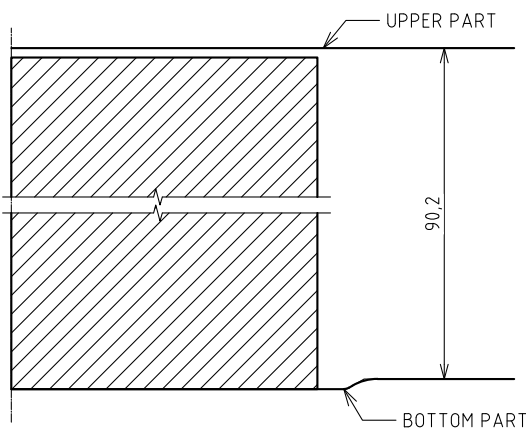
⁸³Components of a node displacement vector \mathbf{u} are denoted by a symbol u_i [m].

6.9 Series of Operations

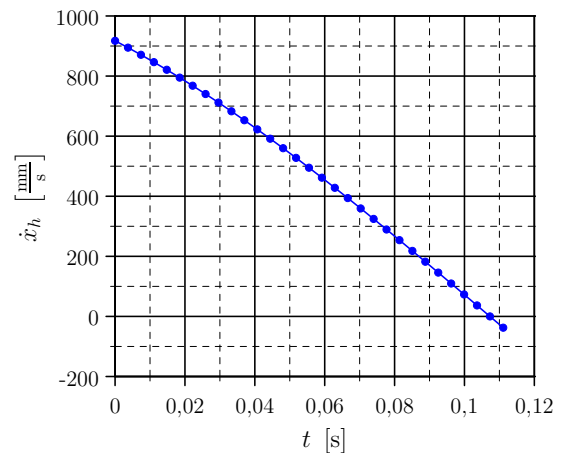
The following description is related to settings of each piecewise analysis, this means solved time range, time stepping, adaptive meshing, tool's kinematics definition, results storage etc. An analysis of type Temp-Disp, Explicit, so fully coupled thermal-stress analysis solved explicitly, is used for a solution. Large deflections (NLGEOM) are considered for a solution. An adaptive meshing is used only during forming phases. A double precision is used because of a high amount of time increments.

6.9.1 Upsetting (Operation 1)

The first operation serves to reduce input material's height for blocking. In Fig. 6.11a is displayed an initial configuration of tools. An tool's upper part is moved from the initial position about a distance of $\Delta h = 53\text{ mm}$ for time $t \doteq 0.1073\text{ s}$. A time step of a solution is set as $\Delta t = 1.5 \times 10^{-7}\text{ s}$, what is reached by a mass scaling. During this time range twenty sub-results into a result file are stored. An adaptive meshing takes place after each five time increments.



(a) Initial position



(b) Velocity dependency

Fig. 6.11: Upsetting

An unload follows, it runs through during a time $t = 0.0038\text{ s}$ with the same time step. During this time range five sub-results into a result file are stored. After finishing this operation it is appropriate to let an inhomogeneous temperature field

to level off, this means in a global scale $\frac{\partial T}{\partial t} \rightarrow 0$. Simulations proved, that a time range $t = 0.2\text{ s}$ is long enough. Because there are not expected any large deformation changes, this interval is split into more sub-intervals with a stepwise increasing time step up to value $\Delta t = 6 \times 10^{-7}\text{ s}$ to an analysis speed-up. A dependency of a velocity amplitude is displayed in Fig. 6.11b.

6.9.2 Blocking (Opeation 2)

A blocking operation serves to a shape change from a barrel, which is a typical result of the upsetting operation (see Fig. 6.12a), to a shape close to a final one. An upper tool's part is moved about a distance of $\Delta h = 22.8\text{ mm}$ for time $t \doteq 0.06893\text{ s}$. In comparison with the previous operation, a time step was reduced to $\Delta t = 1 \times 10^{-7}\text{ s}$ because bigger material's motion and more complicated shape changes are expected. Results storage and adaptive meshing settings are same as in the previous operation.

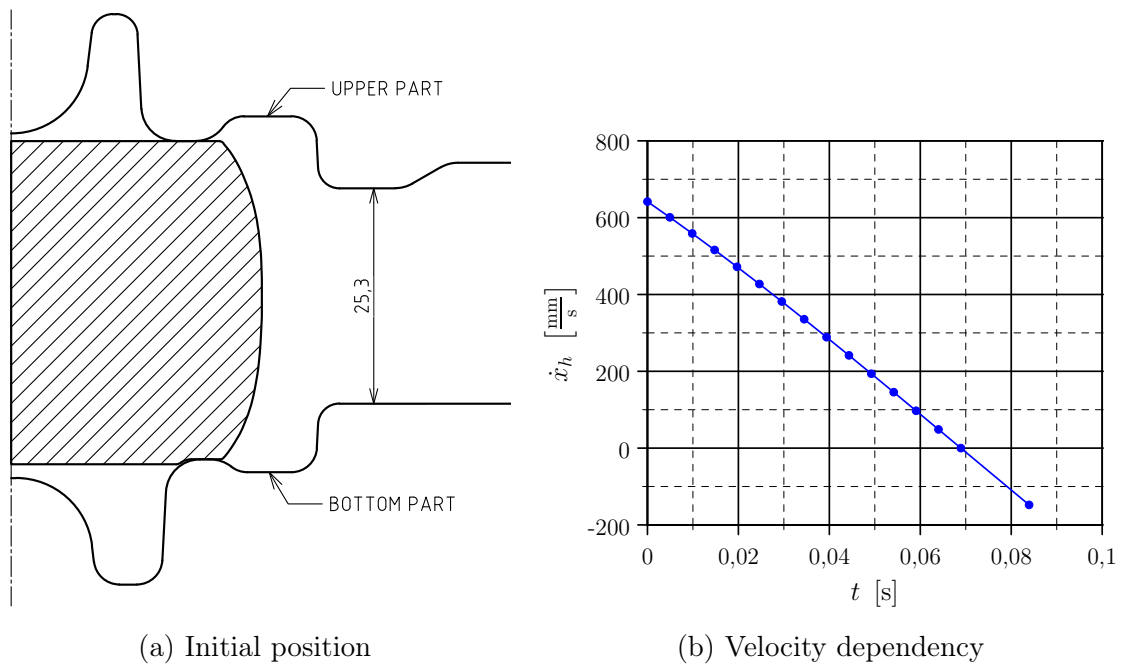


Fig. 6.12: Blocking

An unload follows, which is due to more complicated geometry extended up to time $t = 0.015\text{ s}$ with the same time step. There are again saved five sub-

results during this time interval. As well as in case of the previous operation, the same procedure follows to level off a temperature field. A dependency of a velocity amplitude is displayed in Fig. 6.12b.

6.9.3 Finishing (Operation 3)

Thereafter, the final shape of the forging is created. An upper part of the tool is moved from it's initial position (see Fig. 6.13a) about a distance of $\Delta h = 4.3$ mm for a time $t \doteq 0.02958$ s. A solution takes place with the same time step as a blocking operation while the results storing and the adaptive meshing settings are preserved.

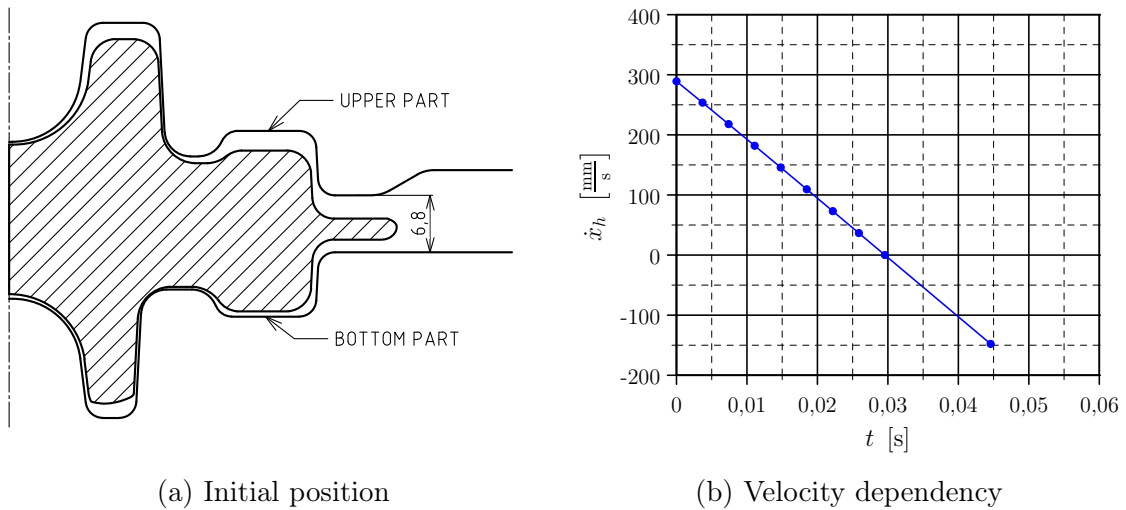


Fig. 6.13: Finishing

The unloading process is identical to the previous operations.

6.9.4 Trimming (Operation 4)

A flash is removed during trimming in a way that a punch pushes the forging towards a trimming tool (see Fig. 6.14a). As it is mentioned in a schematic figure, a punch is moved in a indicated direction about a distance of 11 mm for a time $t \doteq 0.0976$ s. A time increment is reduced to $\Delta t = 7.5 \times 10^{-8}$ s to reduce the impact of mass-scaling on the direction and the rate of crack propagation. An adaptive meshing is not necessary during a trimming operation anymore. Hundred results are saved to create a detailed history of a crack propagation direction and rate. A velocity amplitude dependency is displayed in Fig. 6.14b.

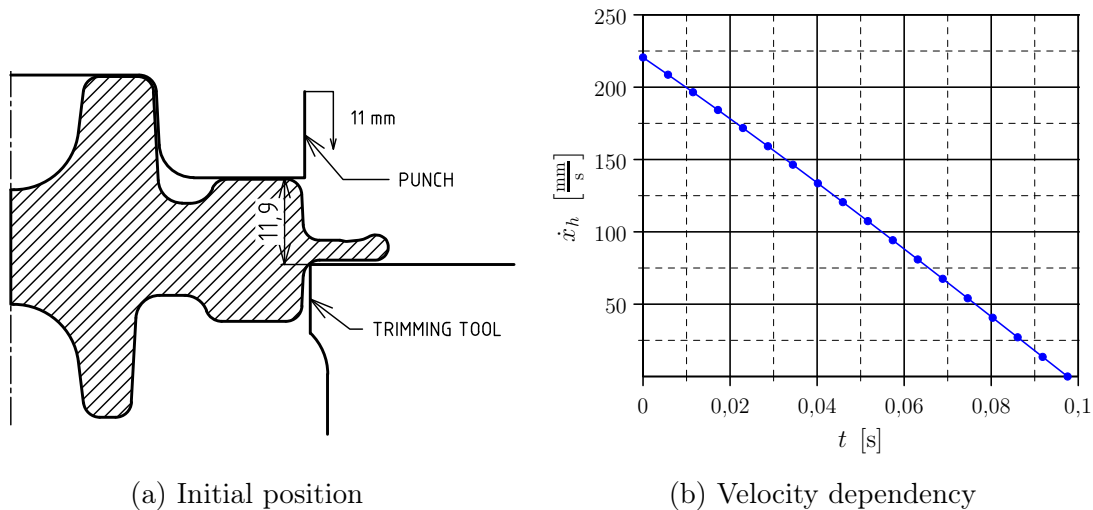


Fig. 6.14: Flash trimming

An additional information about contacts is necessary to be mentioned. An element elimination method used for a crack propagation leads to creation of new surfaces. That is why it is necessary to define a contact pair, where one part of a pair is formed of trimming tool edges and the second one is formed of mesh entities. Element edges/surface are usually chosen as mesh entities and in this way a "surface to surface" contact type is created. However, it is possible to chose only one direction of a normal for common edge of two neighbour elements in Abaqus when a planar elements are used for discretization. This is why a "node to surface" contact type is necessary to be chosen and define a contact between trimming tool edges and an area of nodes, where a crack should probably propagate.

7 Results

7.1 Simulation without Ductile Damage

In this part of the thesis are considered influences of input material dimensions and its initial temperature on an equivalent plastic strain $\bar{\epsilon}_p$ and a temperature T fields. All combinations of used dimensions and initial temperatures are mentioned in Tab. tab. 7.1.

Tab. 7.1: Combinations of input material dimensions and temperatures

Input material ⁸⁴	Initial temperature [°C]
Ø36 – 89.5	900
	1000
	1100
Ø38 – 82.5	900
	1000
	1100

All analysis were performed with settings mentioned in Chap. 6, they were terminated after reaching a final position of a tool during a finishing operation for saving of time, so there were not performed an unload and a temperature field level off. It is necessary to add, that a coarser mesh was necessary to use for an input material with a diameter 38 mm because of problems with an adaptive meshing, so results cannot be in some areas compared properly because of a different number of elements.

Deformed shaped after each operation displayed schematically in Sec. 6.9, are displayed in Fig. 7.1a up to 7.1c after expanding of a planar geometry into a 3D space. Further, three chosen combinations from Tab. 7.1 are compared chronologically after each operation. In conclusion, a time dependencies of force in a rod axial direction for all tools are compared for all combinations.⁸⁵

⁸⁴Denotation: diameter-length, dimensions in mm.

⁸⁵A force in an axial direction should represent a forming force.

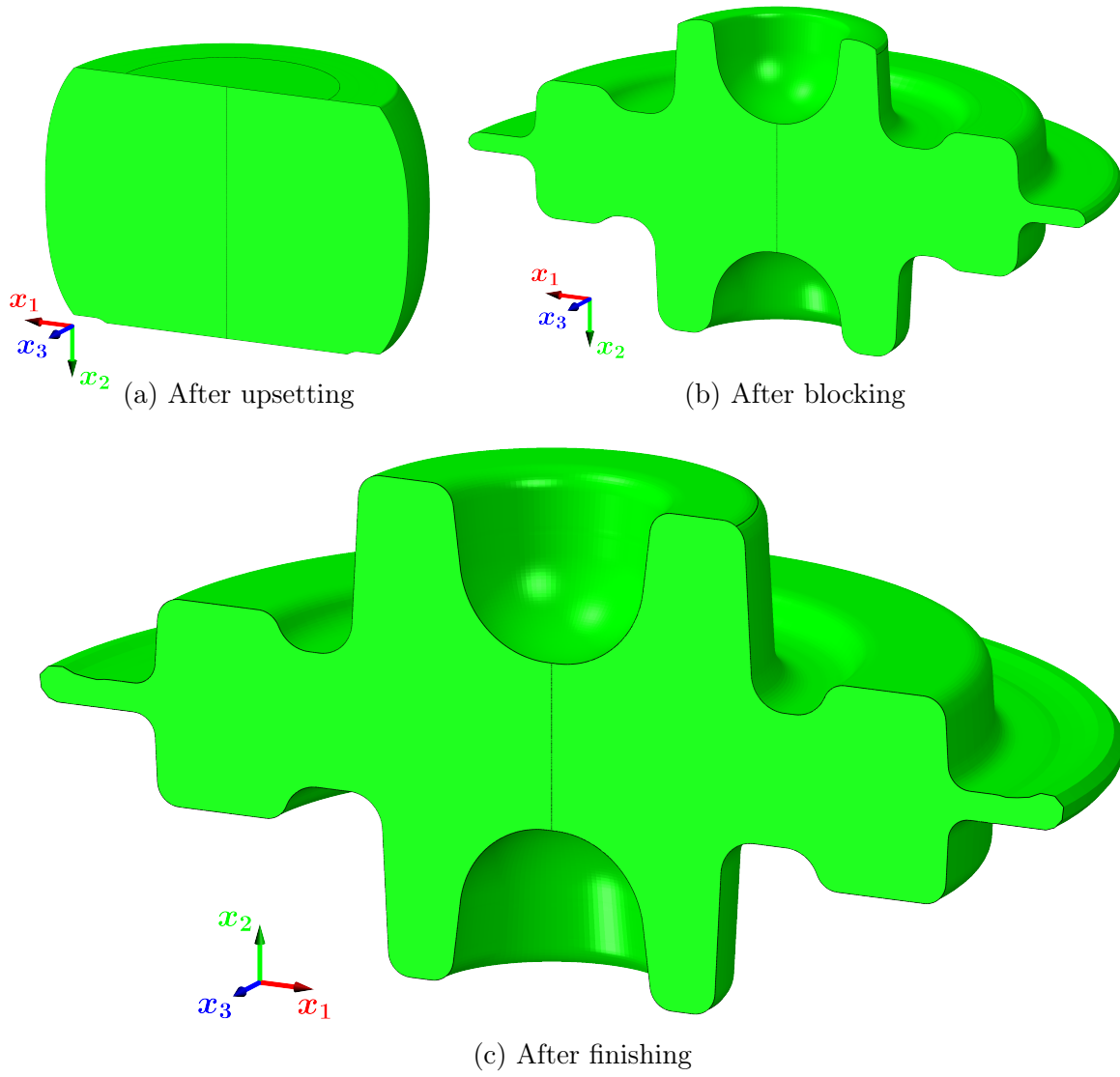


Fig. 7.1: Deformed shapes

7.1.1 Upsetting

Results of an equivalent plastic strain $\bar{\varepsilon}_p$ and a temperature T after upsetting are displayed in Fig. 7.2 up to 7.4. It is visible from displayed results that there is present no hourglassing in a range of an acquired deformation. A hourglassing often causes a local steep growth of a strain. If we aim at an area around a barrel axis in a middle of it's length, so differences in values of an equivalent plastic strain are given just by an initial rod length, because a final barrel length is same for all combinations.⁸⁶ As for a temperature field, there are only small differences in a qualitative aspect. A difference in a maximal temperature change in the rod $\varnothing 36$ and $\varnothing 38$ for temperature 1000 °C is probably given only by a difference in a value of an acquired plastic strain. A significant difference is visible for the rod $\varnothing 36$ and a initial temperature 1100 °C because a temperature time variation $\frac{\partial T}{\partial t}$ is dependent on thermal material properties according to Eq. (5.1a) which are strongly temperature dependent..

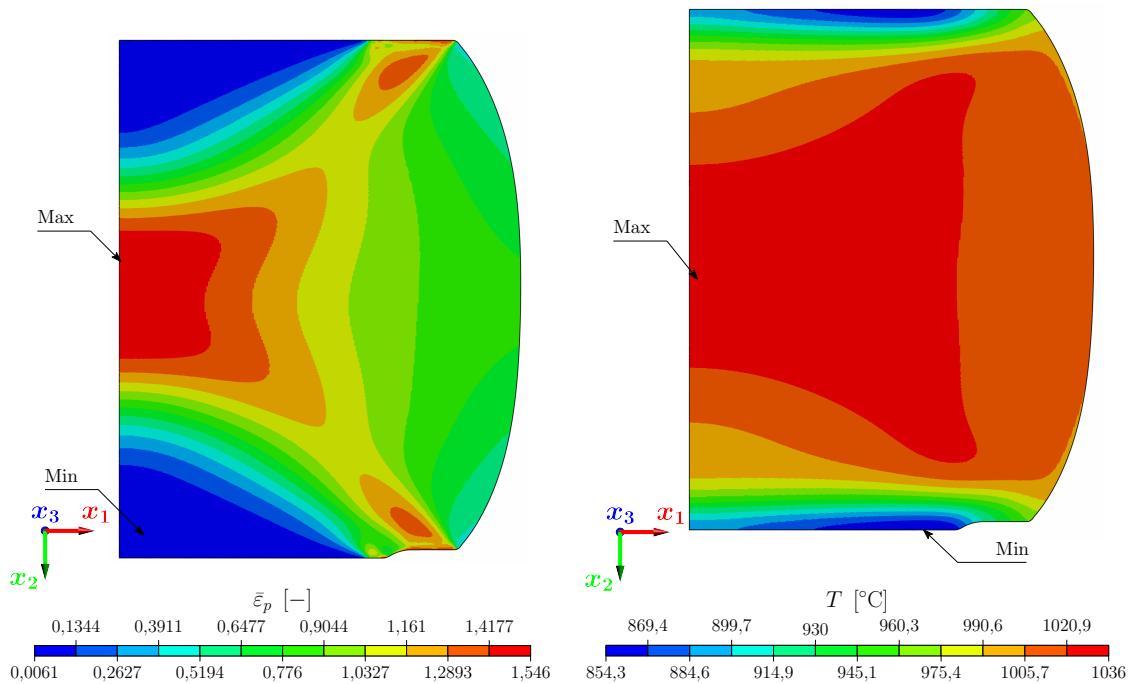


Fig. 7.2: Results after upsetting-rod $\varnothing 36$, temperature 1000 °C

⁸⁶As previously said in Chap. 6, a deformation caused by a temperature is involved geometry yet and there is zero strain state at a process beginning of a forming process.

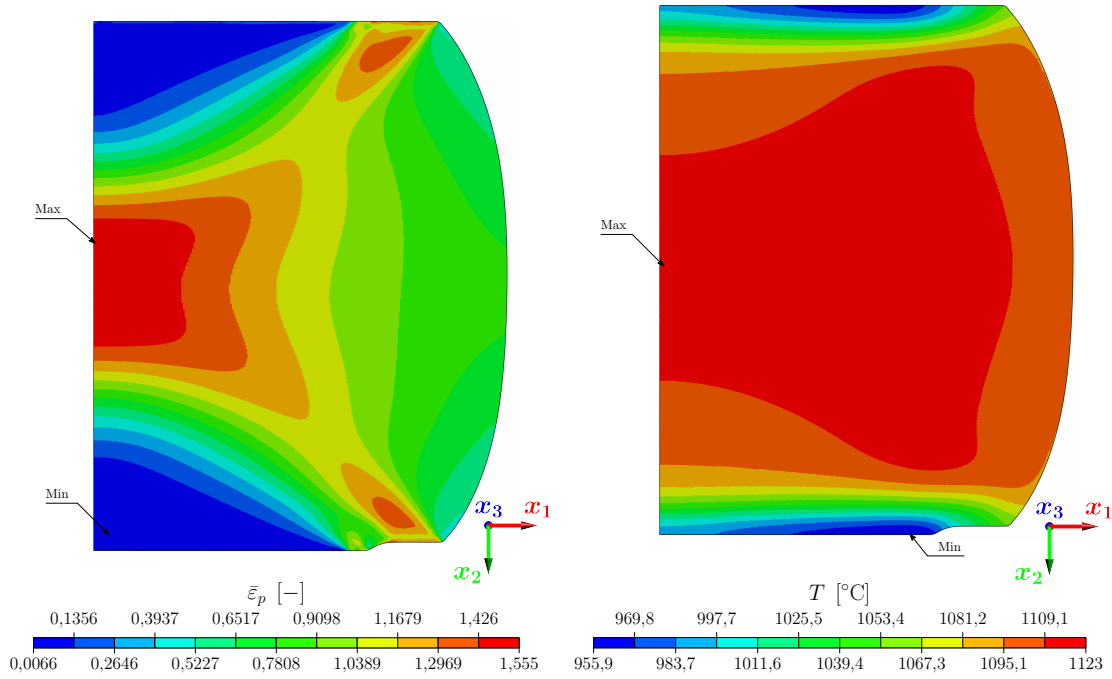


Fig. 7.3: Results after upsetting-rod $\varnothing 36$, temperature 1100 °C

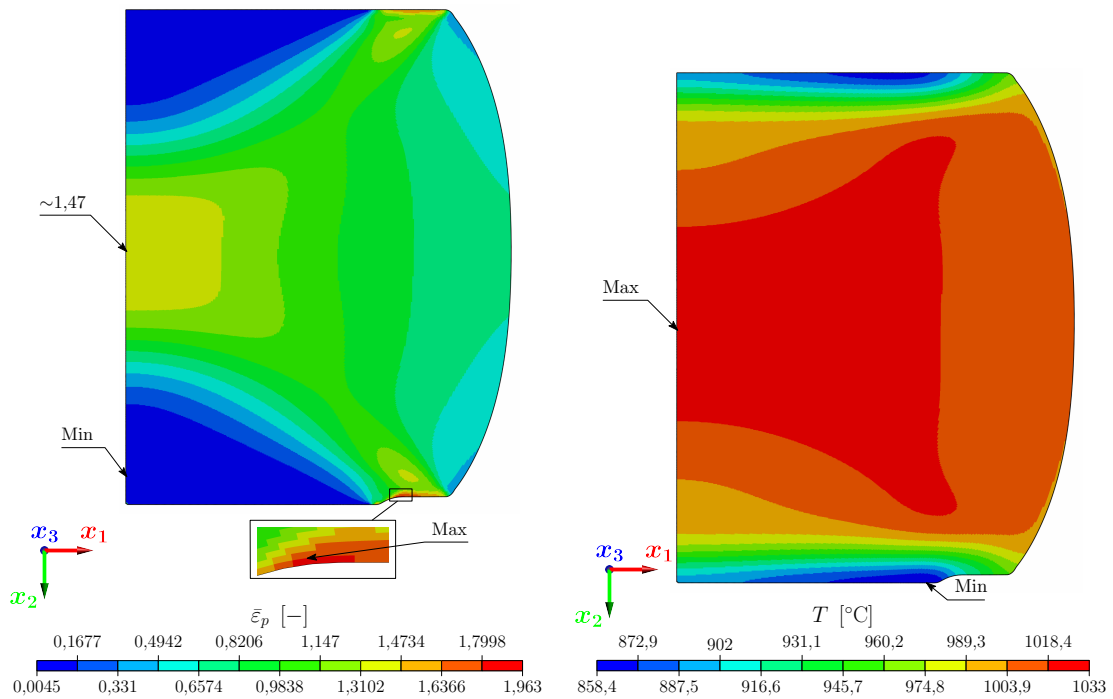


Fig. 7.4: Results after upsetting-rod $\varnothing 38$, temperature 1000 °C

7.1.2 Blocking

Larger shape changes and larger deformations occur during a blocking operation, which would lead without an adaptive meshing to an analysis termination (see Fig. C.2). Nevertheless there occur a local growth of strain with no visible reasons (e.g see Fig. 7.6). A running of strain in an element with a maximal acquired value of strain is displayed in Fig. 7.5. It is visible from the graph, that a steep growth of strain occurs paradoxically during an unload phase, which should be purely *elastic*.

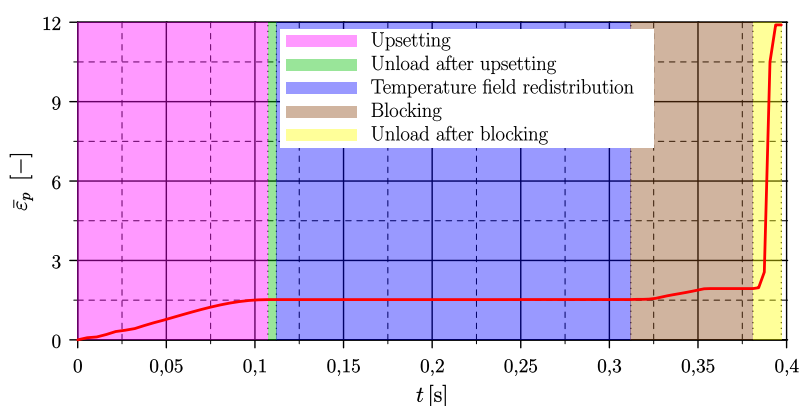


Fig. 7.5: Running of strain in element

There could be an explanation that originally square elements were deformed into rectangles with a big ration of sides, which do not describe properly a stiffness distribution over an element. What is more, a hourglassing can appear because of a reduced integration and it is visible more or less in all solved combinations. A material thermal expansion has minority influence because a contact pressure decreases with a stepwise decreasing load, which has influence on an intensity of transferred heat in a contact. This leads to a quite fast levelling off of temperatures on surfaces with a temperature inside a forging. All these effects are supported by a high mass-scaling necessary for reaching a required time increment size, so inertia forces may occur locally.

In comparison with the rod $\varnothing 36$, an effect of a steep strain growth around an axis does not occur for the rod $\varnothing 38$. On the other hand there is visible a large strain growth in a flash area with a visible mesh degradation. This is caused because of almost half amount of elements (259 200) used for a solution because an

adaptive meshing algorithm crashed during a blocking operation with the same mesh refinement. Because of bigger elements a mass-scaling is decreased too, so this could be an explanation for a reduced strain growth in elements around a forging axis.

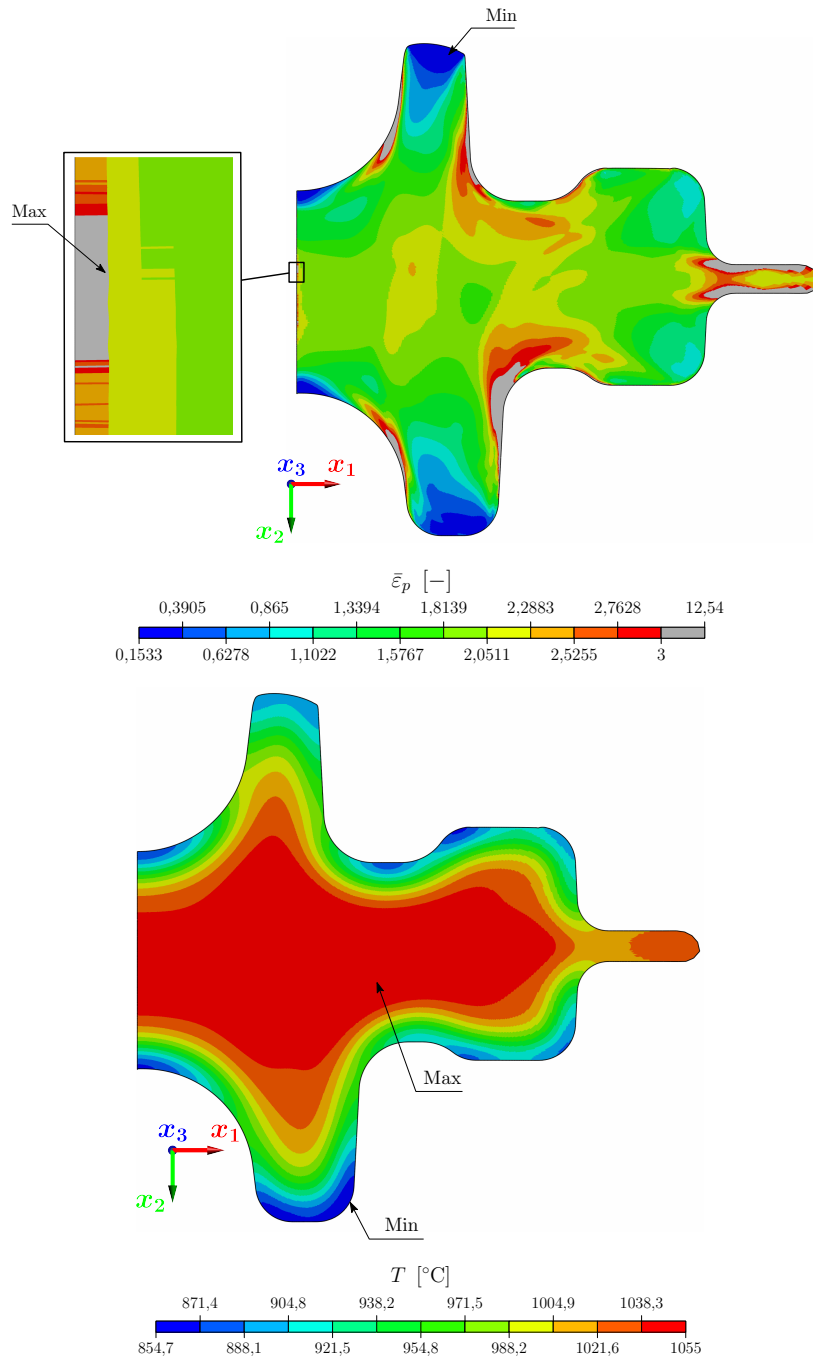


Fig. 7.6: Results after blocking-rod $\varnothing 36$, temperature 1000 °C

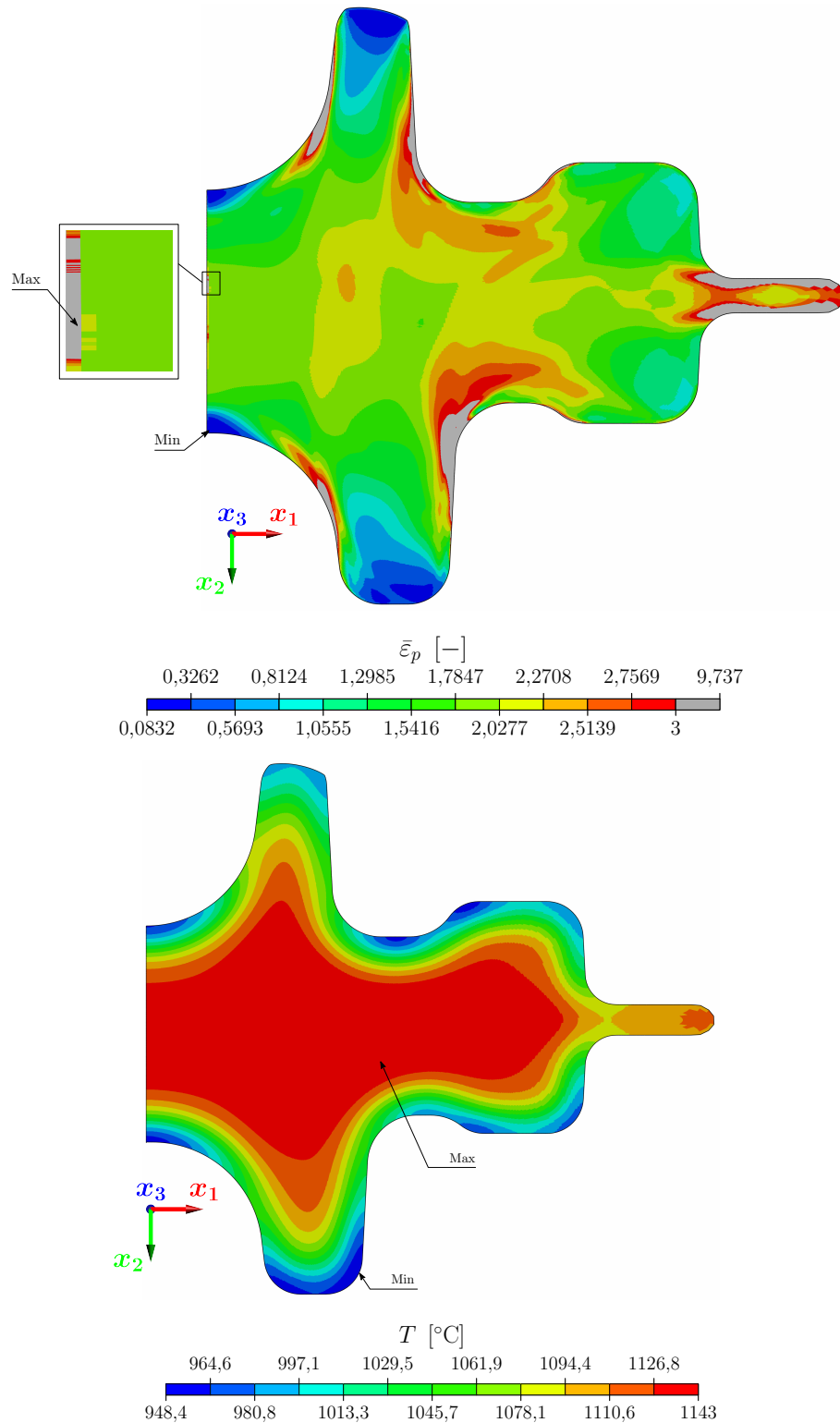


Fig. 7.7: Results after blocking-rod $\varnothing 36$, temperature 1100 °C

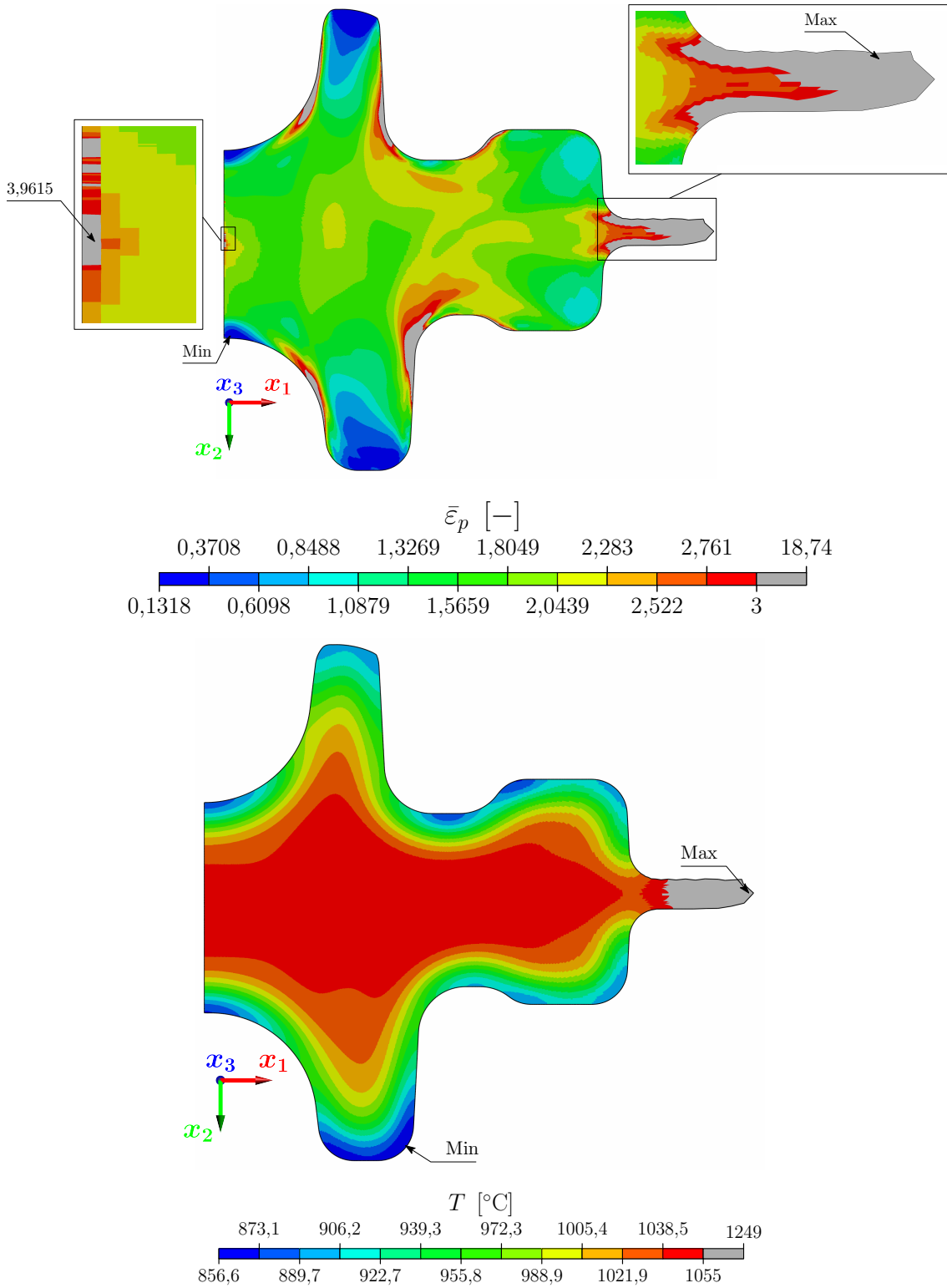


Fig. 7.8: Results after blocking-rod $\varnothing 38$, temperature 1000 °C

7.1.3 Finishing

Results after a finishing operation are similar to results after a blocking operation in a qualitative aspect. On the other hand it is necessary to point out some important facts. The first one is a comparison of maximal value of strain in Fig. 7.6 and 7.9. We can see that value after a blocking operation is higher than after a finishing one. This absolutely contradicts a definition of *acumulative* equivalent plastic strain (see Eq. (4.11) on p. 46) is characterized by that $\dot{\bar{\epsilon}}_p(t) \geq 0$, where $t \in \langle 0; t_a \rangle$. This phenomenon is caused by that an acquired value of strain is slightly changed by an adaptive meshing.

The second one is a steep strain growth in the rod $\varnothing 38$ on a forging axis, which occurred in the other cases already after a blocking operation due to a hourglassing and a mass-scaling. In this case the growth occurs during a straining phase, what is more, a mesh is regular for the whole time with no visible hourglassing, so results should not be influenced by it. A question is if this high level of strain does not cause a continuity break-up and if a crack appears. A conclusion can be stated after checking an evolution of a stress triaxiality η in an area with a high strain that a continuity break-up should not appear because a stress triaxiality is significantly negative for the whole time ($\eta < -2$). According to figures in Sec. 4.3.2 a fracture strain has high value in this area or a stress state is in a cut-off region if a criterion contains it.

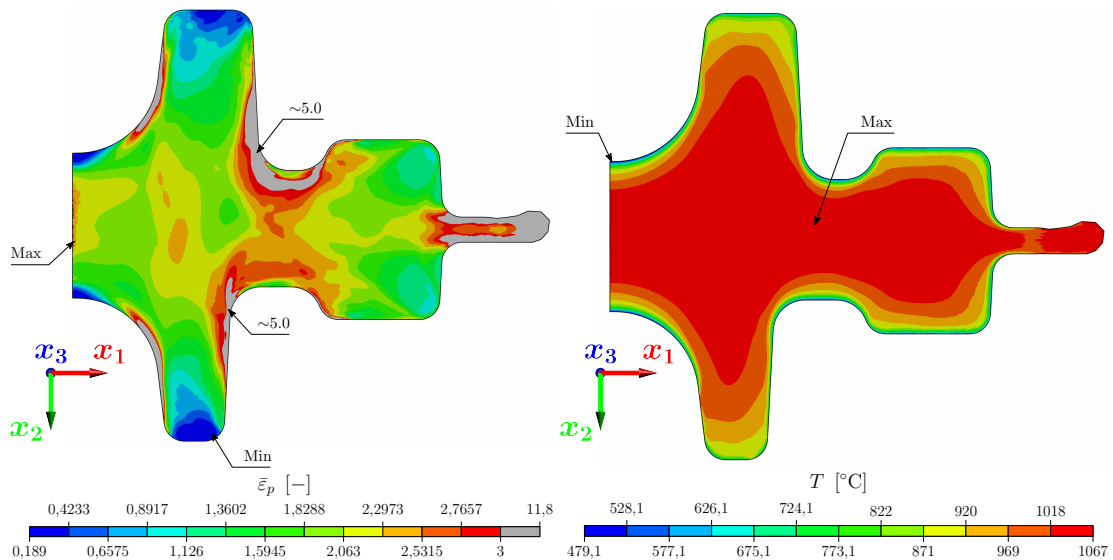


Fig. 7.9: Results after finishing-rod $\varnothing 36$, temperature $1000\text{ }^{\circ}\text{C}$

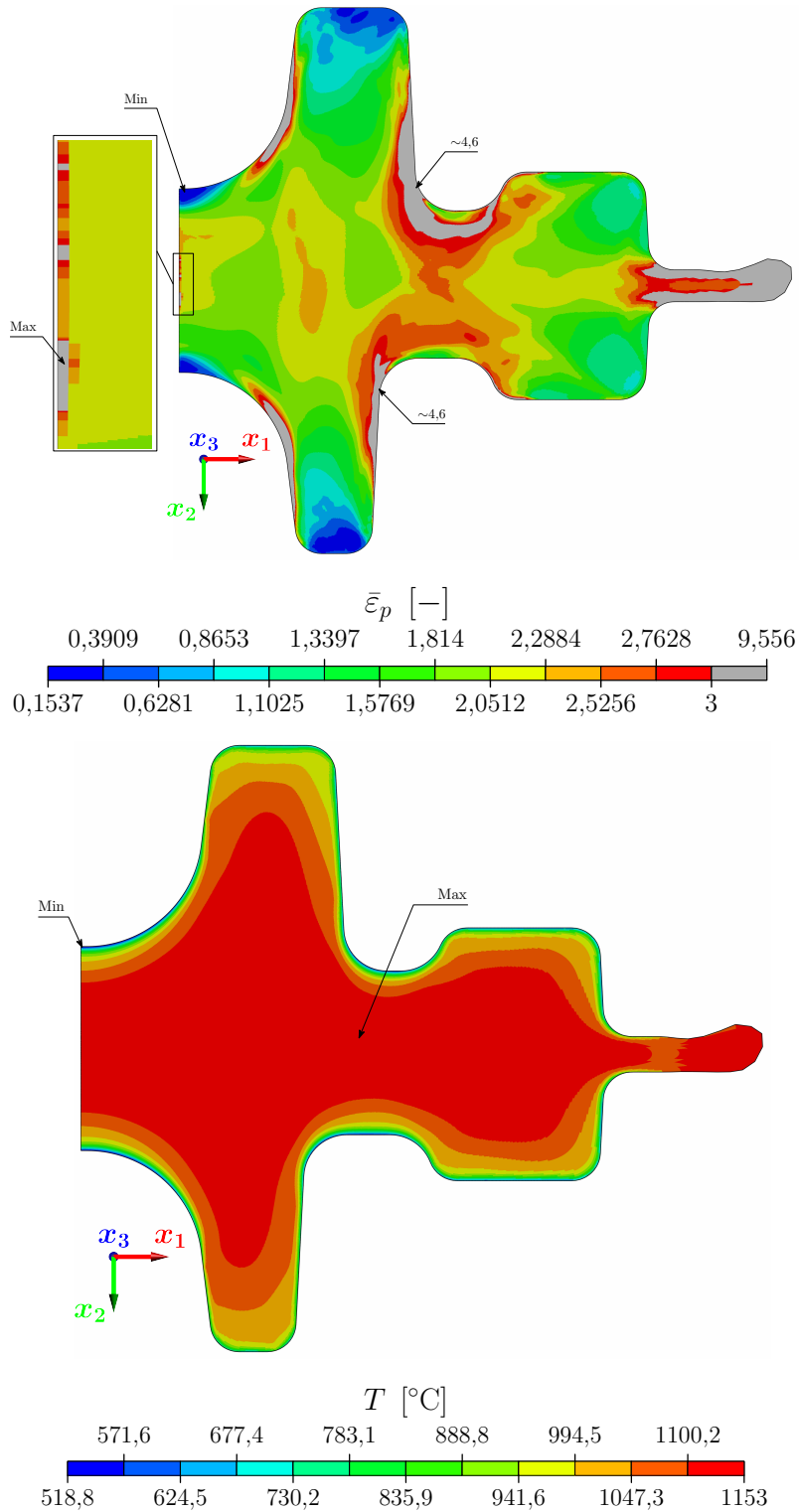


Fig. 7.10: Results after finishing-rod $\varnothing 36$, temperature 1100°C

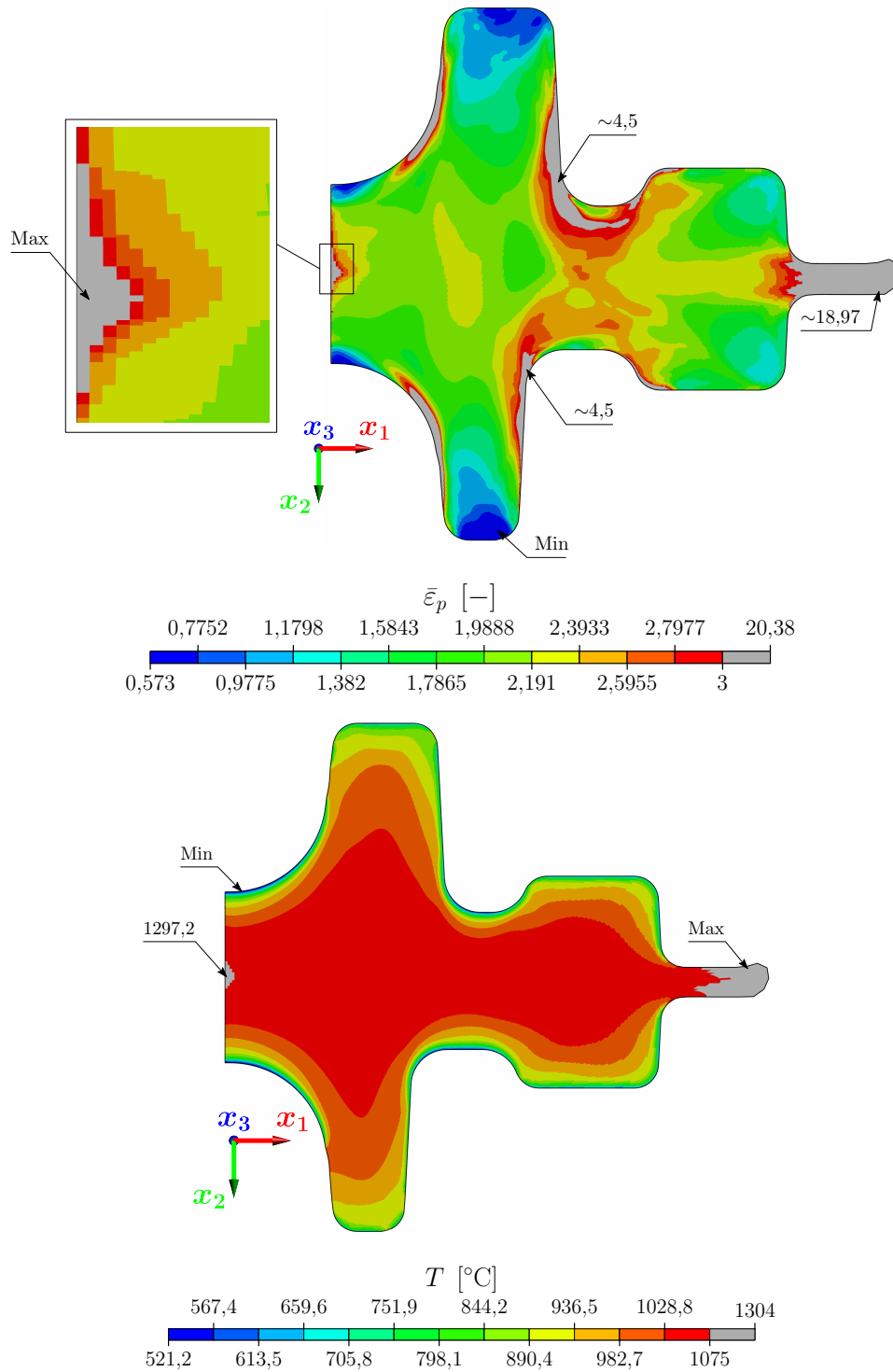


Fig. 7.11: Results after finishing-rod $\varnothing 38$, temperature 1000°C

The other dangerous places are regions, where a material which has to overcome filleted surfaces (grey areas in figures under outer surfaces of a forging) occurs. Areas around a preforged hole has a lower value of strain, so a strain value is written only for outer diameters.

7.1.4 Forming forces

In Fig. 7.12 up to 7.14 are displayed evolutions of a reaction force in an axial direction for non-moving parts of tools. In all graphs is visible a fact that time axes for the rod $\varnothing 36$ and $\varnothing 38$ are different. As previously said in Sec. 6.7, moving parts of tools move along only necessary part of their trajectory, which is given by a distance between an initial and a final configuration Δh . This distance influences a process duration according to Eq. (6.6a) and (6.6b) on p. 77. Because a final barrel height is the same for both diameters and the rod $\varnothing 38$ is shorter, so a time required for an upsetting is shorter too.

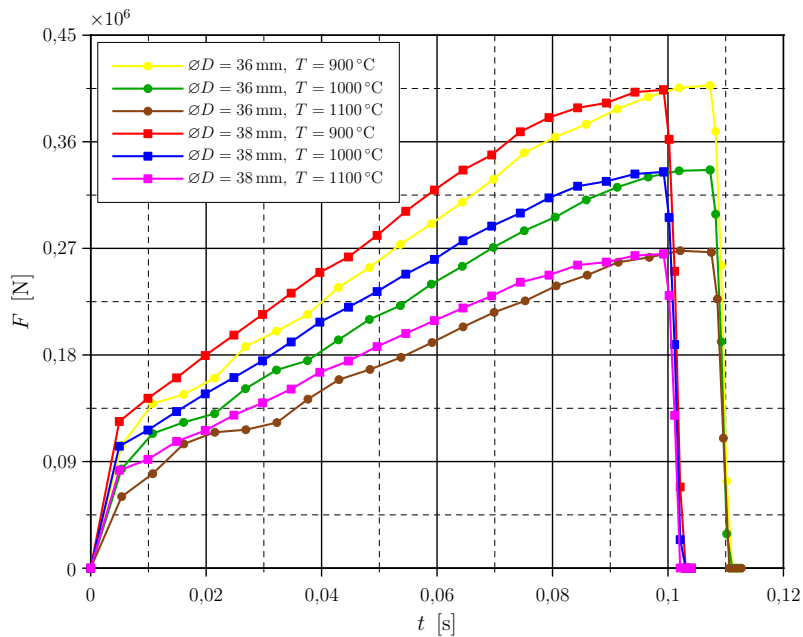


Fig. 7.12: Evolution of axial force during upsetting

It is visible from Fig. 7.12 that a temperature T has more significant influence on a force magnitude, an influence of a diameter for the same temperature is not as big.

A similar trend is visible in Fig. 7.13. A higher sampling frequency should be considered for results saving according to that more complicated shape changes and a motion of material occur during a blocking operation. However, result files consumed about 7.8 GB for the rod $\varnothing 36$, respectively about 5.7 GB for the rod $\varnothing 38$ with settings mentioned in Sec. 6.9. So it would be tricky to store so much data for all analysis with a higher sampling frequency.

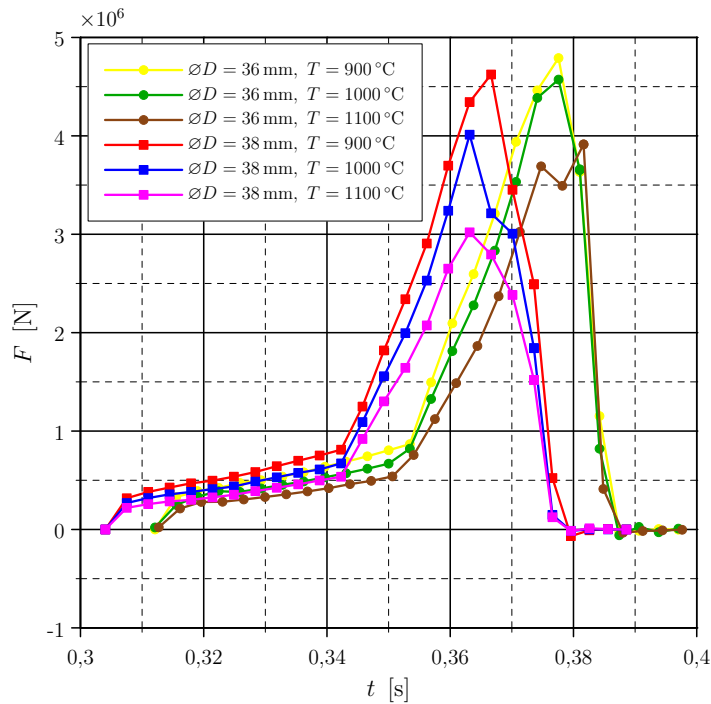


Fig. 7.13: Evolution of axial force during blocking

A trend that an axial decreases with increasing temperature T is not visible properly for the rod $\varnothing 38$ any more. An evolution for the rod $\varnothing 38$ and a the temperature $1000\text{ }^{\circ}\text{C}$ can be zkrslen by a low sampling frequency, because some local extrema may be situated between two neighbour existing samples. A result for the rod with the same diameter and a temperature $1100\text{ }^{\circ}\text{C}$ is surprising too, where a force is maximal for the diameter 38 mm . A possible explanation is that a force, decreased because of a decreased stiffness due to a higher temperature, was compensated because bigger volume compression was needed. Volumes for all solved combinations are mentioned in Tab. 7.2.

Tab. 7.2: Input material volume

Input material	Initial temperature [°C]	Rod volume after heating [mm ³]
∅36 – 89.5	900	94 287.1
	1000	94 919.3
	1100	95 566.2
∅38 – 82.5	900	96 837.8
	1000	97 488.7
	1100	98 154.0

In comparison with the rod ∅36, volumes for the rod ∅38 are bigger, because else a total fill of a die was not acquired, meanwhile a tool size was the *same* for all combinations. This means that a higher ratio of diagonal components was present in an elastic strain tensor ϵ_e for the rod ∅38. These components have influence on a volume change during straining (see Sec. 4.1 on p. 43).

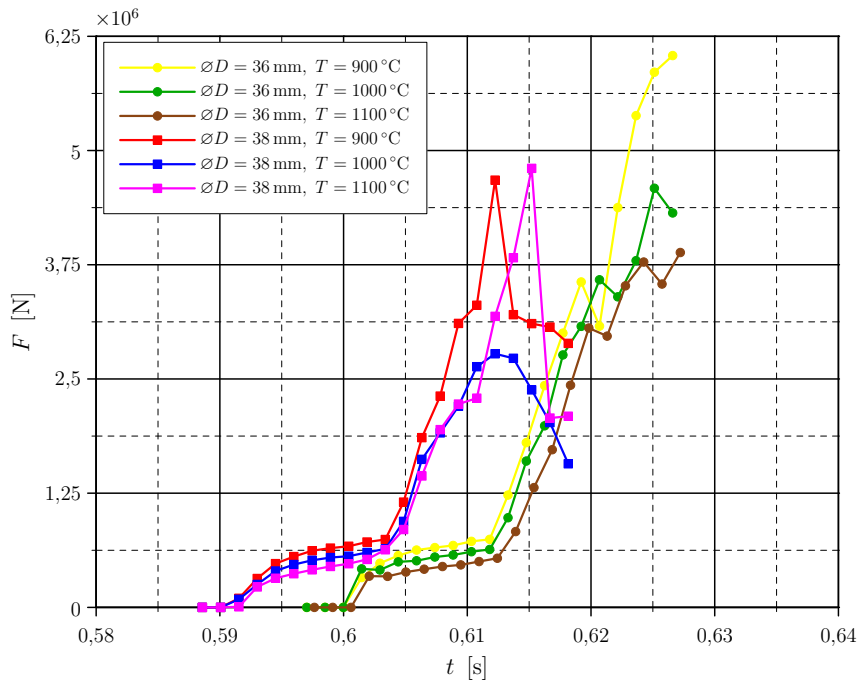


Fig. 7.14: Evolution of axial force during finishing

7.2 Simulation with Ductile Damage

A combination of the rod $\varnothing 38$ and 1000°C is solved now only, where an evolution of a damage parameter according to Johnson-Cook ductile damage criterion is observed how a forming goes on.

A damage parameter field after upsetting (see Fig. 7.15) is very similar to an equivalent plastic strain field in Fig. 7.2 on p. 87. This is because there are no significant changes of quantities characterizing stress state (here only η), which influences a fracture strain according to Eq. (4.23) on p. 55

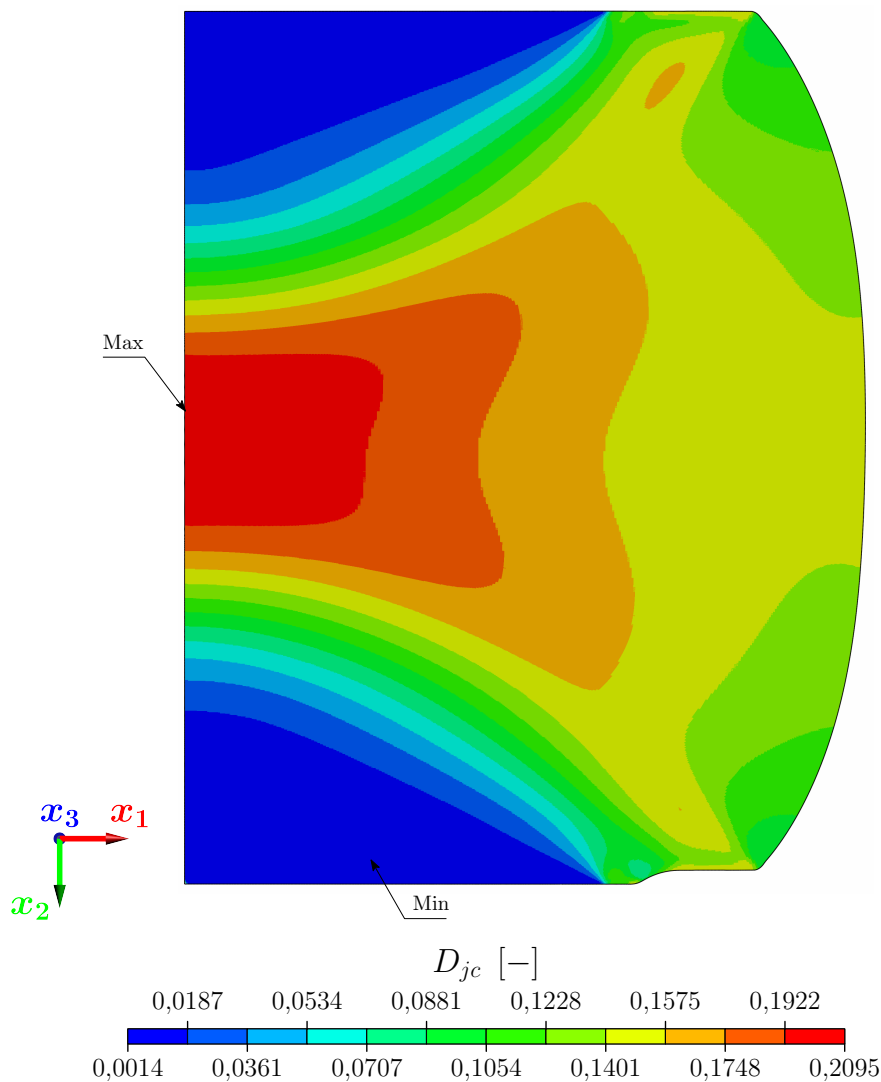


Fig. 7.15: Damage parameter after upsetting

A situation after blocking (see Fig. 7.16) is slightly different. If we omit a maximum nearby a forging axis, which is probably caused by a hourglassing (see Sec. 7.1.2), then a high value is visible by outer diameters of a forging.

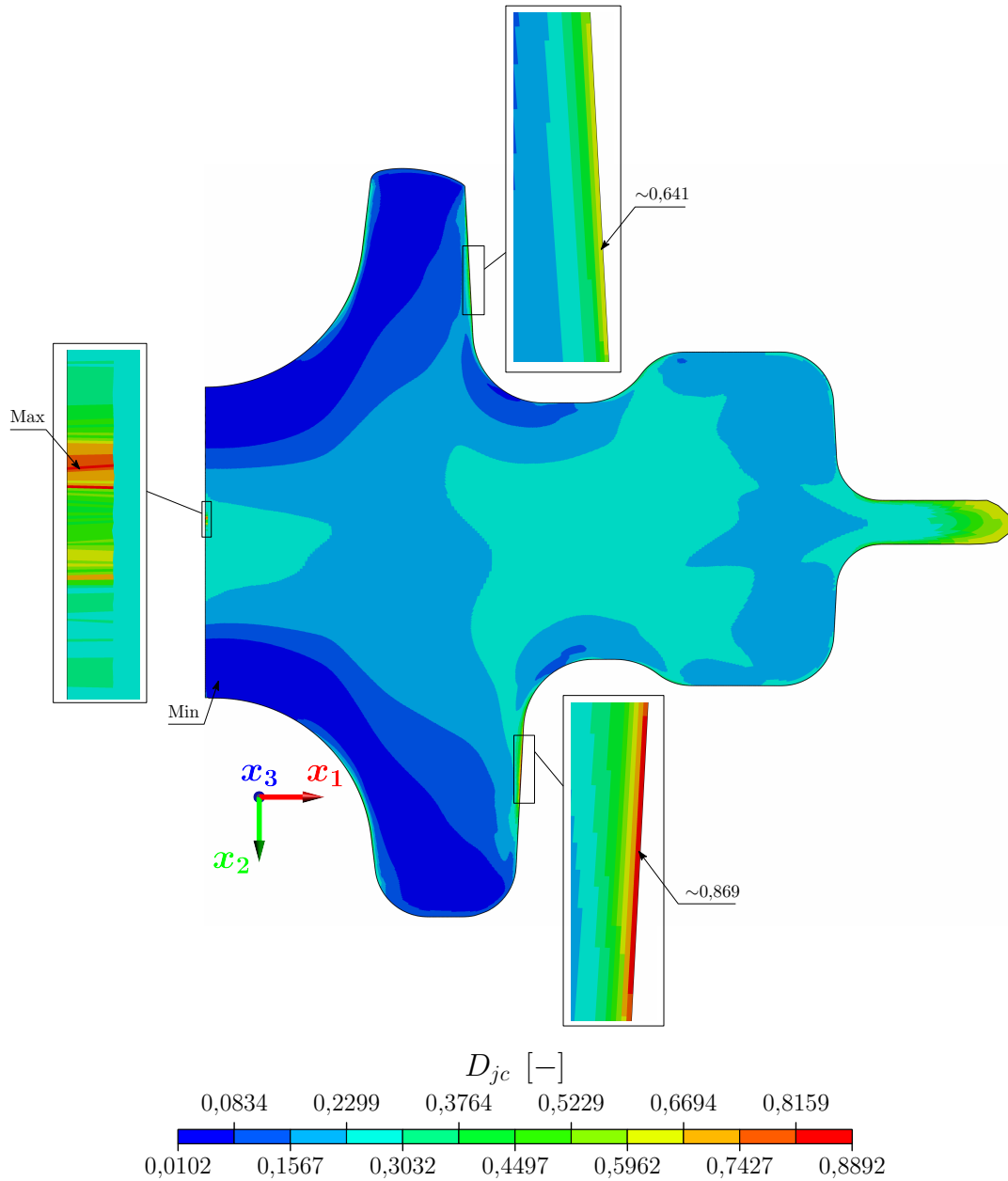


Fig. 7.16: Damage parameter after blocking

This is caused by motion of material over a filleted surface with a smaller fillet radius than preforged holes have. This causes a steep growth of strain, however a damage parameter given by Eq. 4.24 on p. 55 is also dependent on an evolution of a fracture strain. The second aspect is a rubbing on die surfaces, which causes a significant shear stress. A simple shear stress is situated in $\eta - \xi$ coordinate system in point $[0; 0]$, where a resistance of material against damage cumulation is in general smaller than in compression stress state, which was dominant during upsetting.

However, elements were not eliminated because the condition $D_{jc} = 1$ was not fulfilled. An elimination of elements would mean an initiation of surface cracks and a subsequent stress concentration. Furthermore, two cases may occur. The first one is that cracks might propagate and could lead on up to failure during a forming or a subsequent service. The second one is that a crack stops.

Values in above described areas do not change significantly during finishing (see Fig. 7.17) and a part continuity was not broken up. However, some elements were eliminated in an area of a flash as can be seen in the figure. However, a redundant material is situated in this area, which is subsequently removed by trimming (see Sec. 3.3.2).

In Fig. 7.18 on p. 103 is displayed a damage parameter in area of a fracture surface where a large distortion of elements is visible. As was shown yet in a thesis [28], the Johnson-Cook criterion is not the most inappropriate for simulations of processes with damage where a shear stress state is dominant. In Fig. 7.19 on p. 104 is displayed an expanded deformed shape after trimming of a flash

In Sec. 2.5.1 was mentioned a tolerated amount of an artificial energy E_a .⁸⁷ An evolution of an internal energy E_i and a ratio of mentioned energies is displayed in Fig. 7.20 on p. 104. It is visible from a graph that a mentioned condition is fulfilled.

⁸⁷Energy caused by a hourglassing.

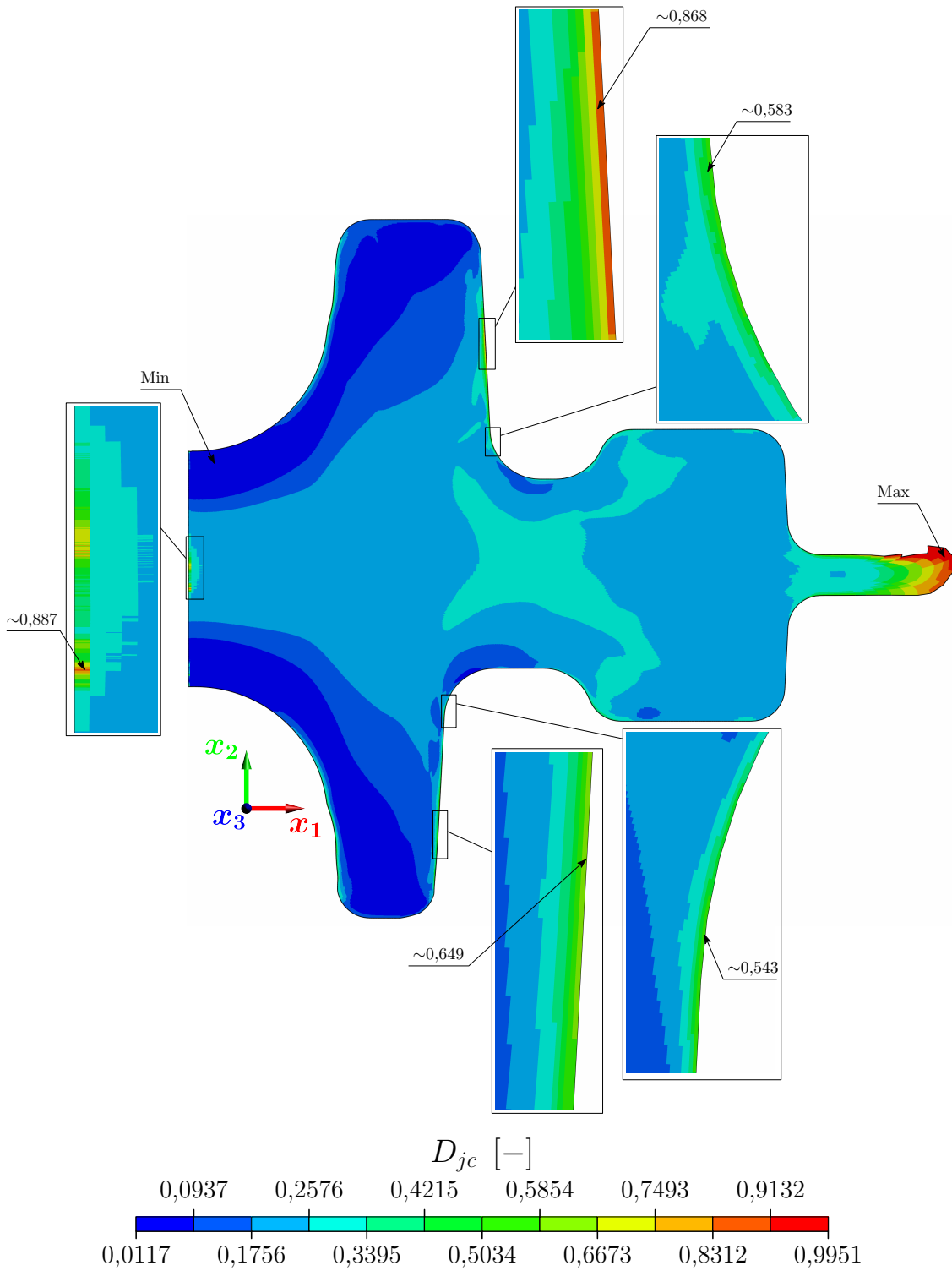


Fig. 7.17: Damage parameter after finishing

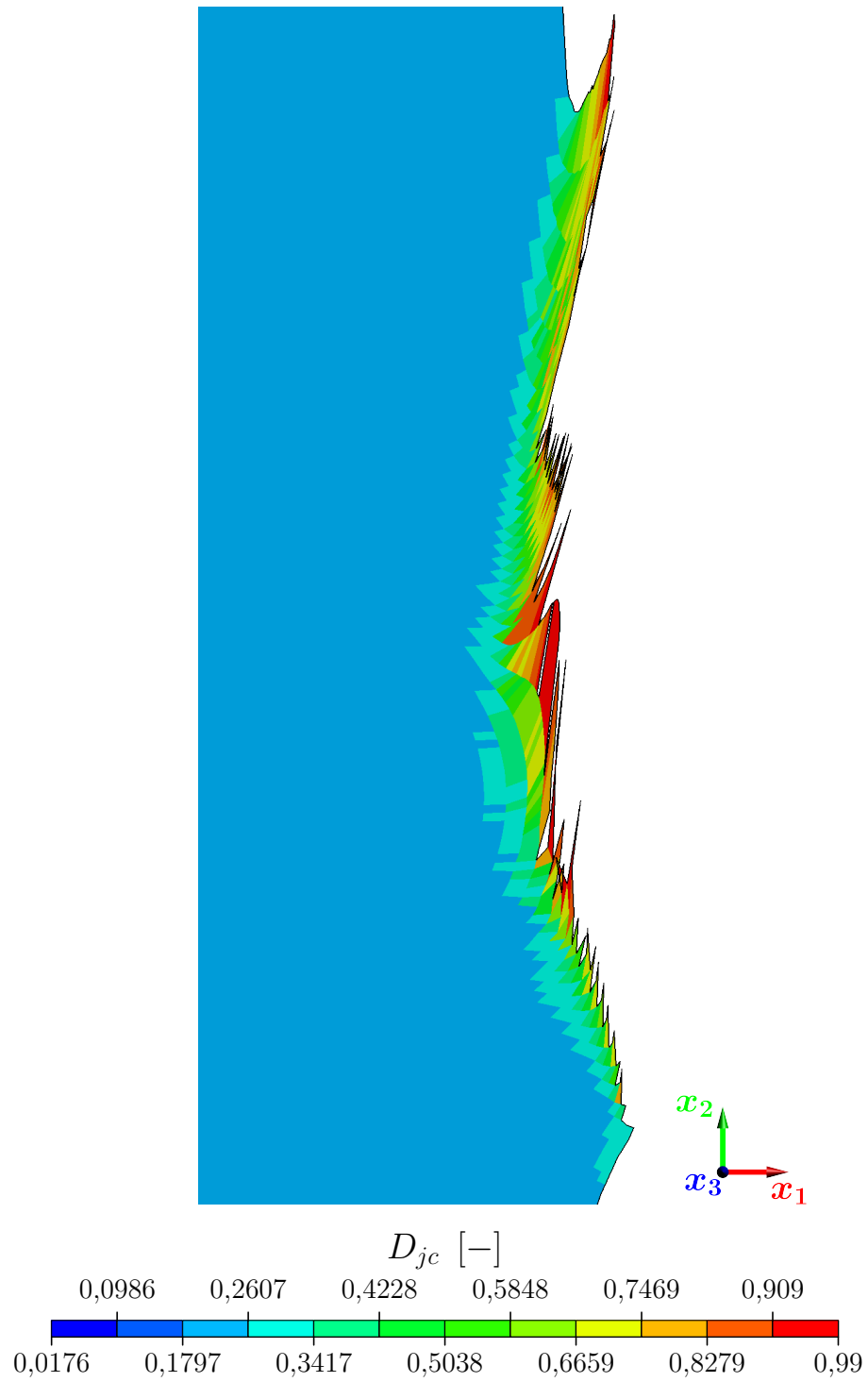


Fig. 7.18: Fracture surface

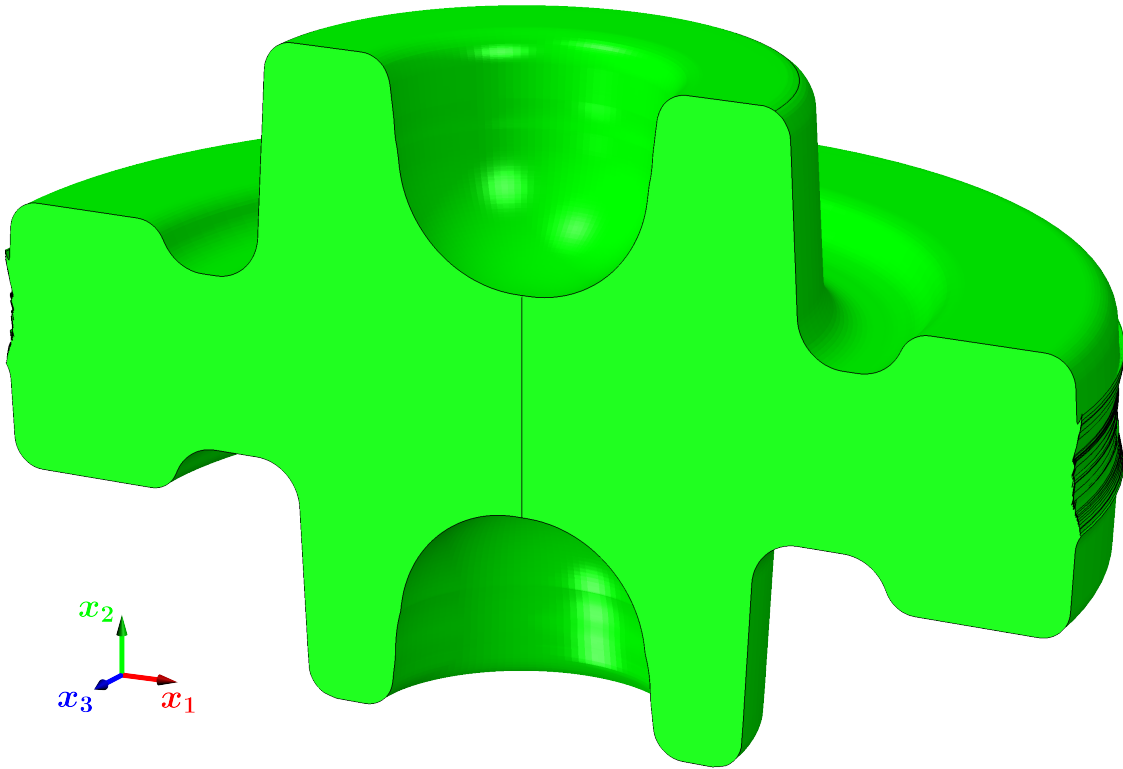


Fig. 7.19: Deformed shape after trimming of flash

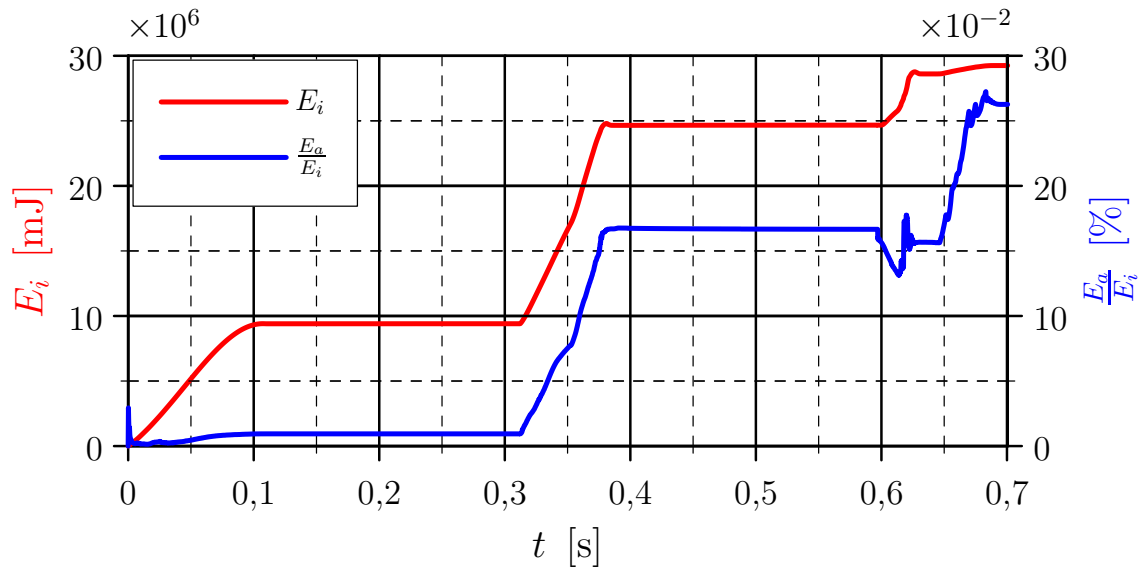


Fig. 7.20: Evolution of internal and artificial energy

8 Conclusion

8.1 Summarization

This thesis is aimed on a FEM simulation of a closed-die forging process belonging into a group of bulk forming methods. It's a *strongly non-linear* problem from an aspect of solid mechanics because it's bonded with large deflections (mainly plastic), non-linear behaviour of material (large plastic strain, important temperature dependency) and large non-stationary contacts (friction, cooling in close surrounding of contacts leading to a local stiffness change).

In an introductory part is a reader acquainted with motivation leading to an origin of this thesis and its targets. Follows a description of a solved problem, an evaluation of essential variables incoming into a solution, a method's choice and its short description. There is also shown a concrete mechanical part, which a spur gear from a car gearbox

After this there are three chapters focused more theoretically, but serve to understand the context and patterns connected to the solved problematics, especially possibilities and limits of a closed-die forging technology (see Chap. 3), constitutive laws for metal based solid substances (especially iron) and characteristics of material required for a solution (see Chap. 4) and in conclusion patterns for heat transfer in solid substances, between solid substances and their surroundings and between bodies in a contact (see Chap. 5).

For the whole thesis is the most important Chap. 6, where is in detail described a procedure how to create a computational model in a software Abaqus CAE, which serves to create an input file for FEM solver of the mentioned software. There have been created within this chapter auxiliary programs in IDE Delphi and a language Pascal making easier to gain inputs for the computational model. There has been chosen an explicit solver for all forming simulations from these reasons

1. Beyond the thesis has been a will to simulate flash trimming after a finishing operation. An element elimination method serving for a crack initiation and propagation in solid bodies is available only for the explicit solver, an implicit solver terminates after eliminating a couple of elements.

2. An author expected large deflections and shape changes connected with the bulk forming become unmanageable for the implicit solver and the forming terminates before a final phase. The explicit solver is also better because of a large amount of contacts in this analysis.
3. A fine time stepping which is a condition for a stability of an explicit algorithm (see Sec. 2.5.1) makes better to solve strongly non-linear problems of the solid body mechanics.⁸⁸
4. On simulation basis has been found out for fully coupled thermal-structural analysis solved by the implicit algorithm doesn't work a heat transfer between a deformable body and a "Discrete Rigid" body type. This problem has been discussed with a support of a software provide, however it hasn't been solved.

8.2 Future Works

- Make experiments to calibrate flow curve for temperatures up to ca. 1200 °C.
- Design and calibrate ductile damage criterion which depends on a stress tri-axiality η (see Eq. (4.19) on p. 53), a normalized third invariant of deviatoric stress tensor ξ (see Eq. (4.20b) na str. 54) and a temperature T , e.g. extend KHPS criterion by a temperature dependency.
- Assess a solution possibilities of the similar forming problems type with the implicit algorithm
- Try a closed-die forging simulation on a 3D geometry.
- Assess an influence of a finite stiffness of dies and a formign machines on a final forging's deformation.

⁸⁸A very small time step has also some risks (rounding error).

Bibliography

- [1] KUBÍK, Petr. *Implementace, kalibrace a využití podmínek tvárného lomu v programech MKP*. Brno, 2015. 106 s. Dizertační práce. Vysoké učení technické v Brně, Fakulta strojního inženýrství. Vedoucí práce prof. Ing. Jindřich Petruška, CSc..
- [2] JANÍČEK, Přemysl. *Systémová metodologie: brána do řešení problémů*. Brno: Akademické nakladatelství CERM, 2014, 374 s. ISBN 978-80-7204-887-8.
- [3] ČSN 41 2050. *Ocel 12050*. Praha: Vydavatelství Úřadu pro normalizaci a měření, 1978. 16 s. Třídící znak 41 2050.
- [4] PETRUŠKA, Jindřich. *MKP v inženýrských výpočtech* [online]. Brno, 2011 [cit. 2019-03-05]. Dostupné z <http://www.umd.fme.vutbr.cz/images/opory/MKP%20v%20inzenyrskych%20vypoctech/RIV.pdf>.
- [5] JANÍČEK, Přemysl. *Mechanika těles: pružnost a pevnost I*. 3. přeprac. vyd. Brno: CERM, 2004. 287 s. ISBN 80-214-2592-X.
- [6] DASSAULT SYSTÈMES. *Abaqus 6.11 documentation collection* [online]. 2011 [cit. 2019-03-05]. Available from: <http://130.149.89.49:2080/v6.11/index.html>
- [7] BOŘKOVEC, Jan. *Výpočtová simulace procesu dělení materiálu*. Brno, 2008. 100 s. Dizertační práce. Vysoké učení technické v Brně, Fakulta strojního inženýrství. Vedoucí práce prof. Ing. Jindřich Petruška, CSc..
- [8] HAŠEK, Vladimír. *Kování*. 1. vyd., Praha: SNTL, 1965. 732 s. ISBN 04.233-65.
- [9] FOREJT, Milan. *Teorie tváření*. 2. vyd., Brno: Akademické nakladatelství CERM, 2004. 167 s. ISBN 80-214-2764-7.
- [10] DVOŘÁK, Milan. *Technologie II*. 3. vyd., Brno: Akademické nakladatelství CERM, 2004. 238 s. ISBN 80-214-2683-7.
- [11] FOREJT, Milan a Miroslav PÍŠKA. *Teorie obrábění, tváření a nástroje*. Brno: Akademické nakladatelství CERM, 2006. 225 s. ISBN 80-214-2374-9.

- [12] ČSN EN 10243-1. *Ocelové zápusťkové výkvy - Mezní úchytky rozměrů - Část 1: Výkvy kované na bucharech a svislých kovacíh lisech*. Praha: Český normalizační institut, 2003. 40 s. Třídící znak 42 9031.
- [13] ČSN 42 9030. *Výkvy ocelové zápusťkové: Příkladky na obrábění, mezní úchytky rozměrů a tvarů*. Praha: Vydavatelství Úřadu pro normalizaci a měření, 1987. 24 s. Třídící znak 42 9030.
- [14] DVOŘÁK, Milan, František GAJDOŠ a Karel NOVOTNÝ. *Technologie tváření: plošné a objemové tváření*. 4. vyd., Brno: Akademické nakladatelství CERM, 2007. 169 s. ISBN 978-80-214-3425-7.
- [15] ČSN 22 8308. *Zápusťky pro buchary: Směrnice pro konstrukci*. Praha: Vydavatelství Úřadu pro normalizaci a měření, 1971. 20 s. Třídící znak 22 8308.
- [16] ČSN 22 8306. *Zápusťky pro svislé kovací lisy: Technické požadavky na konstrukci*. Praha: Vydavatelství norem, 1991. 40 s. Třídící znak 22 8306.
- [17] ONDRÁČEK, Emanuel. *Mechanika těles: pružnost a pevnost II*. 4. vyd., Brno: Akademické nakladatelství CERM, 2006. 262 s. ISBN 80-214-3260-8.
- [18] PETRUŠKA, Jindřich. *Přednášky z předmětu RNU (Nelineární úlohy mechaniky v MKP)* [online]. Akademický rok 2017/2018. Vysoké učení technické v Brně, Fakulta strojního inženýrství, 2018 [cit. 2018-09-29]. Dostupné z: <http://www.umt.fme.vutbr.cz/images/opory/Nelinearni%20ulohy%20mechaniky%20v%20MKP/RNK.zip>.
- [19] TÖRNQVIST, Rikard. *Design of Crashworthy Ship Structures*. Kongens Lyngby, 2003. 268 p. ISBN 87-89502-74-4. PhD Thesis. Technical University of Denmark, Department of Mechanical Engineering. Thesis supervisors Associated Professor Bo Cerup Simonsen, Professor Preben Terndrup Pedersen.
- [20] ŠEBEK, František. *Ductile Fracture Criteria in Multiaxial Loading – Theory, Experiments and Application*. Brno, 2016. 116 p. PhD Thesis. Brno University of Technology, Faculty of Mechanical Engineering. Thesis supervisor prof. Ing. Jindřich Petruška CSc..
- [21] INCROPERA, Frank P. *Fundamentals of heat and mass transfer*. 6th ed. Hoboken, New Jersey: John Wiley, 2007, 997 s. ISBN 978-0-471-45728-2.

- [22] KVAPIL, Jiří. *Tepelný odpor v kontaktu těles za vysokých teplot*. Brno, 2016. 93 s. Dizertační práce: Vysoké učení technické v Brně, Fakulta strojního inženýrství. Vedoucí dizertační práce prof. Ing. Jaroslav Horský, CSc..
- [23] TANG, Qingyun and Weifang ZHANG. *The effect of pressure on thermal contact conductance of superalloys under high temperature*. International Journal of Heat and Mass Transfer [online]. 2016, **103**, 1208-1213 [cit. 2018-05-25]. DOI: 10.1016/j.ijheatmasstransfer.2016.08.028. ISSN 00179310. Available from: <https://linkinghub.elsevier.com/retrieve/pii/S0017931016303118>.
- [24] ČSN EN 10060. *Ocelové tyče kruhové válcované za tepla - Rozměry, mezní úchytky rozměrů a tolerance tvaru*. Praha: Český normalizační institut, 2004. 12 s. Třídící znak 42 5551.
- [25] KOUDELA, Lukáš. *Numerické modelování a optimalizace procesů lisování za tepla*. Plzeň, 2015. 72 s. Dizertační práce. Západočeská univerzita v Plzni, Fakulta elektrotechnická, 2015.72 s. Vedoucí práce doc. Ing. Pavel Karban, Ph.D.
- [26] JORGE JR., Alberto Moreira and Oscar BALANCIN. *Prediction of steel flow stresses under hot working conditions*. Materials Research [online]. 2005, **8**(3), 309-315 [cit. 2018-11-14]. DOI: 10.1590/S1516-14392005000300015. ISSN 15161439. Available from: <https://linkinghub.elsevier.com/retrieve/pii/S0017931016303118>.
- [27] DUAN, Chun Zheng, Hai Yang YU, Yu Jun CAI and Yuan Yuan LI. Finite Element Simulation and Experiment of Chip Formation during High Speed Cutting of Hardened Steel. *Applied Mechanics and Materials*. 2010, **29-32**, 1838-1843. DOI: 10.4028/www.scientific.net/AMM.29-32.1838. ISSN 1662-7482. Available from: <https://www.scientific.net/AMM.29-32.1838>.
- [28] HŮLKA, Jiří. *Aplikace modelů tvárného porušování při výpočtové simulaci technologických operací*. Brno, 2008. 84 s. Diplomová práce. Vysoké učení technické v Brně, Fakulta strojního inženýrství. Vedoucí práce prof. Ing. Jindřich Petruška, CSc..
- [29] HOLZAPFEL, Gerhard A. *Nonlinear Solid Mechanics: A Continuum Approach for Engineering*. New York: John Wiley, 2000. ISBN 04-718-2304-X.

- [30] NĚMEC, Ivan, Miroslav TRCALA a Václav REK. *Nelineární mechanika*. Brno: Vysoké učení technické v Brně, nakladatelství VUTIAM, 2018. ISBN 978-80-214-5519-1.
- [31] BURŠA, Jiří. *Přednášky z předmětu RK0 (Konstitutivní vztahy materiály)* [online]. Akademická rok 2018/2019. Brno: Vysoké učení technické v Brně, Fakulta strojního inženýrství, 2019 [cit. 2018-11-23]. Dostupné z <http://www.old.umt.fme.vutbr.cz/~jbursa/Konstitutivni%20modely.7z>.

List of Most Frequent Abbreviations and Symbols

Latin Abbreviations and Symbols

Sign	Unit	Description	Note
A_{jc}	[Pa]	Flow curve Johnson-Cook constant	
B_{jc}	[Pa]	Flow curve Johnson-Cook constant	
c	$\left[\frac{\text{J}}{\text{kgK}}\right]$	Specific heat	
c_{jc}	[–]	Strain rate hardening exponent (coefficient)	
$C_{1,\dots,4}$	[–]	Xue-Wierzbicki ductile damage criterion material constants	
d_r	[m]	Calculus rod diameter	(6.2), p. 68
D	[m]	Rod diameter	
$D_{1,\dots,5}$	[–]	Johnson-Cook ductile damage criterion material constants	
D_{ab}	[–]	Damage parameter according to criterion ab	4.3.2, p. 53
e^{eng}	[–]	Engineering strain	
e^{true}	[–]	True strain	
f_f	[–]	Friction coefficient	
E	[Pa]	Young's modulus, tensile modulus	
G	[Pa]	Shear modulus	(4.2b), p. 43
Δh	[m]	Distance between an initial and a final position	
J	[–]	Volume ratio	(A.3), p. 118
K	[Pa]	Bulk modulus	$K = \frac{E}{3(1-2\nu)}$

l_{cr}	[m]	Connecting rod length	
L	[m]	Rod length	
m_{jc}	[−]	Temperature softening exponent	
n	[min ^{−1}]	Revolve rate	
n_{jc}	[−]	Flow curve Johnson-Cook strain hardening exponent	
n_{sh}	[−]	Xue-Wierzbicki ductile damage criterion strain hardening exponents	
$N_{1,\dots,6}$	[−]	Bai-Wierzbicki ductile damage criterion material constants	
p, q, r	[Pa]	Stress invariants	(4.14c), p. 47; (4.14d), p. 47; (4.20c), p. 54
p_c	[Pa]	Contact pressure	
$P_{1,\dots,5}$	[−]	KHPS ductile damage criterion material constants	
\dot{Q}^*	[$\frac{W}{m^3}$]	Internal heat sources	
r_{cs}	[m]	Crank radius of a crankshaft	
R_a	[μm]	Arithmetical mean deviation of the assessed profile	
s^{eng}	[Pa]	Engineering stress	
s^{true}	[Pa]	True stress	
S	[m ²]	Actual cross-section size	
S_0	[m ²]	Initial cross-section size	
t	[s]	Time	
Δt	[s]	Time increment	
Δt_c	[s]	Critical time increment	(2.3), p. 24
t_f	[s]	Final time of a process	(6.6b), p. 77
t_i	[s]	Initial time of a process	(6.6a), p. 77
T	[K]	Actual temperature	
T_m	[K]	Melting temperature	
T_r	[K]	Room temperature	
T_∞	[K]	Environment temperature	
T^*	[−]	Homological temperature	(4.17c), p. 50
T_ω	[s]	Period	

v	$[m^3]$	Deformed volume	
V	$[m^3]$	Undeformed volume	
V_f	$[m^3]$	Forging volume	
V_f^*	$[m^3]$	Extended forging volume	
x_i	$[m]$	Deformed configuration coordinates	
x_h	$[m]$	Piston position of a crank mechanism	(3.4a), p. 38
X_i	$[m]$	Undeformed configuration coordinates	
z	$[m]$	Crank mechanism stroke	
\mathbf{C}	$[-]$	Right Green-Cauchy strain tensor	(A.4), p. 118
\mathcal{D}^σ	$[Pa]$	Deviatoric component of a stress tensor	(4.14b), p. 47
$\mathcal{D}^{\varepsilon_p}$	$[-]$	Deviatoric component of a plastic strain tensor	(4.7), p. 45
\mathbf{E}^L	$[-]$	Green-Langrange strain tensor	(A.9), p. 119
\mathbf{E}^{tr}	$[-]$	True (logarithmic) strain tensor	(A.12), p. 120
\mathbf{F}	$[-]$	Deformation gradient	(A.1), p. 117
\mathbf{F}_e	$[N]$	External forces matrix	
\mathbf{F}_i	$[N]$	Internal forces matrix	(2.5), p. 25
\mathbf{I}	$[-]$	Second order identity tensor	
\mathbf{M}	$[kg]$	Mass matrix	
\dot{q}	$[\frac{W}{m^2}]$	Specific heat flux	(5.5), p. 60
\mathbf{R}	$[-]$	Revolve tensor	
\mathbf{U}	$[m]$	Displacement matrix	(2.6b), p. 25
\mathbf{U}_s	$[-]$	Right stretch tensor	
\mathbf{V}_s	$[-]$	Left stretch tensor	
CAE		Complete Abaqus Environment, Computer Aided Engineering	
FEM		Finite Element Method	
IDE		Integrated Development Environment	
VUMAT		Vectorised User MATerial	

Greek Symbols

α	$\left[\frac{\text{W}}{\text{m}^2\text{K}}\right]$	Heat transfer coefficient	
α_c	$\left[\frac{\text{W}}{\text{m}^2\text{K}}\right]$	Conductance	
α_{te}	$[\text{K}^{-1}]$	Temperature expansion coefficient	
δ_f	$[-]$	Addition to forging volume	
δ_{ij}	$[-]$	Kronecker delta	
Δ	$[\text{m}^{-2}]$	Laplace operator	$\Delta = \frac{\partial^2}{\partial x_i^2}$
ε_{rd}	$[-]$	Surface emissivity	
$\bar{\varepsilon}_f$	$[-]$	Fracture strain	4.3.2, p. 53
$\bar{\varepsilon}_p$	$[-]$	<i>Cumulative</i> equivalent plastic strain	(4.11), p. 46
$\dot{\bar{\varepsilon}}_{0p}$	$[\text{s}^{-1}]$	Reference plastic strain rate	
$\dot{\varepsilon}_p^*$	$[-]$	Dimensionless plastic strain rate	(4.17b), p. 50
η	$[-]$	Stress triaxilality	(4.19), p. 53
θ	$[\text{rad}]$	Lode angle	(4.20a), p. 54
$\bar{\theta}$	$[-]$	Normalised Lode angle	(4.21), p. 54
λ_{hc}	$\left[\frac{\text{W}}{\text{mK}}\right]$	Heat conductivity	
λ_l	$[\text{Pa}]$	Lamé constant	(4.2a), p. 43
λ_u	$[-]$	Rod length ratio	$\lambda_u \leq 2.5$
Λ	$\left[\frac{\text{J}}{\text{m}^3} = \text{Pa}\right]$	Strain energy density	(A.13), p. 122
μ	$[-]$	Lode parameter	(4.20d), p. 54
ν	$[-]$	Poisson's ratio	
ξ	$[-]$	Normalised third invariant of the deviatoric stress component	(4.20b), p. 54
ρ	$[\text{m}]$	Cylindrical/spherical coordinate system coordinate	
ρ_d	$\left[\frac{\text{kg}}{\text{m}^3}\right]$	Density	
$\sigma_1, \sigma_2, \sigma_3$	$[\text{Pa}]$	Principal stress	(4.1), p. 43
σ_{eq}	$[\text{Pa}]$	Equivalent stress	

σ_{sb}	$\left[\frac{\text{W}}{\text{m}^2 \text{K}^4}\right]$	Stefan-Boltzmann constant	$\sigma_{sb} = 5.67 \times 10^{-8} \frac{\text{W}}{\text{m}^2 \text{K}^4}$
σ_u	[Pa]	Ultimate stress	
σ_y	[Pa]	Yield stress	
$\bar{\sigma}$	[Pa]	von Mises equivalent stress	(4.14d), p. 47
φ	[rad]	Crankshaft revolve angle	
ϕ	[rad]	Cylindrical/spherical coordinate system coordinate	
Φ	[Pa]	Yield function	(4.3), p. 44
ψ	[rad]	Spherical coordinate system coordinate	
ω	$\left[\frac{\text{rad}}{\text{s}}\right]$	Angular velocity	
ε_e	[-]	Elastic strain tensor	
ε_p	[-]	Plastic strain tensor	
σ	[Pa]	(Cauchy) stress tensor	

A Tensors for Large Deflections

A.1 Strain Tensors

A.1.1 Deformation Gradient

A deformation gradient \mathbf{F} is used for a transformation between deformed and undeformed geometry and its components are defined as

$$F_{ij} = \frac{\partial x_i}{\partial X_j}, \quad (\text{A.1})$$

and in general it is unsymmetric, so it has nine independent components. Its components are non-zero even for a rigid body rotation, so the deformation gradient *cannot* be a measure of a strain [18].

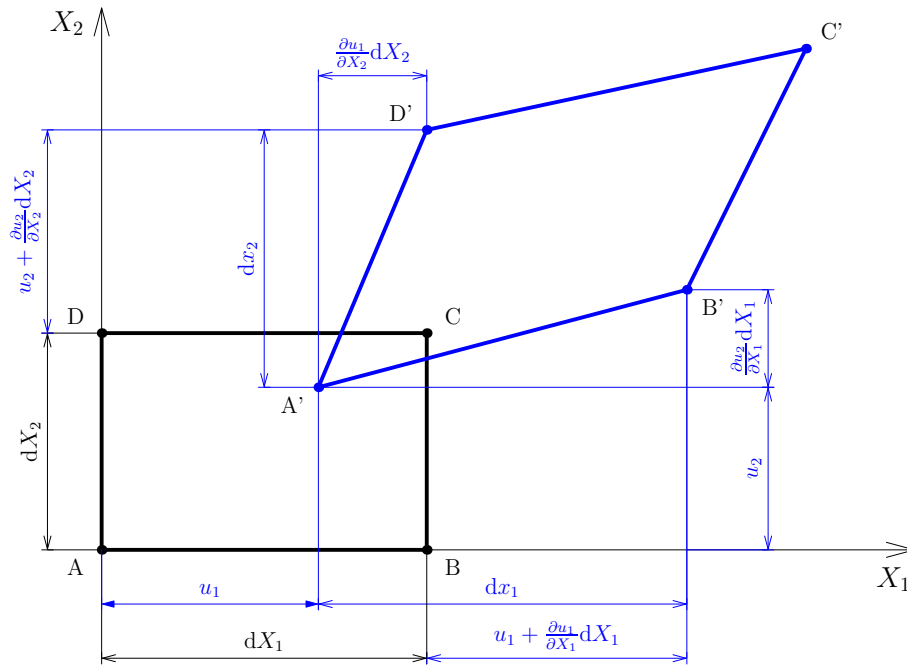


Fig. A.1: Elementary element deformation [18]

So there is performed a polar decomposition defined as

$$\mathbf{F} = \mathbf{R}\mathbf{U}_s = \mathbf{V}_s\mathbf{R}, \quad (\text{A.2})$$

where:

- \mathbf{U}_s $[-]$, respectively \mathbf{V}_s $[-]$ is a right, respectively a left stretch tensor and
- \mathbf{R} $[-]$ is a rotation matrix applying to $\det(\mathbf{R}) = 1$ [18].

The stretch tensors and the rotation matrix are symmetric now, moreover the rotation matrix is orthogonal, so $\mathbf{R}^{-1} = \mathbf{R}^T$. The deformation gradient also quantifies a volume change during a deformation

$$\frac{dv}{dV} = J = \det(\mathbf{F}) = \det(\mathbf{U}_s) \quad [18, 29, 30]. \quad (\text{A.3})$$

It is possible to use the deformation gradient to express several strain tensor, which are symmetric and the rigid body motion is not included.

A.1.2 Right Cauchy-Green Strain Tensor

Right Cauchy-Green Strain Tensor is defined by formulas

$$\mathbf{C} = \mathbf{F}^T \mathbf{F} = \mathbf{U}_s^2, \quad (\text{A.4})$$

eventually in an index notation

$$C_{ij} = F_{ki} F_{kj} \quad [18, 29, 30]. \quad (\text{A.5})$$

In the solid mechanics, there is a big significance of its invariants defined in a *principal* coordinate system as

$$I_1^{\mathbf{C}} = \lambda_1^2 + \lambda_2^2 + \lambda_3^2 = \lambda_k^2, \quad (\text{A.6a})$$

$$I_2^{\mathbf{C}} = \lambda_1^2 \lambda_2^2 + \lambda_1^2 \lambda_3^2 + \lambda_2^2 \lambda_3^2 = \frac{\lambda_i^2 \lambda_j^2 (1 - \delta_{ij})}{2}, \quad (\text{A.6b})$$

$$I_3^{\mathbf{C}} = \lambda_1^2 \lambda_2^2 \lambda_3^2 = \det(\mathbf{C}) = J^2 \quad [31]. \quad (\text{A.6c})$$

These invariant have a big significance mainly in a hyperelastic theory, where the invariant are used to express a strain energy density Λ . It is necessary to mention that Eq. (A.6a), (A.6b) a (A.6c) apply for incompressible or almost incompressible materials.⁸⁹ In the opposite case, it is necessary to use deviatoric components of principal stretches $\bar{\lambda}_i$ for which applies

$$\bar{\lambda}_i = \frac{\lambda_i}{\sqrt[3]{J}} \quad [31]. \quad (\text{A.7})$$

⁸⁹The material can be considered as incompressible if $K > 100G$, where $K = \frac{E}{3(1-2\nu)}$ [Pa] is a bulk modulus.

A.1.3 Green-Lagrangian Strain Tensor

In the solid mechanics, there is used mostly a Lagrangian continuum mechanics description when trajectories of all mesh nodes are observed. A mass motion is bonded with a mesh nodes motion. There is used a Green-Lagrangian strain tensor in the Lagrangian continuum mechanics description expressed as

$$\mathbf{E}^L = \frac{1}{2} (\mathbf{U}_s^2 - \mathbf{I}) = \frac{1}{2} (\mathbf{C} - \mathbf{I}), \quad (\text{A.8})$$

respectively in components from a displacement field

$$E_{ij}^L = \frac{1}{2} \left(\frac{\partial u_i}{\partial X_j} + \frac{\partial u_j}{\partial X_i} + \frac{\partial u_k}{\partial X_i} \frac{\partial u_k}{\partial X_j} \right), \quad (\text{A.9})$$

where $\frac{\partial}{\partial X_i}$ is a change from *initial* configuration [18, 30]. The Green-Lagrange Strain Tensor expresses a deformation against an *initial* geometry.

A.1.4 Eulerian-Almansi Strain Tensor

Eulerian continuum mechanics description is used mostly in the fluid mechanics, where the mass motion is not bonded with the mesh motion, but the mesh is fixed in space. There is used an Eulerian-Almansi strain tensor in the Eulerian continuum mechanics description expressed by formulas

$$\mathbf{E}^A = \frac{1}{2} (\mathbf{I} - \mathbf{U}_s^{-2}) = \frac{1}{2} (\mathbf{I} - \mathbf{C}^{-1}), \quad (\text{A.10})$$

respectively in components from a displacement field

$$E_{ij}^A = \frac{1}{2} \left(\frac{\partial u_i}{\partial x_j} + \frac{\partial u_j}{\partial x_i} - \frac{\partial u_k}{\partial x_i} \frac{\partial u_k}{\partial x_j} \right), \quad (\text{A.11})$$

where $\frac{\partial}{\partial x_i}$ is a change from *actual* configuration [18, 30].

A.1.5 Hencky Strain Tensor

Components of a Hencky Strain Tensor are better known as true/logarithmic strain. Its increment is defined as a deformation increment related to an *actual* deformation

$$dE^{tr} = \frac{dl}{l}.$$

By integration there can be gained a formula for the true strain

$$E^{tr} = \int_{l_0}^l \frac{d\zeta}{\zeta} = \left[\ln |\zeta| \right]_{l_0}^l = \ln \frac{l}{l_0} = \ln \lambda.$$

By generalizing there can be gained a formula for a strue strain tensor \mathbf{E}^{tr} as

$$\mathbf{E}^{tr} = \log \mathbf{U}_s = \frac{1}{2} \log \mathbf{C} \quad [18, 31]. \quad (\text{A.12})$$

The true strain tensor is in the most common cases used to represent FEM results. For non-diagonal components engineering shear strains

$$\gamma_{ij} = 2\varepsilon_{ij}, \quad i \neq j$$

are used. This might be very important for writing user subroutines, because a strain increment gained from a FEM solver differs for Abaqus/Standard and Abaqus/Explicit subroutines as is shown below.

$(\Delta\varepsilon_{11}; \Delta\varepsilon_{22}; \Delta\varepsilon_{33}; \Delta\varepsilon_{12}; \Delta\varepsilon_{23}; \Delta\varepsilon_{13})^T$: Abaqus/Explicit VUMAT

$(\Delta\varepsilon_{11}; \Delta\varepsilon_{22}; \Delta\varepsilon_{33}; \Delta\gamma_{12}; \Delta\gamma_{23}; \Delta\gamma_{13})^T$: Abaqus/Standard UMAT

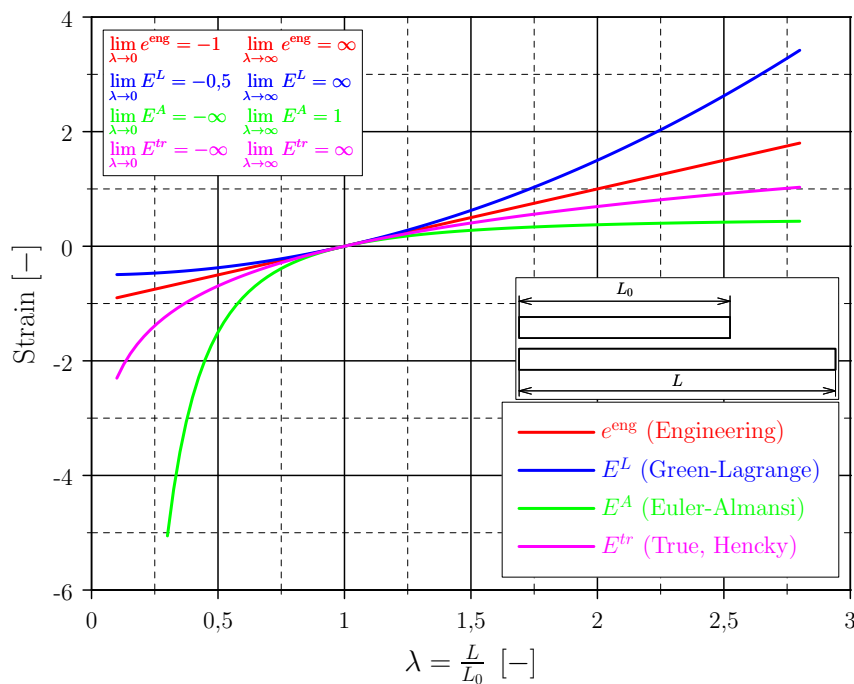


Fig. A.2: Comparison of strain definitions

A.2 Stress Tensors

A.2.1 Cauchy Stress Tensor

A Cauchy stress tensor $\boldsymbol{\sigma}$ is mostly used form to represent stress, because its definition is a force related to an *actual deformed* area, so it has a clear physical principle. Another advantage realted is that it is a symmetric tensor, so applies

$$\sigma_{ij} = \sigma_{ji}$$

and this tensor has six independent components [18, 31, 29, 30]. This tensor is mostly in an output in results of FEM analysis.

A.2.2 First Piola-Kirchhoff Stress Tensor

As well as the tensor mentioned above, First Piola-Kirchhoff stress tensor \mathbf{P} has a clear physical principle and it is a force related to an *initial undeformed* area. Its big disadvantage is asymmetry for big deflections, so it has all nine components independent. In this way, uniaxial tensile tests for materials based on metals are usually evaluated (see Sec. 4.2.3) [18, 31, 29, 30].

A.2.3 Second Piola-Kirchhoff Stress Tensor

A motivation to define Second Piola-Kirchhoff stress tensor \mathbf{S} was elimination of tensor \mathbf{P} asymmetry. The next motivation was to gain an energetically conjugated pair (see further) with the Green-Lagrangian strain tensor \mathbf{E}^L (see Sec A.1.3). On the other hand, this tensor has no physical principle, its a *modified* force related to an *initial undeformed* area [18, 31, 29, 30].

Tab. A.1: Conversion formulas for stress tensors [30]

Input \ Output	$\boldsymbol{\sigma}$	\mathbf{P}	\mathbf{S}
$\boldsymbol{\sigma}$		$\frac{1}{J}\mathbf{P}\mathbf{F}^T$	$\frac{1}{J}\mathbf{F}\mathbf{S}\mathbf{F}^T$
\mathbf{P}	$J\boldsymbol{\sigma}\mathbf{F}^{-T}$		$\mathbf{F}\mathbf{S}$
\mathbf{S}	$J\mathbf{F}^{-1}\boldsymbol{\sigma}\mathbf{F}^{-T}$	$\mathbf{F}^{-1}\mathbf{P}$	

A.3 Energetically Conjugated Tensors

Energetically conjugated tensors are such pairs of stress tensor \mathbf{T}^σ and a strain tensor \mathbf{T}^ϵ , the double dot product of which gives an internal energy density Λ

$$\Lambda = \frac{1}{2} (\mathbf{T}^\sigma : \mathbf{T}^\epsilon). \quad (\text{A.13})$$

Among the energetically conjugated tensors pairs belongs e.g. the Green-Lagrangian strain tensor \mathbf{E}^L and the second Piola-Kirchhoff stress tensor \mathbf{S} , the Eulerian-Almansi strain tensor \mathbf{E}^A and the Cauchy stress tensor $\boldsymbol{\sigma}$ and more. In the solid mechanics, where dominates the Lagrangian continuum mechanics description, the first mentioned pair is used.

B Geometry Creation

B.1 Mechanical Part

There was an effort to determine parameters of a transmission and individual gears, where a module, a profile angle, a unit profile shift etc. belong. A reverse transmission scheme is displayed in Fig. B.1.

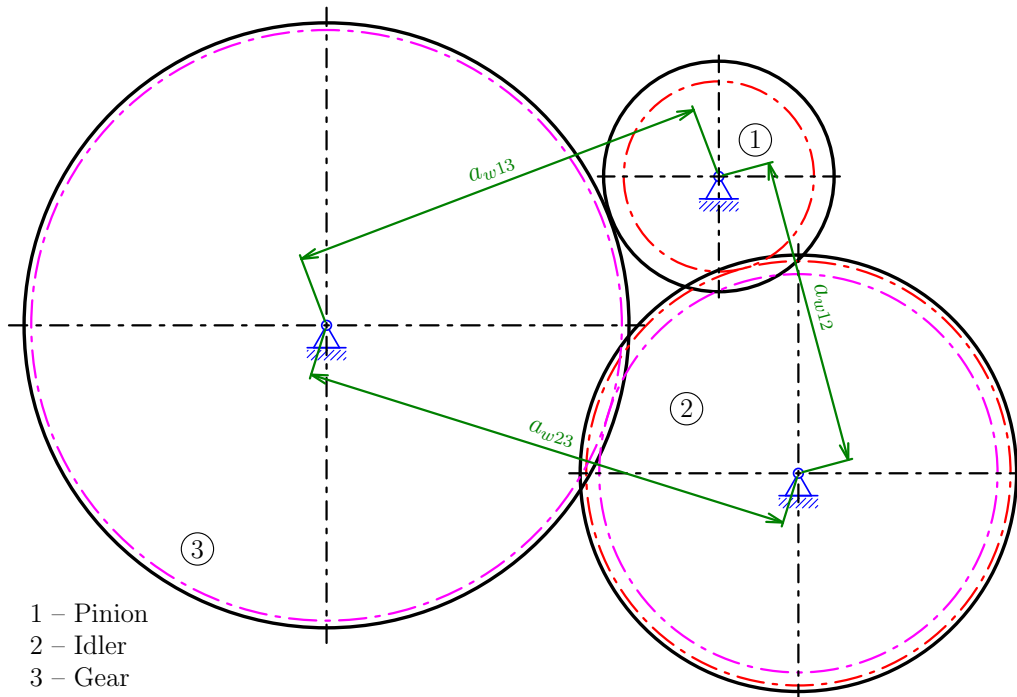


Fig. B.1: Reverse transmission scheme

A symbol a_{wij} denotes an axis distance between gears i and j . Axis distances mentioned below were determined based on a measurement of a gearbox cover where shafts are mounted.

$$a_{w13} = 65 \text{ mm} \quad a_{w12} = 47.6 \text{ mm} \quad a_{w23} = 76.6 \text{ mm}$$

Transmission parameters and profile parameters of individual gears are stated in Tab. B.1. These parameters were estimated based on further measurements⁹⁰ and subsequent calculations.

⁹⁰Span measurement of teeth, measurement over pins/balls.

Tab. B.1: Gearbox F17 reverse transmission parameters

Quantity	Denotation	Pinion	Idler	Gear
Diametral pitch ⁹¹	$DP_n \left[\frac{1}{\text{in}} \right]$	11.75		
Number of teeth	$z_g [-]$	13	29	43
Helix angle	β	0°		
Profile angle	α_n	24°30'		
Unit profile shift	$x_{ps} [-]$	0.966	0.16	-0.7025
Unit addendum	$h_a^* [-]$	0.9	1	0.9
Unit dedendum	$h_f^* [-]$	1.25	1.15	1.25
Unit root fillet	$r_f^* [-]$	0.25	0.3	0.25

The assembly of all gears composing a reverse transmission is displayed in Fig. B.2. A drawing of a gear is situated on an attached CD in a file R_gear_machining_drawing.pdf.

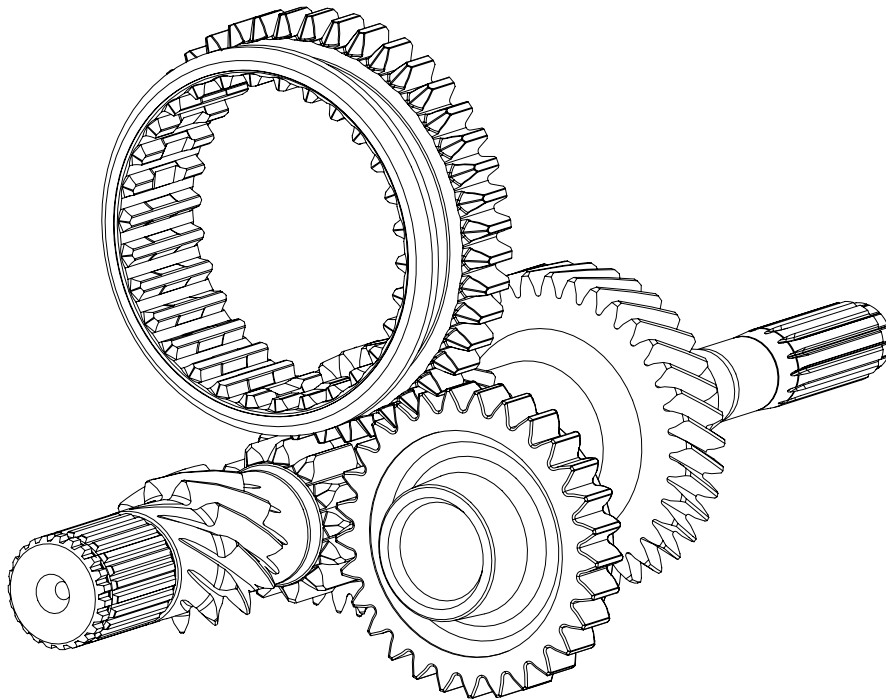


Fig. B.2: Reverse transmission assembly

⁹¹A module is used in countries using the metric system, expressed from a diametral pitch as $m_n = \frac{25.4}{DP_n}$.

B.2 Forging

It was necessary to determine, which surfaces are important for a functionality. These surfaces are denoted by a red colour (see Fig. B.3a) and so it is necessary to put them on a machining addition according to Tab. B.2 (a used value is undercoloured in this table). In Fig. B.3a are also surfaces denoted by a blue colour. They are not functional, but their surface is better than it would be achievable by forging. So an addition only 1.0 mm is used. Surfaces denoted by a thick line and a black colour are not machined. A forging as an envelope body is displayed in Fig. B.3b.

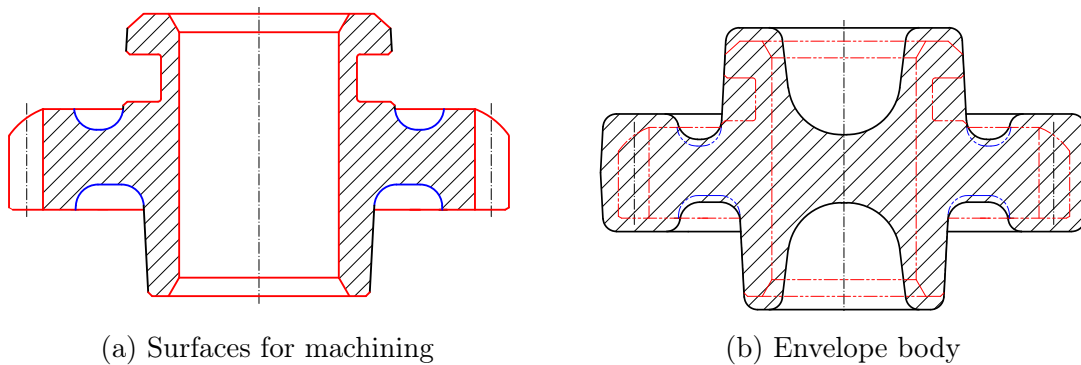


Fig. B.3: Reverse transmission spur gear

The drawings are attached on the CD in subsequent files:

- forging: R_gear_finishing_drawing.pdf,
- preforging: R_gear_blocking_drawing.pdf.

Tab. B.2: Machining additions-common construction [13]

Dimensions in mm

		The biggest forging height								
		over		25	40	63	100	160	250	400
		up to	25	40	63	100	160	250	400	630
The biggest diameter, mean value of width and length of a final product perpendicular to a strike direction	over	up to	Machining additions							
		25	1.5	1.5	2.0	2.0	2.0			
	25	40	1.5	2.0	2.0	2.0	2.5	2.5		
	40	63	2.0	2.0	2.0	2.5	2.5	2.5		
	63	100	2.0	2.0	2.5	2.5	2.5	3.0	3.5	
	100	160	2.0	2.5	2.5	2.5	3.0	3.5	3.5	
	160	250	2.5	2.5	2.5	3.0	3.5	3.5	4.0	4.5
	250	400	2.5	2.5	3.0	3.5	3.5	4.0	4.5	5.0
	400	630	2.5	3.0	3.5	3.5	4.0	4.5	5.0	5.5
	630	1000	3.0	3.5	3.5	4.0	4.5	5.0	5.5	6.0

Tab. B.3: Edge fillet radii [13]

Dimensions in mm

Height (depth) h		Edge fillet radii for ratio					
		$\frac{h}{f} \leq 2$		$2 < \frac{h}{f} \leq 4$		$\frac{h}{f} > 4$	
over	up to	r	R	r	R	r	R
	25	2	6	2	8	3	10
25	40	3	8	3	10	4	12
40	63	4	10	4	12	5	20
63	100	5	12	6	20	8	25
100	160	8	20	8	25	16	40
160	250	12	30	16	45	25	65
250	400	20	50	25	75	40	100
400	630	30	80	40	120	65	150

C Appendix to Results

A problem was described in Chap. 6 that some contact surfaces are not fully separated in an unload phase. The consequences of this error can be seen in Fig. C.1, where one node stays stuck to a tool, a distortion of nearby elements and strain growth occur. According to a small range of a corrupted area, a significant change of rod stiffness does not occur and a distortion does not cause solution termination.

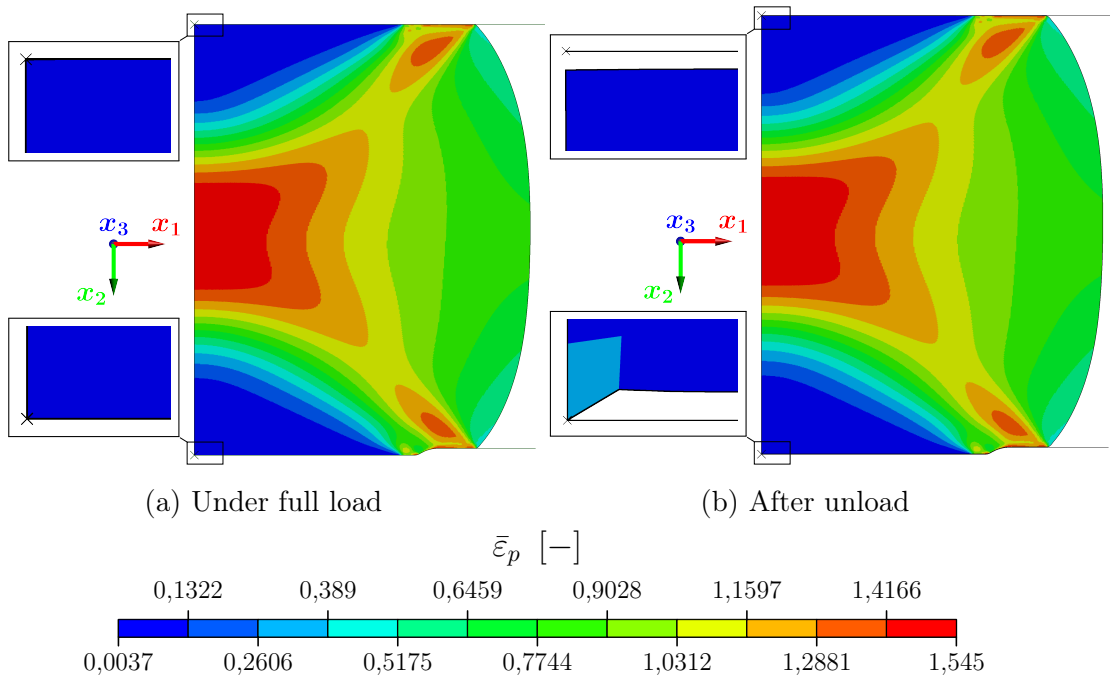


Fig. C.1: Contact (non)separation

Furthermore, there was an effort to use the whole processor power and so a solution without an adaptive meshing was performed with increased number of elements (662 110 in comparison with 459 648). As one can see in Fig. C.2, a mesh was damaged enough by a distortion of many elements mainly nearby contacts with tools, at the end of a blocking operation. So a solution could not continue and it was prematurely terminated. A possible solution would be to increase the number of elements even more, however, this solution is unrealistic for purposes of this thesis because one analysis could take a couple of weeks, perhaps even a couple of months. This implicates that adaptive meshing is unconditionally necessary to realize analysis to their final phase.

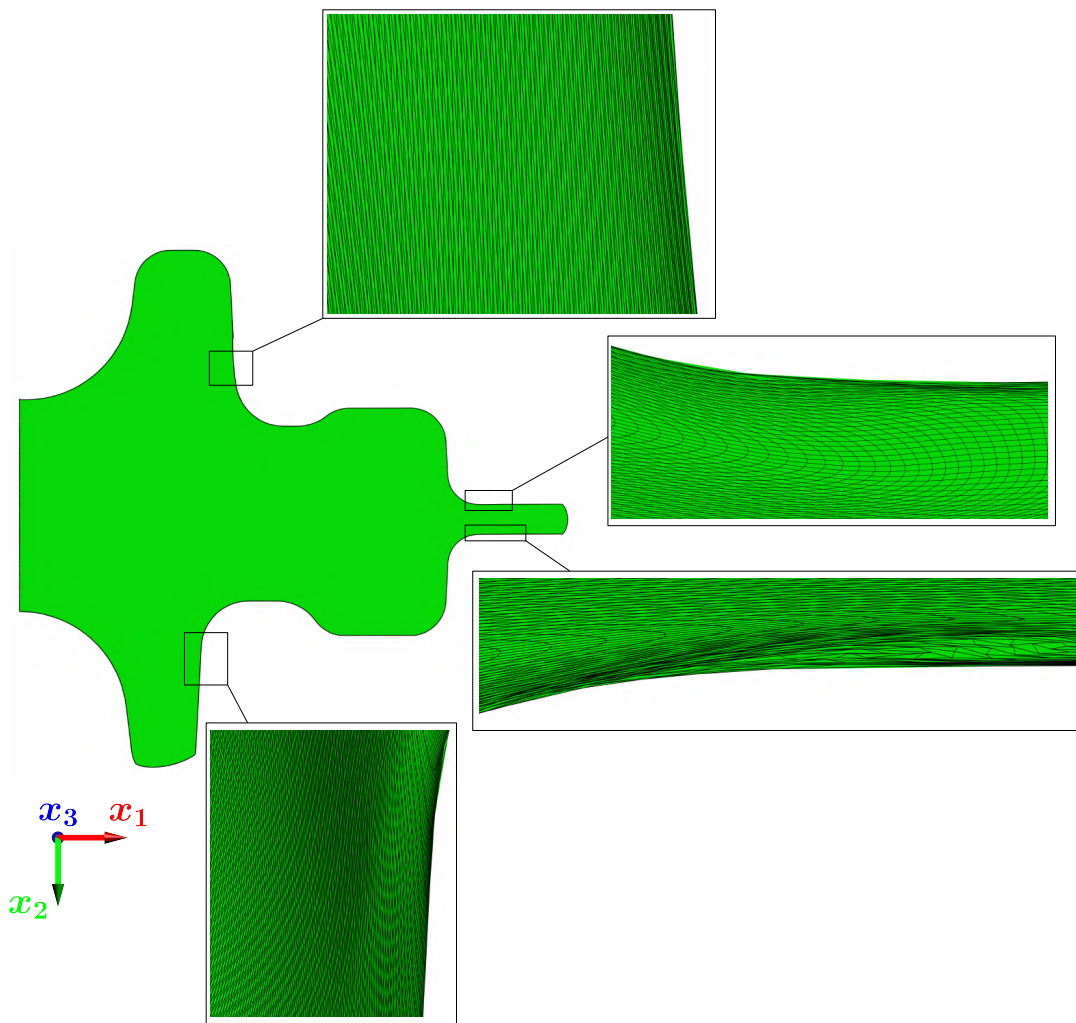


Fig. C.2: Distortion of elements without adaptive meshing

List of Figures

1.1	Biaxial tensile specimen	13
1.2	Central bursting initiation during forward extrusion	14
1.3	Bar shear partitioning	14
2.1	Solved mechanical part	19
2.2	Hertz contact	20
2.3	Uniaxial tensile test	21
2.4	Thin-wall structure post-critical behaviour analysis	21
2.5	Elementary element	23
2.6	Hourglassing symmetric modes	26
3.1	Diagram Fe - Fe ₃ C	27
3.2	Gear production process	28
3.3	Open-die forging operation examples	30
3.4	Assembly die-forging	31
3.5	Parting plane shapes	32
3.6	Forging fillet radii	32
3.7	Preforged hole	33
3.8	Cross section diagram	34
3.9	Roll-forging scheme	34
3.10	Cross wedge rolling scheme	35
3.11	Flash gutters for drop hammers	35
3.12	Crank mechanism scheme	37
3.13	Flash gutters for vertical crank presses	37
3.14	Flash trimming	39
3.15	Forged parts examples 1	41
3.16	Forged parts examples 2	42
4.1	Elastic parameters of the linear isotropic material	43
4.2	von Mises yield surface	44
4.3	Hardening types	48

4.4	Engineering tensile diagram	49
4.5	Johnson-Cook yield stress surfaces	51
4.6	Johnson-Cook flow curves	52
4.7	Ductile damage mechanisms	53
4.8	Johnson-Cook criterion	55
4.9	Xue-Wierzbicki criterion	56
4.10	Bai-Wierzbicki criterion	57
4.11	KHPS criterion	57
4.12	Physical and thermodynamic characteristics of the steel 12 050	58
5.1	Coordinate systems	60
5.2	Illustrative example	63
5.3	Illustrative example-results	64
6.1	Circular rod	68
6.2	Application GUI	69
6.3	Rod	70
6.4	Tool	71
6.5	Specific heat-steel 19 552	71
6.6	Rod's dimensions change	72
6.7	Flow curve for high temperature	72
6.8	Position of ram in time	77
6.9	Kinematic quantities	79
6.10	Crank press amplitude GUI application	80
6.11	Upsetting	81
6.12	Blocking	82
6.13	Finishing	83
6.14	Flash trimming	84
7.1	Deformed shapes	86
7.2	Results after upsetting-rod $\varnothing 36$, temperature 1000°C	87
7.3	Results after upsetting-rod $\varnothing 36$, temperature 1100°C	88
7.4	Results after upsetting-rod $\varnothing 38$, temperature 1000°C	88
7.5	Running of strain in element	89
7.6	Results after blocking-rod $\varnothing 36$, temperature 1000°C	90

7.7	Results after blocking-rod $\varnothing 36$, temperature 1100°C	91
7.8	Results after blocking-rod $\varnothing 38$, temperature 1000°C	92
7.9	Results after finishing-rod $\varnothing 36$, temperature 1000°C	93
7.10	Results after finishing-rod $\varnothing 36$, temperature 1100°C	94
7.11	Results after finishing-rod $\varnothing 38$, temperature 1000°C	95
7.12	Evolution of axial force during upsetting	96
7.13	Evolution of axial force during blocking	97
7.14	Evolution of axial force during finishing	98
7.15	Damage parameter after upsetting	99
7.16	Damage parameter after blocking	100
7.17	Damage parameter after finishing	102
7.18	Fracture surface	103
7.19	Deformed shape after trimming of flash	104
7.20	Evolution of internal and artificial energy	104
A.1	Elementary element deformation	117
A.2	Comparison of strain definitions	120
B.1	Reverse transmission scheme	123
B.2	Reverse transmission assembly	124
B.3	Reverse transmission spur gear	125
C.1	Contact (non)separation	127
C.2	Distortion of elements without adaptive meshing	128

List of Tables

2.1	Steel 12 050 chemical contribution	18
4.1	Variables ranges for ductile damage description	54
6.1	Compatible unit systems	67
6.2	Johnson-Cook flow curve parameters for steel 12 050	73
6.3	Johnson-Cook ductile damage parameters for steel 12 050	73
6.4	Used machines parameters	77
7.1	Combinations of input material dimensions and temperatures	85
7.2	Input material volume	98
A.1	Conversion formulas for stress tensors	121
B.1	Gearbox F17 reverse transmission parameters	124
B.2	Machining additions-common construction	126
B.3	Edge fillet radii	126